

**MODEL PREDICTIVE CONTROL BASED ON
LYAPUNOV FUNCTION AND NEAR STATE VECTOR
SELECTION OF FOUR-LEG INVERTER**

ABDUL MANNAN DADU

**FACULTY OF ENGINEERING
UNIVERSITY OF MALAYA
KUALA LUMPUR**

2018

**MODEL PREDICTIVE CONTROL BASED ON
LYAPUNOV FUNCTION AND NEAR STATE VECTOR
SELECTION OF FOUR-LEG INVERTER**

ABDUL MANNAN DADU

**DISSERTATION SUBMITTED IN FULFILMENT OF
THE REQUIREMENTS FOR THE DEGREE OF MASTER
OF ENGINEERING SCIENCE**

**FACULTY OF ENGINEERING
UNIVERSITY OF MALAYA
KUALA LUMPUR**

2018

UNIVERSITY OF MALAYA
ORIGINAL LITERARY WORK DECLARATION

Name of Candidate: Abdul Mannan Dadu

Matric No: KGA15

Name of Degree: Master of Engineering Science

Title of Dissertation:

MODEL PREDICTIVE CONTROL BASED ON LYAPUNOV FUNCTION
AND NEAR STATE VECTOR SELECTION OF FOUR-LEG INVERTER

Field of Study: Power Electronics

I do solemnly and sincerely declare that:

- (1) I am the sole author/writer of this Work;
- (2) This Work is original;
- (3) Any use of any work in which copyright exists was done by way of fair dealing and for permitted purposes and any excerpt or extract from, or reference to or reproduction of any copyright work has been disclosed expressly and sufficiently and the title of the Work and its authorship have been acknowledged in this Work;
- (4) I do not have any actual knowledge nor do I ought reasonably to know that the making of this work constitutes an infringement of any copyright work;
- (5) I hereby assign all and every right in the copyright to this Work to the University of Malaya ("UM"), who henceforth shall be owner of the copyright in this Work and that any reproduction or use in any form or by any means whatsoever is prohibited without the written consent of UM having been first had and obtained;
- (6) I am fully aware that if in the course of making this Work I have infringed any copyright whether intentionally or otherwise, I may be subject to legal action or any other action as may be determined by UM.

Candidate's Signature

Date:

Subscribed and solemnly declared before,

Witness's Signature

Date:

Name:

Designation:

MODEL PREDICTIVE CONTROL BASED ON LYAPUNOV FUNCTION AND NEAR STATE VECTOR SELECTION OF FOUR-LEG INVERTER

ABSTRACT

Due to the evolution of high processing microprocessors, the model predictive control (MPC) has been widely used in power electronic applications. The model predictive control technique utilizes all the available voltage vectors of power inverter to improve the predictive current control performance. In spite of simplicity, flexibility and fast dynamic response, the conventional model predictive control (C-MPC) has a drawback of computational burden. The computational burden of C-MPC is expensive due to utilize all available voltage vectors of a power inverter to predict the future behavior of the system. This dissertation has focused on Lyapunov model predictive control (L-MPC) methods, in which Lyapunov control law is employed in the cost function to minimize the error between the desired control variables and the actual control variables of a three-phase four-leg inverter to optimize closed-loop system performance. The proposed control algorithm takes advantage of a predefined Lyapunov control law which minimizes the required calculation time by the Lyapunov model equations just once in each control loop to predict future variables. In this dissertation, a near state vector selection-based model predictive control (NSV-MPC) scheme is also proposed to mitigate the common-mode voltage (CMV) with reduced computational burden. The proposed control technique adopts 6 active voltage vectors in the discrete predictive model among 14 available active vectors based on the position of the future reference vector. The position of reference currents is used to detect the voltage vectors surrounding the reference voltage vector in every sampling period. At last, the influencing factor of CMV is revealed based on switching state combination and then the CMV weighting factor is introduced in the cost function to make balance in the ripple content of load currents and the mitigation of CMV. The switching state pattern is selected according to peak to peak

value of CMV and CMV weighting factor is related to peak value of CMV and a user defined co-efficient. The stability of the system is ensured through Lyapunov function with the help of backstepping control method. L-MPC technique improves the digital speed by 23.8% compared to C-MPC and it reduces current tracking error confined within 0.65A and THD in the variation of inverter control parameters of a three-phase four-leg inverter. The CMV can be bounded within one-fourth of the dc-link voltage of a three-phase four-leg inverter using the proposed NSV-MPC technique. MATLAB/Simulink software environment is used for the simulation and the LabVIEW Field programmable gate array (FPGA) rapid prototyping controller is used to validate the proposed control scheme. The results showed that the proposed control techniques had better performance as compared to the C-MPC.

Keywords: Model Predictive Control, Common-Mode Voltage, Total Harmonic Distortion.

ABSTRAK

Oleh kerana evolusi terhadap mikropemproses pemprosesan tinggi, kawalan model ramalan (MPC) telah digunakan secara meluas pada aplikasi elektronik kuasa. Teknik kawalan model ramalan menggunakan semua vektor voltan yang tersedia pada penyongsang kuasa untuk menambahbaik prestasi kawalan arus ramalan. Walaupun mudah, fleksibel dan mempunyai respons dinamik yang pantas, kawalan model ramalan konvensional (C-MPC) mempunyai kelemahan dari segi beban pengkomputeran. Beban pengkomputeran pada C-MPC mempunyai kos yang tinggi kerana ia menggunakan semua vektor voltan yang tersedia pada penyongsang kuasa untuk meramal perilaku akan datang sistem tersebut. Laporan kemajuan kajian ini tertumpu kepada kaedah kawalan model ramalan Lyapunov (L-MPC), di mana hukum kendali Lyapunov digunakan dalam fungsi kos untuk meminimumkan ralat antara pemboleh ubah yang dingini dan pemboleh ubah yang sebenar bagi penyongsang tiga fasa empat kaki. Algoritma yang dicadangkan memanfaatkan hukum kendali Lyapunov pratakrif yang meminimumkan pengiraan masa yang diperlukan oleh persamaan model Lyapunov hanya sekali dalam setiap gelung kawalan untuk meramal pemboleh ubah akan datang. Dalam kajian ini, satu skema kawalan model ramalan berdasarkan pemilihan vektor keadaan berhampiran (NSV-MPC) juga dicadangkan untuk mengurangkan voltan ragam sepunya dengan beban pengkomputeran yang dikurangkan. Teknik kawalan yang dicadangkan menggunakan enam vektor voltan aktif dalam model ramalan diskret antara 14 vektor aktif yang tersedia berdasarkan kepada kedudukan vektor rujukan akan datang. Kedudukan arus-arus rujukan digunakan untuk mengesan vektor voltan di sekeliling vektor voltan rujukan pada setiap tempoh pensampelan. Akhirnya, faktor berpengaruh CMV didedahkan berdasarkan pada kombinasi keadaan penguisan pertama dan kedua, faktor pemberat CMV diperkenalkan dalam fungsi kos untuk mengimbangi kandungan riak pada arus beban dan mitigasi CMV. Pola keadaan penguisan dipilih berdasarkan nilai puncak ke puncak

CMV dan faktor pemberat CMV berkait dengan nilai puncak fungsi CMV dan pekali tentuan pengguna. Kestabilan sistem dipastikan melalui fungsi Lyapunov dengan bantuan kaedah kawalan injak balik. Teknik L-MPC menambahbaik kelajuan digital sebanyak 23.8% berbanding C-MPC dan mengurangkan ralat arus jejak terbatas dalam 0.65A dan THD dalam variasi parameter kawalan penyongsang untuk penyongsang tiga fasa empat kaki. CMV boleh dibataskan dalam satu per empat daripada voltan sambungan dc penyongsang tiga fasa empat kaki menggunakan teknik NSV-MPC yang dicadangkan. Perisian persekitaran MATLAB/Simulink digunakan untuk simulasi dan pengawal pemprototaipan cepat tatasusun medan get boleh aturcara (FPGA) LabVIEW digunakan untuk mengesahkan skema kawalan yang dicadangkan. Keputusan menunjukkan teknik kawalan yang dicadangkan mempunyai prestasi yang lebih baik berbanding C-MPC.

Keywords: kawalan model ramalan, Voltan Mod-Biasa, Penyelewengan Harmonik Jumlah

ACKNOWLEDGEMENTS

First of all, I would like to thank almighty Allah. After that, I want to thank my supervisor Prof. Dr. Saad Mekhilef and Dr. Tey Kok Soon for their endless support and guidance throughout my graduate studies. Their profound knowledge, patience, and creative thinking have been a source of inspiration for me that kept me on the right track. I am very grateful to work with such experienced and cooperative advisor. Special thanks to Prof. Saad for providing research fellowship and research facilities in Power Electronics and Renewable Energy Research Laboratory (PEARL), without it, the study period would have been even tenser. Special thanks to Dr. Tey for friendly supervision and support during the study period.

I am also grateful to many administrative staff in the Department of Electrical Engineering, Faculty of Engineering and Institute of Graduate Studies for facilitating several formalities.

Thanks to the High Impact Research (HIR) secretariat at the University of Malaya for providing fund for this study.

It really has been a great pleasure to work in Power Electronics and Renewable Energy Research Laboratory (PEARL), not only because of talented colleagues but also the friendship. I would like to thank all of my colleagues. I cherish the delightful time that we have worked together.

Last but not least, I offer my deepest gratitude to my parents and BPDB colleagues for their everlasting love, support, and encouragement for all my endeavors.

TABLE OF CONTENTS

Abstract.....	iii
Abstrak.....	v
Acknowledgements.....	vii
Table of Contents.....	viii
List of Figures.....	xii
List of Tables.....	xv
List of Symbols and Abbreviations.....	xvi
CHAPTER 1: INTRODUCTION.....	1
1.1 Introduction.....	1
1.2 Background and Motivation.....	1
1.3 Problem Statement.....	6
1.4 Objectives.....	7
1.5 Outlines of the Research.....	8
CHAPTER 2: STATE OF ART: INVERTER TOPOLOGY AND CONTROL TECHNIQUE 10	
2.1 Introduction.....	10
2.2 Power Inverter Types.....	10
2.2.1 DC to AC Inverter Topology.....	11
2.2.2 Comparison of Inverters.....	12
2.3 Control Techniques of Power Inverter.....	13
2.4 Predictive Control.....	15
2.4.1 Deadbeat Predictive Control.....	15
2.4.2 Hysteresis Based Predictive Control.....	16

2.4.3	Trajectory Based Predictive Control	17
2.4.4	Model Based Predictive Control	17
2.5	Finite Control Set Model Predictive Control.....	18
2.6	Comparison of Inverter Control Techniques	20
2.7	Summary.....	21

CHAPTER 3: DESCRIPTION OF THE INVERTER TOPOLOGY AND THE PROPOSED CONTROL TECHNIQUES.....22

3.1	Introduction.....	22
3.2	Three-Phase Four-leg Inverter System	22
3.2.1	Common Mode Voltage Model.....	23
3.2.2	Mathematical Model.....	25
3.3	Model predictive Control Formulation.....	29
3.4	MPC for Three-Phase Four-Leg Inverter	29
3.4.1	Measurements.....	29
3.4.2	References Generation.....	30
3.4.3	Discrete Time Model.....	30
3.4.4	Predictive Model	31
3.4.5	Cost Function	32
3.4.6	Adding CMV Weighting Factor in the Cost Function	34
3.4.7	Vector Selection Strategy	34
3.5	L-MPC for Three-Phase Four-Leg Inverter.....	35
3.6	Near State Vector Selection Based Model Predictive Control for Three-Phase Four-Leg Inverter	38
3.7	Summary.....	42

CHAPTER 4: RESULT AND DISCUSSION.....	44
4.1 Introduction.....	44
4.2 LabVIEW FPGA Implementation Procedure	44
4.3 Simulation and Experimental Results Analysis.....	47
4.3.1 MPC with CMV Mitigation of Three-Phase Four-Leg Inverter	48
4.3.2 L-MPC for Three-Phase Four-Leg Inverter	53
4.3.3 Near State Vector Based Model Predictive Control for Three-Phase Four-Leg Inverter	60
4.4 Summary.....	67
CHAPTER 5: STABILITY ANALYSIS AND PERFORMANCE ASSESMENT .	68
5.1 Introduction.....	68
5.2 Stability Analysis of Three-phase Four-leg Inverter	68
5.2.1 Lyapunov Law Justification	68
5.2.2 Lyapunov Stability Analysis with Backstepping Control	70
5.3 Performance Assessment of L-MPC	73
5.3.1 Robustness Analysis of Model Parameter Variations	73
5.3.2 Control Algorithm and Implementation Procedure.....	75
5.3.3 Current Reference Tracking and THD	77
5.4 Performance Assessment of NSV-MPC.....	82
5.4.1 Robustness Analysis of Model Parameter Variations	83
5.4.2 Performance Assessment.....	83
5.5 Summary.....	85
CHAPTER 6: CONCLUSION AND FUTURE WORK	87
6.1 Conclusion.....	87
6.1.1 Summary of Major Contributions	87

6.2 Future Work.....	88
References	89
List of Publications and Papers Presented	100

University of Malaya

LIST OF FIGURES

Figure 1.1: The PV system configuration	2
Figure 2.1: Power converter classification (J. Rodriguez & P. Cortes, 2012)	11
Figure 2.2: Different types of converter control technique for power converters	13
Figure 2.3: Classification of predictive control methods used in power electronics (Cortes, Kazmierkowski, Kennel, Quevedo, & Rodriguez, 2008).	15
Figure 2.4: Deadbeat predictive control with RL load.....	16
Figure 2.5: Working principle of MPC	18
Figure 2.6: Finite control set model predictive control technique	18
Figure 3.1: Three-phase four-leg inverter topology.....	23
Figure 3.2: MPC control block diagram	29
Figure 3.3: L-MPC block diagram with three-phase four-leg inverter	35
Figure 3.4: (a) Switching vectors and Prisms (b) Projection of sector on the $\alpha\beta$ coordinate	40
Figure 3.5: Sector identification with near state vector selection	40
Figure 3.6: Near state vector based MPC block diagram.....	41
Figure 4.1: Applications development flow with FPGA compilation (Soghoian, Suleiman, & Akopian, 2014)	45
Figure 4.2: Inverter input DC voltage and output load current acquisition	45
Figure 4.3 Reference current generation for the cost function.....	46
Figure 4.4: Algorithm acquisition using LabVIEW function blocks.....	47
Figure 4.5: Experimental setup in the FPGA platform	48
Figure 4.6: MPC based on all available voltage vector (a) Simulation result (b) Experimental result	49
Figure 4.7: MPC based on active vectors with one zero (pppp) vector (a) Simulation result (b) Experimental result.....	50

Figure 4.8: MPC based on active vectors with one zero (nnnn) vector (a) Simulation result (b) Experimental result.....	51
Figure 4.9: The inverter output current and CMV using CMV weighting factor (a) Simulation result (b) Experimental result.	52
Figure 4.10: Case 1: Balanced references with balanced load and filter (a) Simulation result (b) Experimental Result	54
Figure 4.11: Case 2: Unbalanced references with balanced load and filter (a) Simulation result (b) Experimental Result.	55
Figure 4.12: Case 3: Balanced references with unbalanced load and filter (a) Simulation result (b) Experimental Result	57
Figure 4.13: Case 4: Unbalanced references with unbalanced load and filter (a) Simulation result (b) Experimental Result	58
Figure 4.14: Experimental result with sudden variation in the load from 10 A to 5A of proposed L-MPC.....	59
Figure 4.15: Experimental result with sudden variation in frequency from 50 Hz to 25Hz of L -MPC	59
Figure 4.16: Each phase current and CMV for case 1 (a) Simulation result (b) Experimental result	61
Figure 4.17: Each phase current and CMV for case 2 considering pppp switching state (a) Simulation result (b) Experimental result	62
Figure 4.18: Each phase current and CMV for case 2 considering nnnn switching state (a) Simulation result (b) Experimental result	63
Figure 4.19: Each phase current and CMV for case 3 (a) Simulation result (b) Experimental result	64
Figure 4.20: FFT analysis results of CMV for case 1- 8 vector based NSV-MPC.....	65
Figure 4.21: FFT analysis results of CMV for case 2 considering pppp switching state NSV-MPC.....	65
Figure 4.22: FFT analysis results of CMV for case 2 considering nnnn switching state NSV-MPC.....	66
Figure 4.23: FFT analysis results of CMV for case 3 - NSV-MPC.....	66

Figure 5.1: Comparison of THD between C-MPC and L-MPC with the filter changes (CF) and the controller and filter changes (CCF) at 50 us (a) Simulation result and (b) Experimental result	74
Figure 5.2: Reference tracking error (%) of L-MPC over C-MPC with model parameters variation.....	75
Figure 5.3: Flowcharts of the (a) C-MPC (Rivera, Yaramasu, Llor, et al., 2013) and (b) L-MPC	76
Figure 5.4: Three-phase references and measured load currents (a) C-MPC and (b) L-MPC.....	78
Figure 5.5: Current tracking error of Phase X (a) C-MPC and (b) L-MPC.....	79
Figure 5.6: Experimental result for balanced references with balanced loads (a) C-MPC and (b) L-MPC.....	81
Figure 5.7: The percentages of THD with respect to variation of inductive value	83

LIST OF TABLES

Table 2.1: Comparison of dc-ac power inverters	12
Table 2.2: Comparison of control techniques	20
Table 3.1: Common-Mode Voltage Level with Different Switching States.....	24
Table 3.2: Allowable inverter-switching states.....	25
Table 3.3: The switching states with phase voltages in the $\alpha\beta\gamma$ coordinate.....	39
Table 3.4: CMV for corresponding near state vector of each sector	42
Table 4.1: Parameters of the simulation and experimental results.....	48
Table 4.2: Parameters of the simulation and experimental results.....	53
Table 4.3: Parameters of the experimental results	60
Table 5.1: The improvement of L-MPC over C-MPC per operation.....	77
Table 5.2: Execution time measurement.....	77
Table 5.3 : THD comparison between C-MPC and L-MPC.....	81
Table 5.4 : THD Comparison of Proposed Control Method with Previous Works of Four-leg Inverter	82
Table 5.5: Execution time measurement.....	84
Table 5.6: CMV and percentage of THD and Current tracking error variation at different sampling time.....	84
Table 5.7: THD (%), Current tracking error variation and average switching frequency at different weighting factor.....	85
Table 5.8: Comparison between proposed control technique and previous works.....	85

LIST OF SYMBOLS AND ABBREVIATIONS

PV	:	Photo-voltaic
DC	:	Direct current
AC	:	Alternating current
VSI	:	Voltage source inverter
CCS	:	Continuous control set
FCS	:	Finite control set
MPC	:	Model predictive control
DPC	:	Direct power control
DTC	:	Direct torque control
FOC	:	Flux-oriented control
VOC	:	Voltage oriented control
EMI	:	Electromagnetic interferences
PI	:	Proportional integral
PWM	:	Pulse-width modulation
SVM	:	Space vector modulation
THD	:	Total harmonic distortion
SHE	:	Selective harmonic elimination
CMV	:	Common mode voltage
FPGA	:	Field programmable gate array
CMPC	:	Conventional model predictive control
NSV	:	Near state vector
L-MPC	:	Lyapunov model predictive control

CHAPTER 1: INTRODUCTION

1.1 Introduction

Photo-voltaic (PV) energy has attracted great attention and becoming a mainstream energy source among all the renewable sources due to technological improvements, cost optimization and government incentive programs. This introductory chapter presents a general background of power inverters and its control techniques for energy conversion. A problem statement has been drawn from the background of PV standalone applications. This has been motivated for the research work and found the objectives of this dissertation. The organization of this chapter is as given: the background and motivation behind the research are discussed in section 1.2, the problem statement in section 1.3. The objectives of this dissertation are presented in Section 1.4. Finally, in Section 1.5, the outline of the dissertation is summarized.

1.2 Background and Motivation

The photo-voltaic (PV) energy as a renewable-energy source considered as a clean source of energy is being a more attractive energy source due to minimize environmental impacts, produce minimum secondary wastes and is sustainable based on current and future economic and social societal needs (Panwar, Kaushik, & Kothari, 2011). The PV source totally depends on weather conditions; hence the generated energy is unpredictable and interruptible. PV systems are usually used in the application of roof-top mounted, building-integrated systems with small-scale power utility. Nowadays, most of the PV systems are grid connected or standalone application (PVPS, 2014; Teodorescu, Liserre, & Rodriguez, 2011). The configuration of PV system is shown in Figure 1.1.

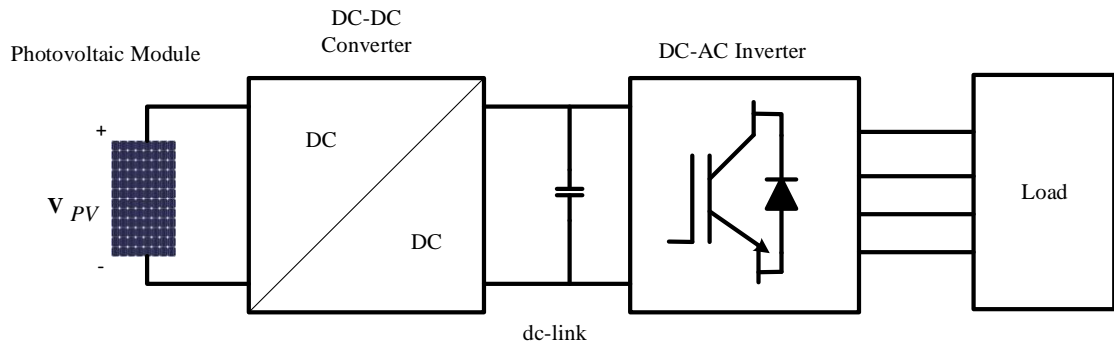


Figure 1.1: The PV system configuration

The PV source generates DC in nature; thus, an inverter is required to convert DC voltage into a desired voltage for feeding into utility grid or specific application at main frequency. The power inverters are used to manage the flow of electrical energy that uses the semiconductor switching devices such as IGBT, MOSFET etc. These switching devices can be used for converting PV energy to different level of desired voltage, current and frequency. Standalone power distribution system is an off-grid interface electricity distribution system and usually this system is tied with PV energy source. At present, the standalone power distribution system of utility industry has to provide uninterrupted and balanced/unbalanced power to its consumer such as data communication, aircraft, home appliances, satellite station and railway system (Singh & Sharma, 2012). A three-phase four-leg inverter can be used for this application. It is also becoming popular in specific applications such as standalone system (Philip et al., 2016), UPS systems (Pichan & Rastegar, 2017) and also islanded mode when the grid supply is failed (Rodriguez, Fuente, Garcera, Figueres, & Moreno, 2013). In modern era, delivering an unbalanced load is a commercial and industrial issue in an energy conversion system. Thus, three-phase four-leg inverter is introduced with providing zero sequence path over the three-phase three-leg inverter to distribute power to the balanced/unbalanced and linear/non-

linear loads (Rivera, Yaramasu, Rodriguez, & Bin, 2013; Yaramasu, Rivera, Narimani, Bin, & Rodriguez, 2014).

The power inverters have a finite number of switching device and these electronic switches can be controlled using discrete control signals. The model of inverters is non-linear in nature with the inclusion of linear and non-linear parts. Therefore, the control strategies are considered with the inclusion of several constraints and restrictions. In modern power electronics applications, researches are not only focused on topological improvement (Fengjiang, Xiaoguang, Fan, & Hoay Beng, 2015; Seung-Hee, Dong-Gyun, Min-Kook, & Byoung-Kuk, 2016), but also control methodology improvement in order to enhance the system performance (Chee-Shen, Levi, Jones, Rahim, & Wooi-Ping, 2014; Geyer & Quevedo, 2014; Rivera, Yaramasu, Llor, et al., 2013). The proportional integral (PI) based control scheme has been implemented in the three phase four-leg inverter topology (Priya & Mabel, 2012). However, the cascaded structure of this control scheme and the tuning of PI controllers are very complicated and time consuming. There are a number of pulse width modulation (PWM) based control techniques such as carrier-based Sinusoidal pulse width modulation (SPWM), Selective harmonic elimination based PWM (SHE-PWM) and three-dimensional space vector based PWM (3D-SVPWM) which is used to control current and voltage of a three-phase four-leg voltage source inverter (VSI) (Choi & Lee, 2015; Fernandes, Costa, & Santos, 2013; George & Mishra, 2009; Prabhakar & Mishra, 2010; F. Zhang & Yan, 2009). PWM is a well-known modulation scheme that has been applied because of its simplicity. However, these classical controllers are easy to be implemented and the PID controller is used to reduce the steady-state current deviation, but the performance is highly depended on the inner control loop (J, Freudenberg, The, & Dieckerhoff, 2015). Apart from that, the modulation stage is also required to generate control signals for the power switches.

As compared to PWM based control, model predictive control (MPC) is a powerful control methodology of power inverters. Continuous control set (CCS) MPC and finite control set (FCS) MPC are the main control methods of MPC in the application of a voltage source inverter (VSI). Owing to control horizon concept, CCS-MPC can be applied with any number of horizon with the low computational burden. Continuous time signals for the control action passes through modulator to generate PWM signals and the mathematical model is very complex (Bordons & Montero, 2015; Vazquez, Montero, Bordons, & Franquelo, 2013). Thus, the FCS-MPC is a remarkable solution to eliminate the inner loop and modulator. FCS- MPC considers a finite number of valid switching states to predict the behavior of the system by a discrete model at every sampling time. The concept of FCS-MPC lies in the optimization of the cost function to ensure the overall performance of the predictive control. A predefined cost function compares each prediction with its respective reference. After that, the switching state that minimizes the cost function is applied to the inverter and this sequence is repeated in every sampling time as mentioned in (Rivera, Yaramasu, Rodriguez, et al., 2013; Yaramasu, Rivera, Bin, & Rodriguez, 2013). This control scheme is carried out without requiring any modulation stage. The goal of this control scheme is to determine the optimum switching state of the inverter, which generates the smallest amount of tracking error with respect to the load reference and optimizes the switching frequency of neutral leg. The optimal switching state will be applied in the next commutation. The FCS-MPC is easy to be implemented and can include additional constraints and nonlinearity in the controller design easily (J. Rodriguez et al., 2013; Scoltock, Geyer, & Madawala, 2015b; Yaramasu et al., 2014). The FCS-MPC algorithm predicts the control variables based on system model acquiring high computational burden in the controller (Rivera, Yaramasu, Llor, et al., 2013; Yaramasu et al., 2013). Apart from the high computational load, FCS-MPC also has higher total harmonic distortion and the ripple content in the current reduces the power

quality as compared to the modulation-based controller at same switching frequency (Akter, Mekhilef, Tan, & Akagi, 2016). In order to improve the inverter output voltage quality and reference tracking with less THD, two-step prediction horizon has been implemented to the four-leg inverter (Yaramasu, Wu, Rivera, Rodriguez, & Wilson, 2012). It has no modulator and inner control loop but the computational burden is increased due to apply two predictions in each switching state. Therefore, several researches have been accomplished to minimize the computational burden in order to obtain better performance in neutral-point-clamped (NPC) multilevel inverter (Barros & Silva, 2008; Barros, Silva, & Jesus, 2013). In (Pozo-Palma & Pacas, 2013, 2014), the FCS-MPC concept has been extended with Luenberg observer and Runge-kutta method to obtain the convergence and delay. However, these works are achieved without control parameter variation performance and modulator is also required.

The common mode voltage (CMV) between the load-neutral point and the midpoint of the dc-link capacitors of the three-phase four-leg inverter causes the drawback in the electromagnetic interference. The mitigation of CMV can be made by hardware improvement such as transistors, capacitors, passive components (Hedayati, Acharya, & John, 2013), common mode filter can be also employed (Tallam, Skibinski, Shudarek, & Lukaszewski, 2011), but modification of hardware is costly, size consuming and complexity. An alternative approach is to modify the algorithm to mitigate CMV at no extra cost. The PWM based algorithm can be incorporated to reduce the CMV as well as to reduce the ripple content in the load current. Therefore, pulse width modulation improvement strategies for the CMV mitigation are established using carrier waves and adjusting the switching vectors (Huang & Shi, 2014) (Hava & Ün, 2011). The algorithm based on near state PWM, NS-3D-SVM are also found to limit the CMV though this can be applicable only in a restricted modulation index (Un & Hava, 2009; M. Zhang, Atkinson, Ji, Armstrong, & Ma, 2014).

The FCS-MPC method can reduce the CMV and control the load current of three-phase three leg inverter mentioned in (Hoseini, Adabi, & Sheikholeslami, 2014; Kwak & Mun, 2015; Vazquez et al., 2014). In (Kwak & Mun, 2015), load current ripple and CMV can be reduced but the selection of two non-zero voltage vector in each sampling period and the determination of each vector duration is very complex. This increases the calculation complexity also. The authors in (Guo, Zhang, Yang, Xie, & Cao, 2016) proposed utilizing four non-zero voltage vector to reduce CMV in every sampling cycle for three-phase three leg inverter. In (L. Guo et al., 2016), the CMV can be confined within $\pm \frac{V_{dc}}{6}$ but the complexity of selecting switching action between opposite voltage vectors increases the switching losses. CMV factor in the cost function is introduced to reduce the CMV though this increases the ripple content in the load current (Xiliang et al., 2016). The work on CMV mitigation with a reduced computational burden for a three-phase four-leg inverter is infrequent. Therefore, further work for this topology is required.

1.3 Problem Statement

The mentioned research problem of energy conversion from PV energy can be achieved using a three-phase four-leg inverter for standalone application. Three-phase four-leg inverter is employed to provide balanced, unbalanced and non-linear load. The main target of this research is to improve the performance of a three-phase four-leg inverter for energy conversion by ensuring the system stability with the dynamic response.

Due to additional leg, the control state increases from 8 (2^3) to 16 (2^4) which increases the number of switching action in every switching period. Furthermore, the fourth leg has to operate at higher switching frequency due to control the zero-sequence voltage/current and it causes higher switching loss (Jose & Patricio, 2012a; Yaramasu et al., 2013; Yaramasu, Wu, Rivera, & Rodriguez, 2012). Therefore, the control perfection, flexibility

and improvement in quality of the inverter load current can be achieved. In order to reduce losses, size and cost in PV energy conversion system, transformer-less inverter is introduced though there has a drawback of the common mode voltage (CMV). In the application of a three-phase four-leg inverter, the drawback of CMV is responsible for the electromagnetic interference, system loss increase, which can affect the other electronic equipment from its usual functionality (Duran, Riveros, Barrero, Guzman, & Prieto, 2012; Kerekes, Teodorescu, Liserre, Klumpner, & Sumner, 2009; Wang, Xiong, Huang, Yao, & Hu, 2008).

There are a number of control methods to operate the power inverters. FCS-MPC is one of them and this control scheme is very interesting due to simple concept, inclusion of non-linearity and constraints with no modulation stage. In spite of these advantages, the FCS-MPC faces the high computational burden due to utilize all available voltage vectors of power inverter to predict the future voltage vector and it is increased with the number of voltage vector.

In this research, Lyapunov function-based model predictive control (L-MPC) is proposed for a three-phase four-leg inverter to optimize computational burden, current reference tracking error and current THD. Near state voltage vector selection-based model predictive control (NSV-MPC) is also proposed to reduce common mode voltage (CMV) with reduced computational burden for a three-phase four-leg inverter. The impact of CMV based on the proposed switching combination and introducing CMV weighting factor in the cost function are also investigated.

1.4 Objectives

1. To propose a Lyapunov function-based model predictive control (L-MPC) and near state voltage vector selection-based model predictive control (NSV-MPC) for a three-phase four-leg inverter.

2. To analyze the reduction of computational burden, current reference tracking, total harmonic distortion and the mitigation of the common mode voltage of a three-phase four-leg inverter.
3. To develop an experimental prototype in a scaled-down laboratory using LabVIEW FPGA platform to validate the effectiveness of the proposed control methods.

1.5 Outlines of the Research

The research outline is presented into six chapters and the work through each chapter is carried out as follows:

Chapter 1: An overview of research background is presented along with the significance to the field study. This chapter describes the scope and motivation behind the research and also presents the research problems. It also finds out the research objectives and therefore, this chapter provides the structure of the dissertation outline.

Chapter 2: This chapter reviews the state of art power inverters and its control techniques employed in the photo-voltaic energy conversion. Thus, this presents the different type of power inverters and the current literature of their control techniques.

Chapter 3: This chapter describes the working principle and mathematical modelling of a three-phase four-leg inverter. The Lyapunov function-based model predictive control technique is proposed for a three-phase four-leg inverter to reduce the computational burden, reference tracking and current ripple content. This chapter also proposes near state vector-based model predictive control for the three-phase four-leg inverter to mitigate the common mode voltage with a reduced computational burden.

Chapter 4: The simulation and experimental results are presented and discussed to verify the feasibility of the proposed control techniques.

Chapter 5: This chapter presents the analysis of system stability using the direct Lyapunov function with the help of backstepping control. Comparative assessment of performance has also presented.

Chapter 6: The main contributions of this research progress report are summarized. Possible extensions for the future work in this research area are suggested.

University of Malaya

CHAPTER 2: STATE OF ART: INVERTER TOPOLOGY AND CONTROL TECHNIQUE

2.1 Introduction

Photo-voltaic energy conversion systems have been widely used in standalone applications to ensure the reliable power distribution. Standalone system is required to provide balanced, unbalanced, linear and non-linear load for uneven load distribution. In modern era, researches are going not only on power inverters improvement but also improvement of the control techniques to ensure the power reliability. Therefore, power inverters and their control technique have been becoming more significant part of the PV energy conversion systems. The arrangement of semi-conductor devices and their proper turn on-off play a crucial role in the research area of energy conversion. In this chapter, a brief literature review on power inverters and their control techniques are explained. An overview of classical control and digital control such as deadbeat, hysteresis, trajectory, and model based predictive controls are discussed.

2.2 Power Inverter Types

Power inverters are used for different applications from industry to resident in a diverse sector such as industrial, transportation, renewable energies, power systems and residential (Bose, 2000). Owing to increasing demand and environmental concern, the application of power inverters has been increasing in the renewable energy conversion system over recent years. Photovoltaic energy system among the different renewable energy sources is a very attractive source of power inverter applications due to deliver power from PV panel to standalone systems. PV system composed of a dc-dc converter for optimal operation of PV panel and an inverter to deliver power to the standalone. Power inverters are made with power semi-conductor devices and for proper operation, it requires some additional elements such as input /output filters, transformer and cooling system for the switching devices.

The power converters can be four main types such as DC-DC, DC-AC, AC-DC, and AC-AC power converters and all these converters are classified in different sub-categories illustrated in Figure 2.1.

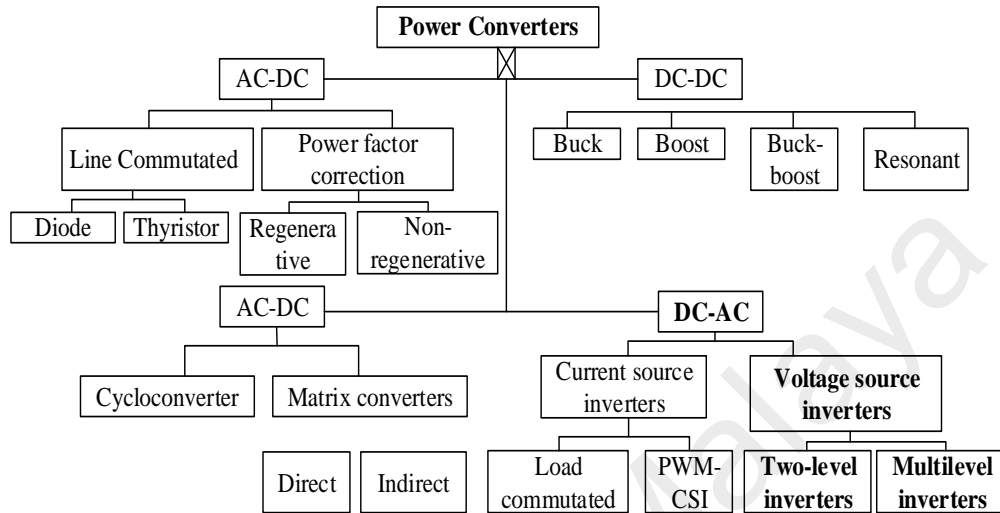


Figure 2.1: Power converter classification (J. Rodriguez & P. Cortes, 2012)

2.2.1 DC to AC Inverter Topology

There are many types of dc-ac voltage source inverter topology and all applications require different specifications to adapt the most appropriate topology and the control techniques. The most commonly used dc-ac inverter is three-phase three-leg inverter in the application of utility grid (Trinh, F. H, & Wang, 2017), standalone power distribution (Jung et al., 2014). Three-phase three level NPC inverter is also very popular in those applications (Calle-Prado et al., 2015). However, those inverter topologies cannot be applicable in some applications where the single phase non-linear load connected or unbalanced loading condition can be happened. In such an application three-phase four-leg inverter topology is the appropriate solution to provide an unbalanced load through the neutral leg (Chen, Luo, Zhang, & Quan, 2017; Rivera, Yaramasu, Llor, et al., 2013).

2.2.2 Comparison of Inverters

The key components of the dc-ac inverter are summarized in Table 2.1. It is clear that there has some compact inverter with low and medium complexity (Mohd et al., 2010; Ortjohann, Mohd, Hamsic, & Lingemann, 2009) (Hurng-Liahng, Jinn-Chang, Kuen-Der, Wen-Jung, & Yi-Hsun, 2005; Jou, Wu, Wu, & Chiang, 2008) but there has no neutral current flowing path. Therefore, these inverters cannot be applicable for some specific application where a neutral path is required. On the other hand, the inverter having neutral paths (Maheshwari, Munk-Nielsen, & Busquets-Monge, 2013) (Rivera, Rodriguez, Yaramasu, & Wu, 2012; Rojas et al., 2017) but these inverters are bulky and high computationally complexity.

Table 2.1: Comparison of dc-ac power inverters

Topology	No. of dc-link capacitor	No. of power switches	No. of Switching state	Zero sequence path	Computational complexity	Size and volume
Split dc-link topology(Mohd et al., 2010; Ortjohann et al., 2009)	2	6	8	No	Medium	Compact
Zigzag transformer(Hurng-Liahng et al., 2005; Jou et al., 2008)	1	6	8	No	Low	Bulky
Four-leg topology(Rivera, Yaramasu, Llor, et al., 2013; M. Zhang et al., 2014)	2	12	16	Yes	High	Compact
NPC inverter(Maheshwari et al., 2013)	2	12	27	No	High	Bulky
Three-phase three-leg inverter (Uddin, Mekhilef, & Rivera, 2015)	1	6	8	No	Low	Very compact
Four-leg NPC inverter(Rivera et al., 2012; Rojas et al., 2017)	2	16	81	Yes	Very High	Bulky
H-Bridge Inverter(Cortes, Wilson, Kouro, Rodriguez, & Abu-Rub, 2010)	6	24	125	No	Very high	Bulky

2.3 Control Techniques of Power Inverter

The improvement of control techniques is an ongoing research topic for the power inverters to comply with control requirements. At present, control requirements are not only associated with the dynamic performance and system stability but also requires technical specifications, constraints and in some cases regulations and codes. The operating limits and conditions are not only dealt with hardware but also with addressing control systems. Hence, the tendency is being focused on more advanced control techniques. The most established control techniques commonly used to be summarized in Figure 2.2.

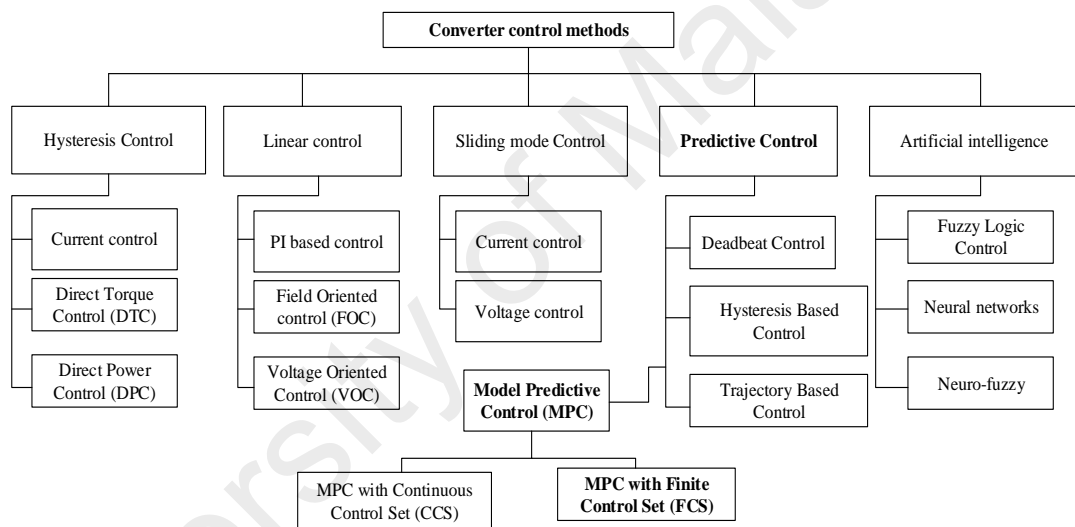


Figure 2.2: Different types of converter control technique for power converters

Hysteresis control and linear control are included in classical control techniques widely accepted by the power inverters. The classical control techniques use the proportional integral (PI) regulators and pulse width/ space vector modulation (PWM/SVM) (Nguyen, Nguyen, & Prasad, 2016). The switching frequency is fixed using classical control techniques with PWM/SVM. Thus, the requirement of optimum switching loss can be fulfilled using lower switching operation at MW-level. Hysteresis control of power inverters includes nonlinear nature and the switching states of

semiconductor devices depend on the error between the measured variable and the reference. This control technique can be used as a current control in simple application and used as direct torque control (DTC) (Basri & Mekhilef, 2016; Xia, Wang, Wang, & Shi, 2016) and direct power control (DPC) in complex applications (Scoltock, Geyer, & Madawala, 2015a; Z. Song, Tian, Yan, & Chen, 2016). This control requires high switching frequency to implement in digital platforms and in some applications, resonance problems arise due to variable switching frequency for nonlinearity of the systems. Thus, expensive and bulky filters are required to control the switching frequency. Linear controller such as PI controller-based modulation stage is the common choice for the power inverters. Field oriented control (FOC) for motor drives based on linear controller and voltage oriented control (VOC) for grid-connected inverters to control current based on the same concept can be applied (Druant, Belie, Sergeant, & Melkebeek, 2016) (Kadri, Gaubert, & Champenois, 2011). The modulation stage used in linear control requires additional coordinate transformation and the performance of this technique is uneven during dynamic range for nonlinear applications.

Sliding mode control, intelligent control and predictive control are included in advanced control techniques based on digital control platforms. Sliding mode control presents the system robustness and considers the switching nature of the power inverters. Fuzzy logic is perfectly applied where the system model or some of its parameters are unknown. At last, the others control techniques are explained in the literature such as neural networks, neuro fuzzy (Ghate & Dudul, 2011). The digital control technique is improving so fast for developing powerful microprocessor and becoming popular due to low-cost and high computational power. Among these control techniques, the predictive control is an alternative and interesting control technique for the control of power inverters. The predictive control (PC) includes hysteresis based, trajectory-based control, deadbeat-based control, and model based predictive control.

2.4 Predictive Control

The predictive control has an emerged control technique for the process control during the 1970s in the oil and chemical industries (Garcia, Prett, & Morari, 1989) (Morari & Lee, 1999). The predictive control utilizes the predictive model to predict the future behavior of a system. The optimal control action is generated using these predictions. The application of predictive control is an interesting research topic in power electronic due to the evolution of DSPs and FPGAs required for fast processing. Different types of predictive control technique are shown in Figure 2.3.

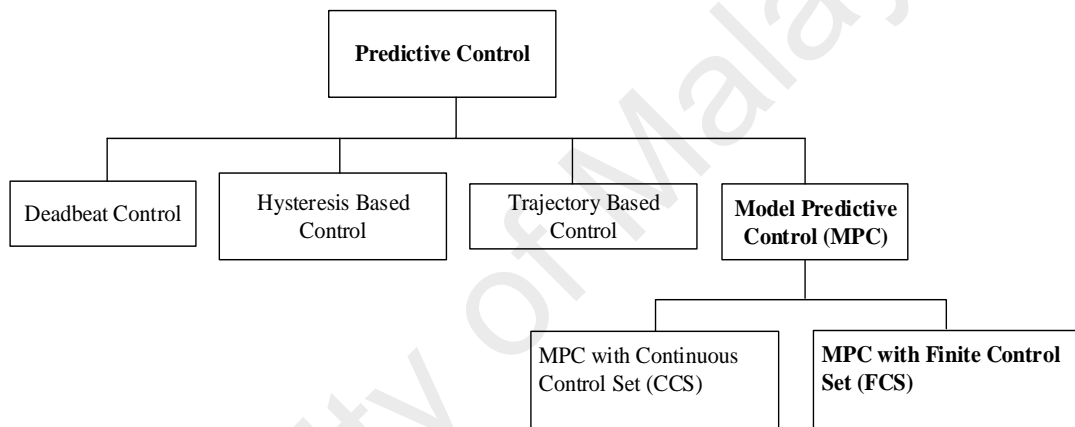


Figure 2.3: Classification of predictive control methods used in power electronics (Cortes, Kazmierkowski, Kennel, Quevedo, & Rodriguez, 2008).

2.4.1 Deadbeat Predictive Control

Deadbeat predictive control is a well-known control system that uses the system model to predict the voltage which makes the error zero in every sampling time. Then a modulation stage is used to apply this predicted voltage to generate the switching signal. A deadbeat control technique uses the predictive controller instead of PI regulators to make the tracking error towards to zero (Alexandrou, Adamopoulos, & Kladas, 2016; W. Song, Ma, Zhou, & Feng, 2016). This controller generates the suitable reference voltage in each sampling period to achieve the desired tracking error. A PWM or SVM modulator is used to generate the control signals to fire the switch of the power inverter. The

perturbation and parameter variation of the systems deteriorate the control performance though the transient response of this control is better compared to classical control. Moreover, this controller excludes the nonlinearity and constraints of the system (Dora & Madhulita, 2013). The parameter's modelling error, fragile and un-modeled delays deteriorate the system performance and cause instability (Bibian & Jin, 2002; Rossiter, 2003). Deadbeat control overall block diagram is shown in Figure 2.4.

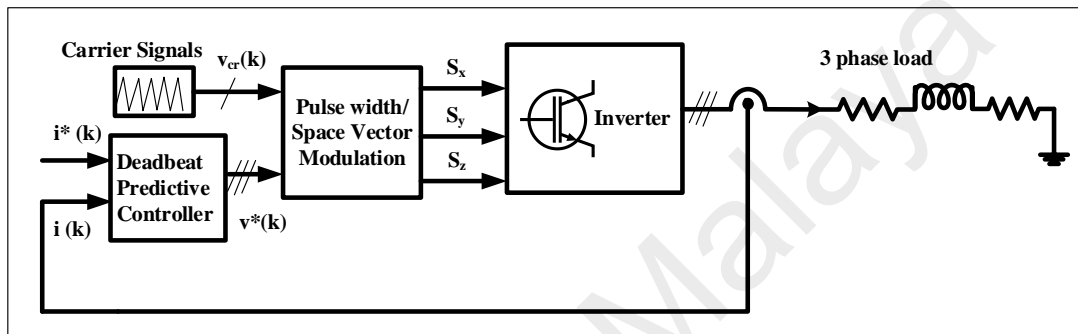


Figure 2.4: Deadbeat predictive control with RL load.

2.4.2 Hysteresis Based Predictive Control

The hysteresis based predictive control maintain the optimization criterion of controlled variable within the boundaries of a hysteresis area (Nauman & Hasan, 2016). This control techniques combine the hysteresis with predictive controller and operates at variable switching frequency. The predictive controller determines the switching states in an appropriate error boundary. When the reference vector reaches at the predefined hysteresis boundary, the next control switching vector is activated using prediction and optimization (Sonawane, Gawande, Kadwane, & Ramteke, 2016; X. Zhang, Wang, Yu, Guo, & Cao, 2016).

2.4.3 Trajectory Based Predictive Control

Trajectory based predictive controller combines the slide mode controller with predictive controller and operates at variable switching frequency. Direct mean torque control and direct self-control are also introduced according to trajectory based predictive control. This control technique forces the control variable of the system to flow a predefined trajectory (Gao & Hu, 2010; Morales-Caporal & Pacas, 2008).

2.4.4 Model Based Predictive Control

Model predictive control (MPC) based on model of the system to represent the future behavior of control variables. MPC is successfully used in industrial application especially chemical process industry from 1970 and the application of MPC in power electronics has been found from the 1980 (Garcia et al., 1989) (Morari & Lee, 1999). The concepts of MPC are very intuitive and easy to implement to a wide variety of systems. The inclusion of non-linearity's and constraints can be easily addressed with MPC and based on specific application, modifications and extensions can be included. A cost function makes the optimal actuation that represents the desired future behavior of the system. The operation principle of MPC is summarized in Figure 2.5. The cost function minimizes the error between the actual and desired variables and this sequence is repeated each sampling period. The whole process considering the new measured data is applied repeatedly for each sampling instant.

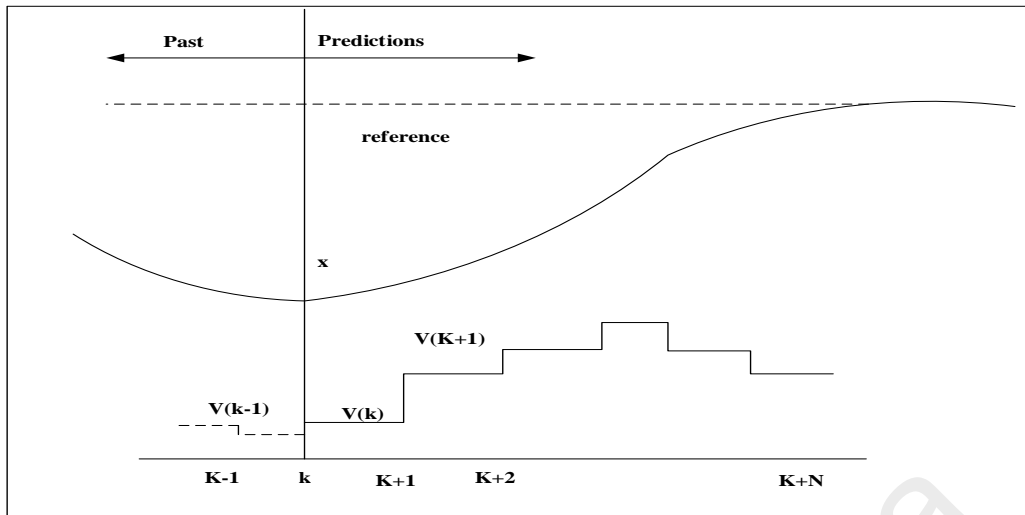


Figure 2.5: Working principle of MPC

2.5 Finite Control Set Model Predictive Control

Recently, Finite control set model predictive control (FCS-MPC) technique is a promising and an intuitive alternative to control the power inverters (Tomlinson, Mouton, Kennel, & Stolze, 2016; Trabelsi, Bayhan, Ghazi, Abu-Rub, & Ben-Brahim, 2016). The FCS-MPC is a non-linear control based discrete model of the system and is employed without modulation stage and linear regulators shown in Figure 2.6.

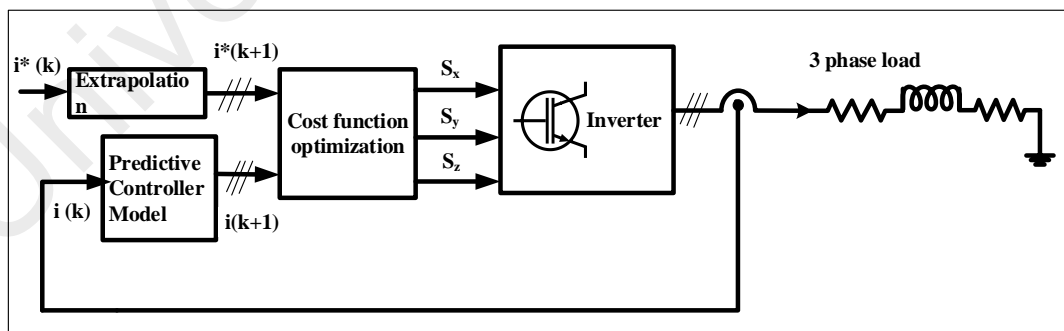


Figure 2.6: Finite control set model predictive control technique

The design and operation of the control technique can be incorporated with the inclusion of constraints and technical requirements in a straight-forward manner. The real behavior of a system to be controlled is needed to design an efficient FCS-MPC controller. A power inverter exhibits the following constraints, properties, and requirements (Kouro, Cortés, Vargas, Ammann, & Rodríguez, 2009; Jose Rodriguez & Patricio Cortes, 2012):

- a) Finite number of switching states, an example for three-phase four-leg VSI, 16 switching states are available.
- b) The maximum current, efficiency, switching loss, tracking error restriction for safe and reliable operation.
- c) Nonlinearity during low switching frequency.
- d) Digital control plat-forms favors discrete time implementation especially in industrial application.

FCS-MPC can easily be applied to power inverters, power quality applications drives and energy storage systems (J. Rodriguez et al., 2013). The main challenges of the FCS-MPC are brief as follows:

- a) Expensive computational burden required
- b) The variable switching frequency operation
- c) The weighting factors selection is not analytical or numerical.
- d) The prediction horizon and modelling of the system affect the control performance.

All these control challenges are investigated in this research and many control solutions have been settled to focus the FCS-MPC technique as the high-performance tool in the next generation.

2.6 Comparison of Inverter Control Techniques

The performance criteria listed in Table 2.2 compare between the existing controls techniques with alternative solutions. Model predictive control shows the best trade-off in terms of inclusion constraints and non-linearity, model-based control without modulation stage. However, the high computational burden of the model predictive control scheme is a possible downside, which means it can be the focus of future research.

Table 2.2: Comparison of control techniques

Control Technique	Control algorithm	Modulation stage	Switching frequency	Constraints and non-linearity	Computational Complexity
Deadbeat predictive control (Alexandrou et al., 2016; W. Song et al., 2016).	Model and PWM based	Needs a modulator	Fixed	Cannot be included	Low
hysteresis predictive control (Sonawane et al., 2016; X. Zhang et al., 2016)	hysteresis based	No modulator	Variable	Included	Moderate
Trajectory predictive controller(Gao & Hu, 2010; Morales-Caporal & Pacas, 2008)	Trajectory based	No modulator	Variable	Included	High
Model predictive control (Tomlinson et al., 2016; Trabelsi et al., 2016)	Model based	No modulator	Variable/Fixed	Included	High
3D-SVM control (Mohd et al., 2010; Ortjohann et al., 2009)	3D-SVM	Needs a modulator	Fixed	Cannot be included	moderate
PWM control (Hurng-Liahng et al., 2005; Jou et al., 2008)	PI-PWM	Needs a modulator	Fixed	Cannot be included	Moderate

2.7 Summary

In this chapter, the review of power inverter topology and their different control techniques has been summarized and followed by the different predictive control techniques explanation. It is clear that the finite control set model predictive control (FCS-MPC) is an interesting digital control technique among these new control techniques. The concept of FCS-MPC has improved over last ten years though its general concept was introduced five decades ago. The operating principle and implementation procedure of FCS-MPC has also explained. In recent years, the rapid growths of innovations are published more than previous. Still there has much more research work in this area that can be done. The challenging issue such as computational burden reduction, improvement of control algorithm, common mode voltage mitigation, and system performance has been presented in details.

CHAPTER 3: DESCRIPTION OF THE INVERTER TOPOLOGY AND THE PROPOSED CONTROL TECHNIQUES

3.1 Introduction

The objective of this research is to propose the Lyapunov model predictive control technique as well as the near state vector selection-based model predictive control technique in the application of a three-phase four-leg inverter. The proposed techniques are applied to this application to improve the system performance, reduce the computational burden, mitigate common mode voltage, and to ensure the system stability. Therefore, this chapter describes the topology with configuration and working principle for dc-ac conversion and also develops a mathematical model for the proposed control techniques. Finite control set model predictive control (FCS-MPC) concept is extended to Lyapunov function based MPC, which has fast controlling with reduced calculation, optimized current tracking error, enhanced system performance and better power quality. Lyapunov function-based model predictive control (L-MPC) technique is applied to three-phase four-leg inverter with RL load. Near state vector selection-based model predictive control is also proposed to the three-phase four-leg inverter to mitigate the common mode voltage with a reduced computational burden.

3.2 Three-Phase Four-leg Inverter System

Three-phase four-leg inverter is introduced over a three-phase three-leg inverter to drive the unbalanced load and non-linear loads (Rivera, Yaramasu, Llor, et al., 2013). An imbalance current to deal with zero sequence current drawn from each phase requires an extra neutral connection due to these loads. The three-phase four-leg power inverter topology with an output RL filter is shown in Figure 3.1. An additional fourth leg is connected to the conventional three-phase inverter, which used to control the zero-sequence current. Due to the neutral leg, the number of control signals increased from 8 (2^3) to 16 (2^4) and thus the control complexity is also increased as compared to three-leg

inverter though the neutral inductance reduces the neutral leg switching frequency current ripple (Rivera, Yaramasu, Llor, et al., 2013). The neutral leg inductance L_{fn} has a more substantial effect on the neutral current than the inductance used in the other legs. Therefore, the neutral inductance L_{fn} can reduce the neutral leg switching frequency current ripple. Besides, the neutral inductor limits the fault current during short circuit or unbalanced loading condition (Liu, Liu, & Li, 2013; Pettersson, Salo, & Tuusa, 2005). Hence, the neutral inductance L_{fn} is introduced in the neutral leg. Though the neutral inductor increases the complexity and computational burden neutral inductor is employed to reduce the THD in neutral current (Bayhan, Abu-Rub, & Balog, 2016; R. Zhang, Prasad, Boroyevich, & Lee, 2002). Neutral inductance L_{fn} is connected through RL filter for the practical applications.

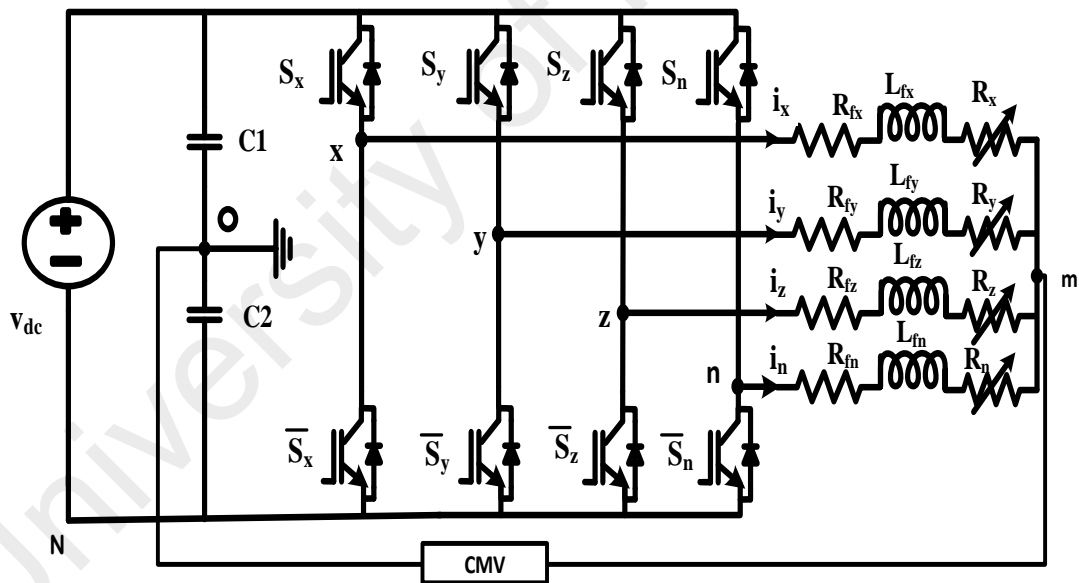


Figure 3.1: Three-phase four-leg inverter topology

3.2.1 Common Mode Voltage Model

The paired IGBT switch in each of the four-legs is turned on and turned off in a complementary mode. If the upper switch of a leg is turned on, the lower one is turned

off and vice versa. The common mode voltage (CMV) is the potential difference between the midpoint of the dc-link capacitors and the load neutral point (v_{mo}) for three-phase four-leg inverter as shown Figure 3.1. The relation of CMV and the voltages with respect to the center of the dc-link can be expressed as (Yaramasu et al., 2015):

$$V_{mo} = \frac{V_{xo} + V_{yo} + V_{zo} + V_{no}}{4} \quad (3.1)$$

The phase voltages based on switching state can have either $+\frac{V_{dc}}{2}$ or $-\frac{V_{dc}}{2}$ voltages level. Therefore, depending on 16 switching state of the three-phase four-leg inverter, the CMV has the value among $\pm \frac{V_{dc}}{2}$, 0 , and $\pm \frac{V_{dc}}{4}$. Based on the relationship of CMV with voltage switching vectors, the 16 switching states are adopted by calculating the CMV using equation (3.1) are presented in Table 3.1. In Table 3.1, p and n are written for 1 and 0 respectively such as pppp=1111 and nnnn=0000.

Table 3.1: Common-Mode Voltage Level with Different Switching States

	pppp	nnnp	pnp	ppnp	nnp	nppp	nnpp	pnpp
V_{xo}	$\frac{V_{dc}}{2}$	$-\frac{V_{dc}}{2}$	$\frac{V_{dc}}{2}$	$\frac{V_{dc}}{2}$	$-\frac{V_{dc}}{2}$	$-\frac{V_{dc}}{2}$	$-\frac{V_{dc}}{2}$	$\frac{V_{dc}}{2}$
V_{yo}	$\frac{V_{dc}}{2}$	$-\frac{V_{dc}}{2}$	$-\frac{V_{dc}}{2}$	$\frac{V_{dc}}{2}$	$\frac{V_{dc}}{2}$	$\frac{V_{dc}}{2}$	$-\frac{V_{dc}}{2}$	$-\frac{V_{dc}}{2}$
V_{zo}	$\frac{V_{dc}}{2}$	$-\frac{V_{dc}}{2}$	$-\frac{V_{dc}}{2}$	$-\frac{V_{dc}}{2}$	$-\frac{V_{dc}}{2}$	$\frac{V_{dc}}{2}$	$\frac{V_{dc}}{2}$	$\frac{V_{dc}}{2}$
V_{fo}	$\frac{V_{dc}}{2}$	$\frac{V_{dc}}{2}$	$\frac{V_{dc}}{2}$	$-\frac{V_{dc}}{2}$	$\frac{V_{dc}}{2}$	$\frac{V_{dc}}{2}$	$\frac{V_{dc}}{2}$	$\frac{V_{dc}}{2}$
V_{mo}	$\frac{V_{dc}}{2}$	$\frac{V_{dc}}{4}$	0	$\frac{V_{dc}}{4}$	0	$\frac{V_{dc}}{4}$	0	$\frac{V_{dc}}{4}$
	pppn	nnnn	pnnn	ppnn	nppn	nppn	nnpn	pnpn
V_{xo}	$\frac{V_{dc}}{2}$	$-\frac{V_{dc}}{2}$	$\frac{V_{dc}}{2}$	$\frac{V_{dc}}{2}$	$-\frac{V_{dc}}{2}$	$-\frac{V_{dc}}{2}$	$-\frac{V_{dc}}{2}$	$\frac{V_{dc}}{2}$
V_{yo}	$\frac{V_{dc}}{2}$	$-\frac{V_{dc}}{2}$	$-\frac{V_{dc}}{2}$	$\frac{V_{dc}}{2}$	$\frac{V_{dc}}{2}$	$\frac{V_{dc}}{2}$	$-\frac{V_{dc}}{2}$	$-\frac{V_{dc}}{2}$
V_{zo}	$\frac{V_{dc}}{2}$	$-\frac{V_{dc}}{2}$	$-\frac{V_{dc}}{2}$	$-\frac{V_{dc}}{2}$	$-\frac{V_{dc}}{2}$	$\frac{V_{dc}}{2}$	$\frac{V_{dc}}{2}$	$\frac{V_{dc}}{2}$
V_{fo}	$-\frac{V_{dc}}{2}$							
V_{mo}	$\frac{V_{dc}}{4}$	$-\frac{V_{dc}}{2}$	$-\frac{V_{dc}}{4}$	0	$-\frac{V_{dc}}{4}$	0	$-\frac{V_{dc}}{4}$	0

3.2.2 Mathematical Model

The paired switch in each of the four-legs is activated in a complementary mode. The voltage applied to the RL filter referring to Figure 3.1 can be written as:

$$\begin{bmatrix} v_{xn} \\ v_{yn} \\ v_{zn} \end{bmatrix} = \begin{bmatrix} S_x - S_n \\ S_y - S_n \\ S_z - S_n \end{bmatrix} * v_{dc} \quad (3.2)$$

Table 3.2 summarizes the allowable inverter-switching states.

Table 3.2: Allowable inverter-switching states

	S_x	S_y	S_z	S_n	v_{xn}	v_{yn}	v_{zn}
1	1	1	1	1	0	0	0
2	1	1	1	0	v_{dc}	v_{dc}	v_{dc}
3	1	1	0	1	0	0	$-v_{dc}$
4	1	1	0	0	v_{dc}	v_{dc}	0
5	1	0	1	1	0	$-v_{dc}$	0
6	1	0	1	0	v_{dc}	0	v_{dc}
7	1	0	0	1	0	$-v_{dc}$	$-v_{dc}$
8	1	0	0	0	v_{dc}	0	0
9	0	1	1	1	$-v_{dc}$	0	0
10	0	1	1	0	0	v_{dc}	v_{dc}
11	0	1	0	1	$-v_{dc}$	0	$-v_{dc}$
12	0	1	0	0	0	v_{dc}	0
13	0	0	1	1	$-v_{dc}$	$-v_{dc}$	0
14	0	0	1	0	0	0	v_{dc}
15	0	0	0	1	$-v_{dc}$	$-v_{dc}$	$-v_{dc}$
16	0	0	0	0	0	0	0

The inverter output voltages according to Kirchoff's voltage law is as follows.

$$\mathbf{v} = (R_f + R)\mathbf{i} + L_f \frac{d\mathbf{i}}{dt} + v_{mN} \quad (3.3)$$

where

$$\mathbf{v} = [v_{xN} \quad v_{yN} \quad v_{zN} \quad v_{nN}]^T$$

$$\mathbf{i} = [i_x \quad i_y \quad i_z \quad i_n]^T$$

$$R_f + R = [R_{fx} + R_x \quad R_{fy} + R_y \quad R_{fz} + R_z \quad R_{fn} + R_n]^T$$

$$L_f = [L_{fx} \quad L_{fy} \quad L_{fz} \quad L_{fn}]^T$$

$$i_n + i_x + i_y + i_z = 0 \quad (3.4)$$

\mathbf{v} is load voltage vector, \mathbf{i} is load vector current, R_f is filter resistance, R is load resistance, L_f is filter inductance and v_{mN} is the voltage between the load neutral and the dc-link negative point (N).

The voltages of each leg from the dc-link negative point (H) can be written as

$$v_{jN} = S_j v_{dc} \quad , j = x, y, z, n \quad (3.5)$$

Where v_{dc} is the dc-link voltage, S_j is switching state of leg j.

The derivative from equation (3.3) can be written in a continuous form in terms of load current vector.

$$\frac{d\mathbf{i}}{dt} = \frac{1}{L_f} [(\mathbf{v} - v_{mN}) - (R_f + R)\mathbf{i}] \quad (3.6)$$

The load neutral voltage (v_{mH}) can be expressed from equation (3.5) and equation (3.6) as

$$v_{mN} = L_{eq} v_{dc} \sum_{k=x,y,z,n} \frac{S_k}{L_{fk}} - L_{eq} \sum_{k=x,y,z,n} \frac{R_{fk} + R_k}{L_{fk}} \mathbf{i}_k \quad (3.7)$$

$$\text{With } L_{eq} = \left(\frac{1}{L_{fx}} + \frac{1}{L_{fy}} + \frac{1}{L_{fz}} + \frac{1}{L_{fn}} \right)^{-1}$$

The state space representation of this system from equation (3.3) as

$$\dot{\mathbf{x}} = \mathbf{Ax} + \mathbf{Bv} \quad \mathbf{y} = \mathbf{Cx} \quad (3.8)$$

$$\text{With } \mathbf{x} = [i_x \quad i_y \quad i_z]^T \text{ and } \mathbf{v} = [v_{xn} \quad v_{yn} \quad v_{zn}]^T$$

Where the coefficients of matrix **A**, **B** and **C** can be calculated according to (Rivera, Yaramasu, Llor, et al., 2013).

$$\mathbf{A} = \begin{bmatrix} a_1 & a_2 & a_3 \\ a_4 & a_5 & a_6 \\ a_7 & a_8 & a_9 \end{bmatrix}$$

Where the coefficients of Matrix A is given below:

$$a_1 = -\frac{R_{fx} + R_x}{L_{fx}} + \frac{L_{eq}}{L_{fx}} \left(\frac{R_{fx} + R_x}{L_{fx}} - \frac{R_{fn} + R_n}{L_{fn}} \right)$$

$$a_2 = \frac{L_{eq}}{L_{fx}} \left(\frac{R_{fy} + R_y}{L_{fy}} - \frac{R_{fn} + R_n}{L_{fn}} \right)$$

$$a_3 = \frac{L_{eq}}{L_{fx}} \left(\frac{R_{fz} + R_z}{L_{fz}} - \frac{R_{fn} + R_n}{L_{fn}} \right)$$

$$a_4 = \frac{L_{eq}}{L_{fy}} \left(\frac{R_{fx} + R_x}{L_{fx}} - \frac{R_{fn} + R_n}{L_{fn}} \right)$$

$$a_5 = -\frac{R_{fy} + R_y}{L_{fy}} + \frac{L_{eq}}{L_{fy}} \left(\frac{R_{fy} + R_y}{L_{fy}} - \frac{R_{fn} + R_n}{L_{fn}} \right)$$

$$a_6 = \frac{L_{eq}}{L_{fy}} \left(\frac{R_{fz} + R_z}{L_{fz}} - \frac{R_{fn} + R_n}{L_{fn}} \right)$$

$$a_7 = \frac{L_{eq}}{L_{fz}} \left(\frac{R_{fx} + R_x}{L_{fx}} - \frac{R_{fn} + R_n}{L_{fn}} \right)$$

$$a_8 = \frac{L_{eq}}{L_{fz}} \left(\frac{R_{fy} + R_y}{L_{fy}} - \frac{R_{fn} + R_n}{L_{fn}} \right)$$

$$a_9 = -\frac{R_{fz} + R_z}{L_{fz}} + \frac{L_{eq}}{L_{fz}} \left(\frac{R_{fz} + R_z}{L_{fz}} - \frac{R_{fn} + R_n}{L_{fn}} \right)$$

Matrix B can be written as

$$\mathbf{B} = \begin{bmatrix} b_1 & b_2 & b_3 \\ b_4 & b_5 & b_6 \\ b_7 & b_8 & b_9 \end{bmatrix}$$

Where the coefficients are as follows

$$b_1 = \frac{v_{dc}}{L_{fx}} \left(1 - \frac{L_{eq}}{L_{fx}} \right)$$

$$b_2 = - \frac{v_{dc}}{L_{fx}} \frac{L_{eq}}{L_{fy}}$$

$$b_3 = - \frac{v_{dc}}{L_{fx}} \frac{L_{eq}}{L_{fz}}$$

$$b_4 = - \frac{v_{dc}}{L_{fy}} \frac{L_{eq}}{L_{fx}}$$

$$b_5 = \frac{v_{dc}}{L_{fy}} \left(1 - \frac{L_{eq}}{L_{fy}} \right)$$

$$b_6 = - \frac{v_{dc}}{L_{fy}} \frac{L_{eq}}{L_{fz}}$$

$$b_7 = - \frac{v_{dc}}{L_{fz}} \frac{L_{eq}}{L_{fx}}$$

$$b_8 = - \frac{v_{dc}}{L_{fz}} \frac{L_{eq}}{L_{fy}}$$

$$b_9 = \frac{v_{dc}}{L_{fz}} \left(1 - \frac{L_{eq}}{L_{fz}} \right)$$

And matrix C can be defined as

$$\mathbf{C} = \begin{bmatrix} 1 & 0 & 0 \\ 0 & 1 & 0 \\ 0 & 0 & 1 \end{bmatrix}$$

3.3 Model predictive Control Formulation

The formulation of MPC technique for three-phase four-leg inverter with resistive – inductive load and grid-connected neutral point clamped inverter has explained in the following section. The MPC technique works based on the discrete time model. Therefore, three-phase four-leg inverter requires the transformation from the continuous time model into a discrete time model at a specific sampling time.

3.4 MPC for Three-Phase Four-Leg Inverter

The required steps to develop the formulation of MPC technique consist of discrete time model, predictive model, construct a cost function and voltage vector selection strategy. The three-phase four-leg inverter with the control block diagram is shown in Figure 3.2

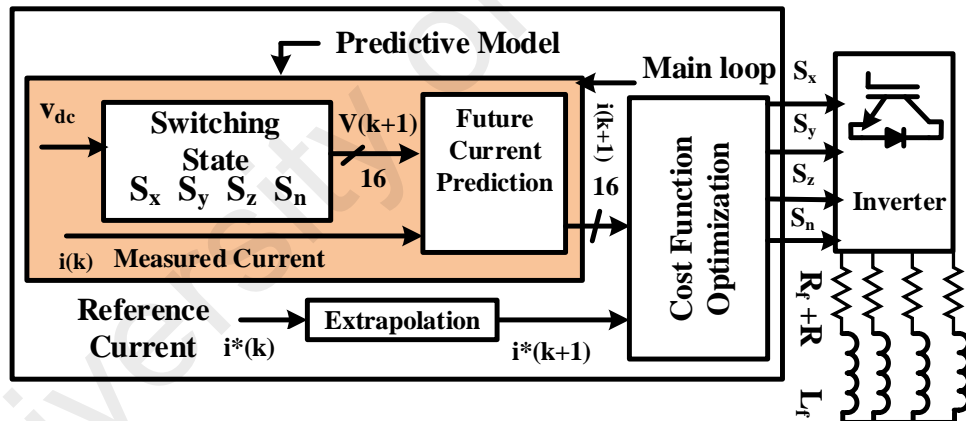


Figure 3.2: MPC control block diagram

3.4.1 Measurements

The predictive model requires the feedback signals. These feedback signals can be voltages, currents, active power and reactive power.

3.4.2 References Generation

Generate the reference control variables $x^*(k)$ based on the specific application. Extrapolate the generated reference of control variable to $(k+1)^{\text{th}}$ instant. The current references are provided by the user at k^{th} instant and then the required extrapolation can be obtained using the following fourth-order Lagrange extrapolation (Yaramasu et al., 2013):

$$\mathbf{i}^*(k+1) = 4\mathbf{i}^*(k) - 6\mathbf{i}^*(k-1) + 4\mathbf{i}^*(k-2) - \mathbf{i}^*(k-3) \quad (3.9)$$

When the sampling period is very small ($T_s < 20 \mu\text{s}$), the extrapolation is not required. In that case, $\mathbf{i}^*(k+1) = \mathbf{i}^*(k)$.

3.4.3 Discrete Time Model

The digital implementation requires a discrete time model to predict the future current's value at sampling interval (k) . The values of the state x at times k^{th} and $(k+1)^{\text{th}}$ instant can be calculated using the solution of (3.8). These are

$$x((k+1)T_s) = e^{A(k+1)T_s}x(0) + e^{A(k+1)T_s} \int_0^{(k+1)T_s} e^{-A\tau} Bv(\tau) d\tau \quad (3.10)$$

$$x(kT_s) = e^{AkT_s}x(0) + e^{AkT_s} \int_0^{kT_s} e^{-A\tau} Bv(\tau) d\tau \quad (3.11)$$

multiply all terms of equation (3.11) by e^{AT_s} to solve for $e^{A(k+1)T_s}x(0)$, obtaining

$$x(kT_s)e^{AT_s} = e^{AkT_s}x(0)e^{AT_s} + e^{AkT_s}e^{AT_s} \int_0^{kT_s} e^{-A\tau} Bv(\tau) d\tau \quad (3.12)$$

$$\text{or, } e^{A(k+1)T_s}x(0) = e^{AT_s}x(kT_s) - e^{A(k+1)T_s} \int_0^{kT_s} e^{-A\tau} Bv(\tau) d\tau \quad (3.13)$$

from (3.8),

$$x((k+1)T_s) = e^{AT_s}x(kT_s) - e^{A(k+1)T_s} \int_0^{kT_s} e^{-A\tau} Bv(\tau) d\tau + e^{A(k+1)T_s} \int_0^{(k+1)T_s} e^{-A\tau} Bv(\tau) d\tau \quad (3.14)$$

$$\text{or, } x((k+1)T_s) = e^{AT_s}x(kT_s) + e^{A(k+1)T_s} [\int_0^{(k+1)T_s} e^{-A\tau} Bv(\tau) d\tau - \int_0^{kT_s} e^{-A\tau} Bv(\tau) d\tau] \quad (3.15)$$

which, by linearity of integration, is equivalent to

$$x((k+1)T_s) = e^{AT_s}x(kT_s) + e^{A(k+1)T_s} [\int_{kT_s}^{(k+1)T_s} e^{-A\tau} Bv(\tau) d\tau]$$

$$x((k+1)T_s) = e^{AT_s}x(kT_s) + e^{A(k+1)T_s} [\int_{kT_s}^{(k+1)T_s} e^{-A\tau} Bv(k+1)T_s d\tau]$$

$$x((k+1)T_s) = e^{AT_s}x(kT_s) + [\int_{kT_s}^{(k+1)T_s} e^{A[(k+1)T_s-\tau]} Bv(k+1)T_s d\tau]$$

$$x((k+1)T_s) = e^{AT_s}x(kT_s) - [\int_{T_s}^0 e^{A\lambda} d\lambda Bv(k+1)T_s]$$

$$x((k+1)T_s) = e^{AT_s}x(kT_s) + [\int_0^{T_s} e^{A\lambda} d\lambda Bv(k+1)T_s] \quad (3.16)$$

3.4.4 Predictive Model

The control variables have to track the reference. The values of inverter output current \mathbf{i} at k^{th} and $(k+1)^{\text{th}}$ instant with sampling time T_s can be calculated using the solution of (3.8) as

$$\mathbf{i}((k+1)T_s) = e^{A(k+1)T_s}\mathbf{i}(0) + e^{A(k+1)T_s} \int_0^{(k+1)T_s} e^{-A\tau} Bv(\tau) d\tau \quad (3.17)$$

$$\mathbf{i}(kT_s) = e^{AkT_s}\mathbf{i}(0) + e^{AkT_s} \int_0^{kT_s} e^{-A\tau} Bv(\tau) d\tau \quad (3.18)$$

After solving $\mathbf{i}((k + 1)T_s)$ from equation (3.17), (3.18) and then changing the variable of integration, the following equation (3.19) can be obtained.

$$\mathbf{i}((k + 1)T_s) = e^{AT_s}\mathbf{i}(kT_s) + A^{-1}(\mathbf{P} - \mathbf{I}_{3 \times 3})\mathbf{B} \mathbf{v}(k + 1)T_s] \quad (3.19)$$

The output current can be expressed at $(k+1)^{\text{th}}$ sample from equation (3.19).

$$\mathbf{i}(k+1) = \mathbf{P}\mathbf{i}(k) + \mathbf{Q}\mathbf{v}(k+1) \quad (3.20)$$

$$\text{Where } \mathbf{P} = e^{AT_s}$$

$$\mathbf{Q} = \int_0^T e^{A\lambda} d\lambda \mathbf{B}$$

$$= \mathbf{A}^{-1} \int_0^T \mathbf{A} e^{A\lambda} d\lambda \mathbf{B}$$

$$= \mathbf{A}^{-1} e^{A\lambda} \Big|_{\lambda=0}^T \mathbf{B}$$

$$= \mathbf{A}^{-1} (e^{AT} - \mathbf{I}) \mathbf{B}$$

$$\mathbf{Q} = \mathbf{A}^{-1} (\mathbf{P} - \mathbf{I}_{3 \times 3}) \mathbf{B}$$

The identity matrix $\mathbf{I}_{3 \times 3}$ and Matrices \mathbf{P} and \mathbf{Q} are to be calculated offline using MATLAB. The load current and dc-link voltage are required to predict the output current.

3.4.5 Cost Function

Each predicted future current value is compared with respective reference in a natural frame to select the optimal switching state by the predefined cost function at the next step by using the following equation:

$$\begin{aligned}
g_a(k+1) &= |\mathbf{i}^*(k+1) - \mathbf{i}(k+1)| \\
&= |i_x^*(k+1) - i_x(k+1)| + |i_y^*(k+1) - i_y(k+1)| + |i_z^*(k+1) - i_z(k+1)| \quad (3.21)
\end{aligned}$$

When the error g_a is zero, the output current equals to its reference. The fourth leg has to change the switching state according to the switching state changes of three phases in order to control the zero-sequence current. Hence, the changing rate of switching state in the fourth leg is higher and it operates at higher switching frequency as compared to the average switching frequency. Therefore, the switching loss of the fourth leg is higher. In order to compensate the neutral leg switching frequency, it's constrained has been included in the cost function, as follows.

$$g_b(k+1) = w_{swc} * swc_n \quad (3.22)$$

Where w_{swc} is the weighting factor related to the switching frequency reduction. The guidelines of weighting factor selection have given but still this is an open research topic (Uddin et al., 2015) The number of switching in fourth leg can be achieved as follows (Jose & Patricio, 2012a).

$$swc_n = |S_n(k+1) - S_n(k_{opt})| \quad (3.23)$$

Where $S_n(k+1)$ is the predicted neutral leg gate signal and $S_n(k_{opt})$ is the optimal gate signal in the previous sample, k . The objective of equation (3.13) is to force the predicted switching signal to remain at the same signal as the previous state. The additional term equation (3.23) must be accomplished in order to improve the performance regarding reference tracking and switching loss, hence w_{swc} is considered to prioritize the objectives empirically. Then, the cost function can be expressed as follows:

$$g(k+1) = g_a(k+1) + g_b(k+1) \quad (3.24)$$

The objective of this cost function is to optimize the error close to zero of load current vectors.

3.4.6 Adding CMV Weighting Factor in the Cost Function

The CMV factor is introduced for three-phase three-leg inverter in (Xiliang et al., 2016). The cost function in equation (3.24) is developed with the term of current tracking and fourth leg switching issue. The CMV factor can be added with these terms to mitigate the common mode interference. Then, the cost function can be written as

$$g(k + 1) = g_a(k + 1) + g_b(k + 1) + w_{cmv} * f_v \quad (3.25)$$

Where w_{cmv} the weighting factor related to CMV term and f_v refers to the peak value function of CMV for every switching voltage vector. The calculated value of CMV using equation (3.1) can be considered the maximum limit of CMV value. The addition term in the cost function is combined with current reference tracking term, which can fulfil the current reference tracking as well as the mitigation of CMV.

3.4.7 Vector Selection Strategy

The conventional model predictive control technique utilizes all the 16 voltage vectors of a three-phase four-leg inverter to improve the predictive current control performance. The common mode voltage (CMV) is expensive owing to utilize all available vectors. The expression from Table 3.1, it is clear that the CMV depends upon the selection of switching state. The basic principle of mitigating CMV is to use only active vectors because of the highest peak value of CMV caused by utilizing zero voltage vectors in switching patterns. As the MPC method is applied based on pre-defined switching state at every sampling period, hence four combinations of switching state of the three-phase four-leg inverter can be preselected according to the peak value of CMV.

1. The most easy and simple switching pattern selection is the cancellation of zero switching state in the predictive model. Therefore, the variation in the amplitude of CMV is confined within $\pm \frac{V_{dc}}{4}$ and the reduction of CMV is 50 % as it is dropped from $\pm \frac{V_{dc}}{2}$.
2. The CMV can be reduced to zero by the inclusion of six switching state in the switching pattern in every sampling period from 16 available switching states.

3.5 L-MPC for Three-Phase Four-Leg Inverter

The L-MPC control method predicts the future load voltage closest to the unique voltage reference generated using Lyapunov control law. At the end of each sampling time, the error optimization between the predicted current and their reference is done by a cost function in terms of the predicted and the future load voltage. The proposed control algorithm generates load reference voltage vector from the measured load current and reference current to achieve efficient reference tracking in Figure 3.3.

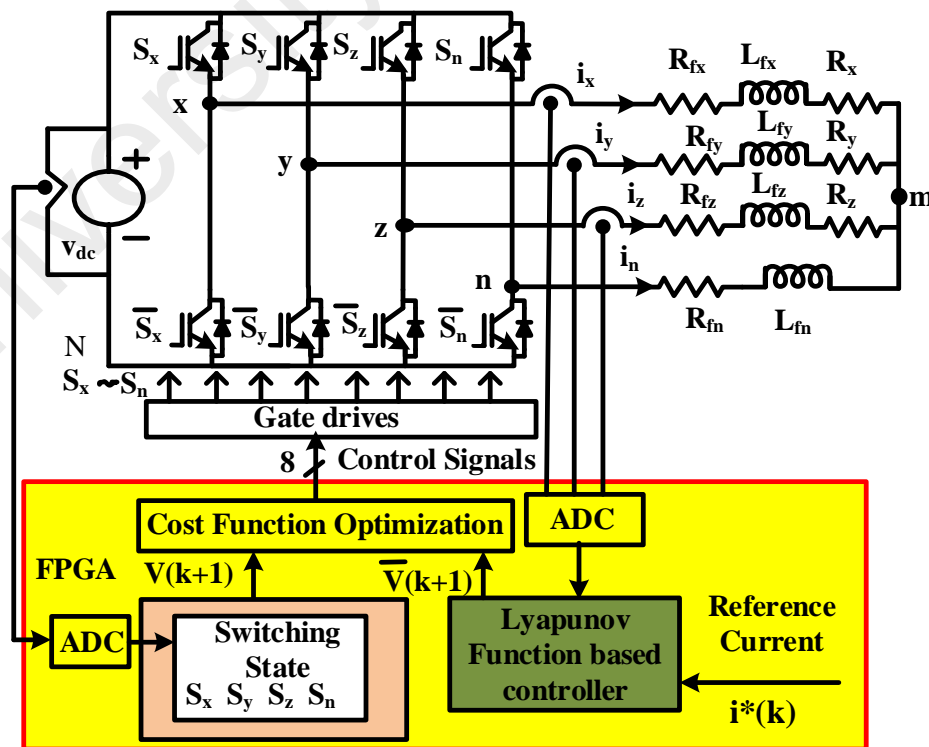


Figure 3.3: L-MPC block diagram with three-phase four-leg inverter

The Lyapunov function-based FCS-MPC uses the Lyapunov model equations just once in each control loop to obtain the inverter output vector by optimizing the error between generated ideal vector and predefined available vector of the inverter. Lyapunov model predictive control (L-MPC) directly applies the voltage vector based on predefined switching state. The inverter output voltage vector constrained with continuous voltage and the unavoidable quantization error vector as follows.

$$\mathbf{v}(k+1) = \bar{\mathbf{v}}(k+1) + \delta(k+1) \quad (3.26)$$

Where $\bar{\mathbf{v}}(k+1)$ are the continuous inverter output voltages, bounded by the finite set and $\delta(k+1)$ is the quantization error.

The L-MPC to modify the C-MPC is necessary for the analysis of three-phase the four-leg inverter with control parameter changes. Therefore, the future current error at the $(k+1)$ th sampling instant in the discrete-time domain is expressed as.

$$\begin{aligned} \mathbf{i}_{er}(k+1) &= \mathbf{i}(k+1) - \mathbf{i}^*(k+1) \\ \mathbf{i}_{er}(k+1) &= \mathbf{P}\mathbf{i}(k) + \mathbf{Q}\mathbf{v}(k+1) - \mathbf{i}^*(k+1) \end{aligned} \quad (3.27)$$

where, $\mathbf{i}^*(k+1)$ is the future reference current vector. In order to ensure the current $\mathbf{i}(k+1)$ is able to track the reference value $\mathbf{i}^*(k+1)$, a productive control algorithm is required for the four-leg inverter. The L-MPC algorithm is fit to this specific purpose. Therefore, a control function is necessary for converging the current tracking error \mathbf{i}_{er} to zero asymptotically.

Taking the discrete Lyapunov function positively as

$$LF\{\mathbf{i}_{er}(k)\} = \frac{1}{2}\{\mathbf{i}_{er}(k)\}^T\{\mathbf{i}_{er}(k)\} \quad (3.28)$$

The rate of change of Lyapunov function from equation (3.27) and equation (3.28) can be expressed as.

$$\begin{aligned}
\nabla \text{LF}\{\mathbf{i}_{er}(k+1)\} &= \text{LF}\{\mathbf{i}_{er}(k+1)\} - \text{LF}\{\mathbf{i}_{er}(k)\} \\
&= \frac{1}{2}\{\mathbf{i}_{er}(k+1)\}^T\{\mathbf{i}_{er}(k+1)\} - \frac{1}{2}\{\mathbf{i}_{er}(k)\}^T\{\mathbf{i}_{er}(k)\} \\
&= \frac{1}{2}\{[\mathbf{P}\mathbf{i}(k) + \mathbf{Q}\mathbf{v}(k+1) - \mathbf{i}^*(k+1)]^T[\mathbf{P}\mathbf{i}(k) + \mathbf{Q}\mathbf{v}(k+1) - \mathbf{i}^*(k+1)]\} \\
&\quad - \frac{1}{2}\{\mathbf{i}_{er}(k)\}^T\{\mathbf{i}_{er}(k)\} \\
&= \frac{1}{2}\{[\mathbf{P}\mathbf{i}(k) + \mathbf{Q}(\bar{\mathbf{v}}(k+1) + \boldsymbol{\delta}(k+1)) - \mathbf{i}^*(k+1)]^T[\mathbf{P}\mathbf{i}(k) + \mathbf{Q}(\bar{\mathbf{v}}(k+1) + \boldsymbol{\delta}(k+1)) - \mathbf{i}^*(k+1)]\} \\
&\quad - \frac{1}{2}\{\mathbf{i}_{er}(k)\}^T\{\mathbf{i}_{er}(k)\} \tag{3.29}
\end{aligned}$$

The rate of change of Lyapunov function (∇LF) always has to be negative in order to converge the tracking error towards zero. Therefore, the future discrete output voltage vector at the next sampling instant assures the rate of change of Lyapunov function equation (3.29) is negative, which can be as follows.

$$\bar{\mathbf{v}}(k+1) = -\frac{\mathbf{P}}{\mathbf{Q}}\mathbf{i}(k) + \frac{1}{\mathbf{Q}}\mathbf{i}^*(k+1) \tag{3.30}$$

In the L-MPC method, the reference voltage vectors are calculated just once in which depend on system parameters and reference currents. This control law with the closed-loop system equation (3.30) is practically exponentially stable in the following compact set.

$$\Lambda = \mathbf{i}_{er} \mid \|\mathbf{i}_{er}\| \leq \mathbf{Q}\sigma \tag{3.31}$$

where σ is the upper bound constant of the quantization error and the quantization error can satisfy $\|\boldsymbol{\delta}(k+1)\| \leq \sigma$ with $\sigma > 0$. In the proposed control system, the Lyapunov

control law equation (3.30) is used in the cost function as a future reference voltage vector $\bar{\mathbf{v}}(k+1)$ to select the closest one of sixteen future voltage vectors. The first part of the cost function defined as follows whereas the second part is same as the conventional model predictive control method.

$$\begin{aligned} g_a(k+1) &= |\bar{\mathbf{v}}(k+1) - \mathbf{v}(k+1)| \\ &= |\bar{v}_{xn}(k+1) - v_{xn}(k+1)| + |\bar{v}_{yn}(k+1) - v_{yn}(k+1)| + |\bar{v}_{zn}(k+1) - v_{zn}(k+1)| \end{aligned} \quad (3.32)$$

Therefore, the optimum future voltage vector of the four-leg inverter is directly selected using Lyapunov control law in a cost function to track the reference vector as.

$$\begin{aligned} g(k+1) &= |\bar{v}_{xn}(k+1) - v_{xn}(k+1)| + |\bar{v}_{yn}(k+1) - v_{yn}(k+1)| + \\ &|\bar{v}_{zn}(k+1) - v_{zn}(k+1)| + w_{swc} * swc_n \end{aligned} \quad (3.33)$$

3.6 Near State Vector Selection Based Model Predictive Control for Three-Phase Four-Leg Inverter

In three - dimensional coordinate system for three-phase four-leg inverter, there is six prisms to express the switching voltage vectors. These prisms can be divided into six sectors from I to VI such that each sector is combined with half of the two-adjacent prism shown in Figure 3.4. The sixteen-voltage vector of the three-phase four-leg inverter can be transformed from abc into $\alpha\beta\gamma$ coordinate using the following transformation in equation (3.34).

$$\mathbf{T} = \begin{bmatrix} \frac{2}{3} & -\frac{1}{3} & -\frac{1}{3} \\ 0 & \frac{1}{\sqrt{3}} & -\frac{1}{\sqrt{3}} \\ \frac{1}{3} & \frac{1}{3} & \frac{1}{3} \end{bmatrix} \quad (3.34)$$

The voltage vector expressed in $\alpha\beta\gamma$ coordinate are shown in Table 3.3.

Table 3.3: The switching states with phase voltages in the $\alpha\beta\gamma$ coordinate

Switching States	Phase voltage in $\alpha\beta\gamma$ coordinate			Switching States	Phase voltage in $\alpha\beta\gamma$ coordinate		
	V_α	V_β	V_γ		V_α	V_β	V_γ
pppp	0	0	0	pppn	0	0	V_{dc}
nnnp	0	0	$-V_{dc}$	nnnn	0	0	0
pnpn	$\frac{2V_{dc}}{3}$	0	$-\frac{2V_{dc}}{3}$	pnnn	$\frac{2V_{dc}}{3}$	0	$\frac{V_{dc}}{3}$
ppnp	$\frac{V_{dc}}{3}$	$\frac{V_{dc}}{\sqrt{3}}$	$-\frac{V_{dc}}{3}$	ppnn	$\frac{V_{dc}}{3}$	$\frac{V_{dc}}{\sqrt{3}}$	$\frac{2V_{dc}}{3}$
npnp	$-\frac{V_{dc}}{3}$	$\frac{V_{dc}}{\sqrt{3}}$	$-\frac{2V_{dc}}{3}$	npnn	$-\frac{V_{dc}}{3}$	$\frac{V_{dc}}{\sqrt{3}}$	$\frac{V_{dc}}{3}$
npnp	$-\frac{2V_{dc}}{3}$	0	$-\frac{V_{dc}}{3}$	nppn	$-\frac{2V_{dc}}{3}$	0	$\frac{2V_{dc}}{3}$
nnpp	$-\frac{V_{dc}}{3}$	$-\frac{V_{dc}}{\sqrt{3}}$	$-\frac{2V_{dc}}{3}$	nnpn	$-\frac{V_{dc}}{3}$	$-\frac{V_{dc}}{\sqrt{3}}$	$\frac{V_{dc}}{3}$
pnpn	$\frac{V_{dc}}{3}$	$-\frac{V_{dc}}{\sqrt{3}}$	$-\frac{V_{dc}}{3}$	pnpn	$\frac{V_{dc}}{3}$	$-\frac{V_{dc}}{\sqrt{3}}$	$\frac{2V_{dc}}{3}$

The projection of the reference vector on the $\alpha\beta$ coordinate is used to determine the sector of reference vector. Two tetrahedron lies in two prisms in each sector. When the reference switching vector is in sector I, four non-zero switching vector are required to synthesize the reference vector in Figure 3.5. In order to minimize ripple and harmonic content in the current, near state switching vectors to the reference vector are addressed and four adjacent switching vectors to the reference vector should be selected. Therefore, two sets of four switching reference vectors are to be selected in each sector. There are six active vectors and two zeros vectors in each sector. In order to reduce CMV and utilize high dc-link voltage, six active switching vectors are selected to synthesize the reference in each sector. Assumed that, the reference voltage vector is located in the sector I on the $\alpha\beta$ plane in $\alpha\beta\gamma$ coordinate. All sector lies on the projection in $\alpha\beta$ coordinate. The first sector is identified between 330° to 30° and similarly, other sectors location according to Figure 3.5. Voltage vector closest to the reference voltage vector is being selected by evaluating the six-active vector using the same predictive model mentioned

in section III. Depending on the cost function in equation (3.14), the optimal voltage vector is being selected among six active vectors.

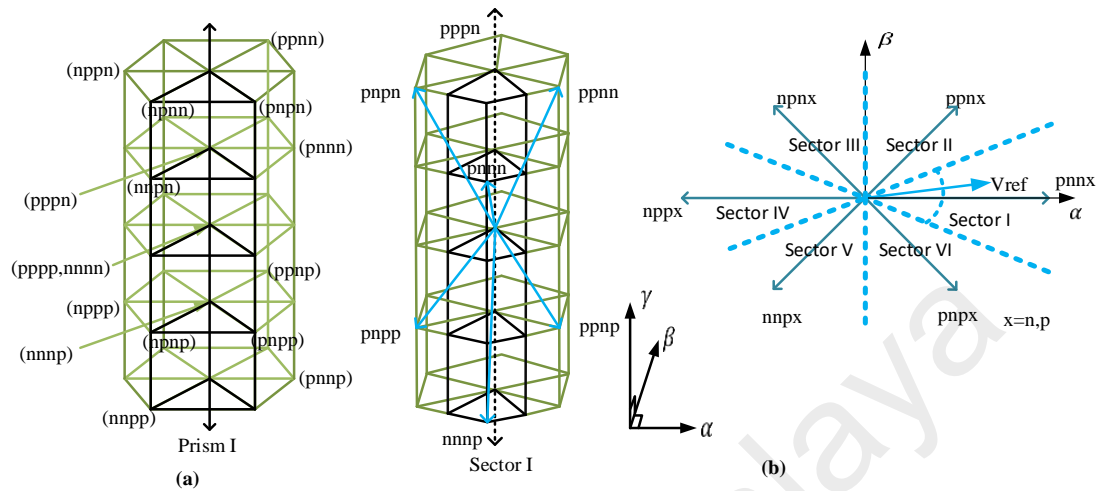


Figure 3.4: (a) Switching vectors and Prisms (b) Projection of sector on the $\alpha\beta$ coordinate

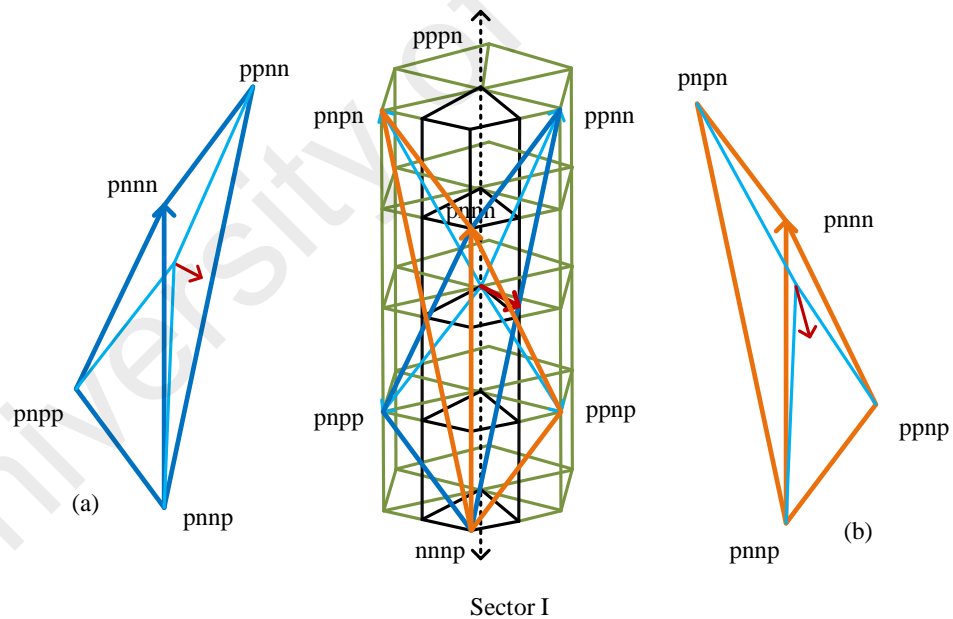


Figure 3.5: Sector identification with near state vector selection

Model predictive control technique based on near state voltage vector is employed to find the closest voltage vector to reduce the error between the desired and reference

currents. The proposed control method predicts the reference vector at every sampling time from the pre-defined sector. Six active vectors among the available 14 active vectors are to be selected surrounding the reference vector based on near state voltage vector illustrated in Table 3.4. The CMV can be confined using only six active vectors within $\pm \frac{V_{dc}}{4}$ with reduced computational burden due to the reduced number of switching state in obtaining the future voltage vector. However, this increases the ripple content marginally in the load current as like conventional MPC. Hence, one zero vector either pppp or nnnn can be considered with six active vectors at each control cycle and this causes the CMV variation between $\pm \frac{V_{dc}}{4}$ and $+\frac{V_{dc}}{2}$ or $-\frac{V_{dc}}{2}$. Therefore, seven voltage vectors are selected for determining the closest voltage vector to reference vector in proposed NSV-MPC whereas the 15 voltage vectors are considered in conventional MPC scheme. Thus, the computational burden is reduced due to the reduction of switching vectors from 16 to 8(considering both zero vectors), 15 to 7 (considering one zero vector) and 14 to 6 (considering only active vectors) in Figure. 3.6. As a result, near state vector based MPC can demonstrate the same performance as conventional MPC with reduced CMV and computational burden.

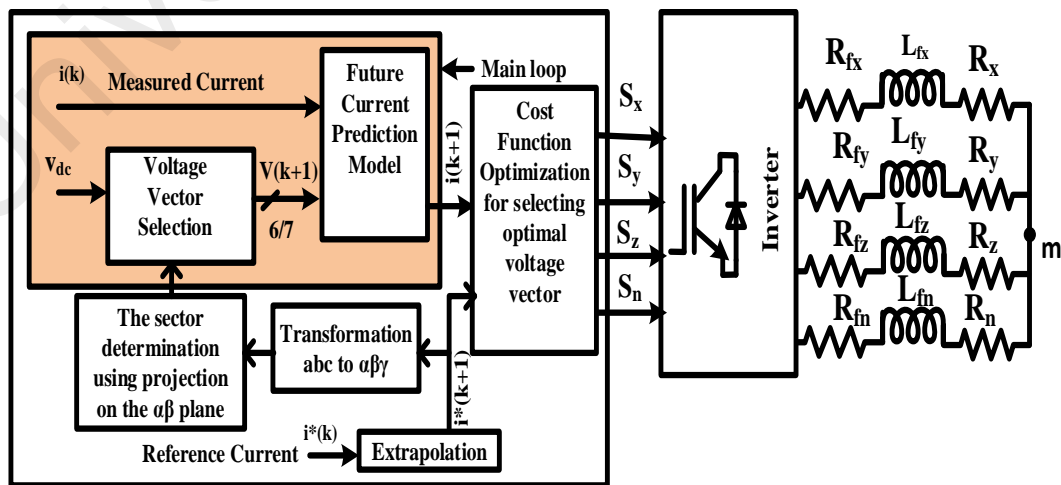


Figure 3.6: Near state vector based MPC block diagram

Table 3.4: CMV for corresponding near state vector of each sector

SECTOR I							SECTOR II						
	$pnpp$	$pnpn$	$pnnn$	$ppnn$	$pnpn$	$ppnp$		$pnpn$	$ppnp$	$pnnn$	$pnnp$	$pnnn$	$pnnp$
V_{xo}	$\frac{V_{dc}}{2}$	$\frac{V_{dc}}{2}$	$\frac{V_{dc}}{2}$	$\frac{V_{dc}}{2}$	$\frac{V_{dc}}{2}$	$\frac{V_{dc}}{2}$	V_{xo}	$\frac{V_{dc}}{2}$	$\frac{V_{dc}}{2}$	$\frac{V_{dc}}{2}$	$-\frac{V_{dc}}{2}$	$\frac{V_{dc}}{2}$	$-\frac{V_{dc}}{2}$
V_{yo}	$-\frac{V_{dc}}{2}$	$-\frac{V_{dc}}{2}$	$-\frac{V_{dc}}{2}$	$\frac{V_{dc}}{2}$	$-\frac{V_{dc}}{2}$	$\frac{V_{dc}}{2}$	V_{yo}	$-\frac{V_{dc}}{2}$	$\frac{V_{dc}}{2}$	$\frac{V_{dc}}{2}$	$\frac{V_{dc}}{2}$	$-\frac{V_{dc}}{2}$	$\frac{V_{dc}}{2}$
V_{zo}	$\frac{V_{dc}}{2}$	$-\frac{V_{dc}}{2}$	$-\frac{V_{dc}}{2}$	$-\frac{V_{dc}}{2}$	$\frac{V_{dc}}{2}$	$-\frac{V_{dc}}{2}$	V_{zo}	$-\frac{V_{dc}}{2}$	$-\frac{V_{dc}}{2}$	$-\frac{V_{dc}}{2}$	$-\frac{V_{dc}}{2}$	$-\frac{V_{dc}}{2}$	$-\frac{V_{dc}}{2}$
V_{no}	$\frac{V_{dc}}{2}$	$\frac{V_{dc}}{2}$	$-\frac{V_{dc}}{2}$	$-\frac{V_{dc}}{2}$	$-\frac{V_{dc}}{2}$	$\frac{V_{dc}}{2}$	V_{no}	$\frac{V_{dc}}{2}$	$\frac{V_{dc}}{2}$	$-\frac{V_{dc}}{2}$	$-\frac{V_{dc}}{2}$	$-\frac{V_{dc}}{2}$	$\frac{V_{dc}}{2}$
V_{mo}	$\frac{V_{dc}}{4}$	0	$-\frac{V_{dc}}{4}$	0	0	$\frac{V_{dc}}{4}$	V_{mo}	0	$\frac{V_{dc}}{4}$	0	$-\frac{V_{dc}}{4}$	$-\frac{V_{dc}}{4}$	0
SECTOR III							SECTOR IV						
	$ppnp$	$npnp$	$npnn$	$nppn$	$ppnn$	$nppp$		$npnp$	$nppp$	$nppn$	$nnpn$	$npnn$	$nnpp$
V_{xo}	$\frac{V_{dc}}{2}$	$-\frac{V_{dc}}{2}$	$-\frac{V_{dc}}{2}$	$-\frac{V_{dc}}{2}$	$\frac{V_{dc}}{2}$	$-\frac{V_{dc}}{2}$	V_{xo}	$-\frac{V_{dc}}{2}$	$-\frac{V_{dc}}{2}$	$-\frac{V_{dc}}{2}$	$-\frac{V_{dc}}{2}$	$-\frac{V_{dc}}{2}$	$-\frac{V_{dc}}{2}$
V_{yo}	$\frac{V_{dc}}{2}$	$\frac{V_{dc}}{2}$	$\frac{V_{dc}}{2}$	$\frac{V_{dc}}{2}$	$\frac{V_{dc}}{2}$	$\frac{V_{dc}}{2}$	V_{yo}	$\frac{V_{dc}}{2}$	$\frac{V_{dc}}{2}$	$\frac{V_{dc}}{2}$	$-\frac{V_{dc}}{2}$	$\frac{V_{dc}}{2}$	$-\frac{V_{dc}}{2}$
V_{zo}	$-\frac{V_{dc}}{2}$	$-\frac{V_{dc}}{2}$	$-\frac{V_{dc}}{2}$	$\frac{V_{dc}}{2}$	$-\frac{V_{dc}}{2}$	$\frac{V_{dc}}{2}$	V_{zo}	$-\frac{V_{dc}}{2}$	$\frac{V_{dc}}{2}$	$\frac{V_{dc}}{2}$	$\frac{V_{dc}}{2}$	$-\frac{V_{dc}}{2}$	$\frac{V_{dc}}{2}$
V_{no}	$\frac{V_{dc}}{2}$	$\frac{V_{dc}}{2}$	$-\frac{V_{dc}}{2}$	$-\frac{V_{dc}}{2}$	$-\frac{V_{dc}}{2}$	$\frac{V_{dc}}{2}$	V_{no}	$\frac{V_{dc}}{2}$	$\frac{V_{dc}}{2}$	$-\frac{V_{dc}}{2}$	$-\frac{V_{dc}}{2}$	$-\frac{V_{dc}}{2}$	$\frac{V_{dc}}{2}$
V_{mo}	$\frac{V_{dc}}{4}$	0	$-\frac{V_{dc}}{4}$	0	0	$\frac{V_{dc}}{4}$	V_{mo}	0	$\frac{V_{dc}}{4}$	0	$-\frac{V_{dc}}{4}$	$-\frac{V_{dc}}{4}$	0
SECTOR V							SECTOR VI						
	$nppp$	$nnpp$	$nnpn$	$pnpn$	$nppn$	$pnpp$		$nnpp$	$pnpp$	$pnpn$	$pnnn$	$nnpn$	$pnpn$
V_{xo}	$-\frac{V_{dc}}{2}$	$-\frac{V_{dc}}{2}$	$-\frac{V_{dc}}{2}$	$\frac{V_{dc}}{2}$	$-\frac{V_{dc}}{2}$	$\frac{V_{dc}}{2}$	V_{xo}	$-\frac{V_{dc}}{2}$	$\frac{V_{dc}}{2}$	$\frac{V_{dc}}{2}$	$\frac{V_{dc}}{2}$	$-\frac{V_{dc}}{2}$	$\frac{V_{dc}}{2}$
V_{yo}	$\frac{V_{dc}}{2}$	$-\frac{V_{dc}}{2}$	$-\frac{V_{dc}}{2}$	$-\frac{V_{dc}}{2}$	$\frac{V_{dc}}{2}$	$-\frac{V_{dc}}{2}$	V_{yo}	$-\frac{V_{dc}}{2}$	$-\frac{V_{dc}}{2}$	$-\frac{V_{dc}}{2}$	$-\frac{V_{dc}}{2}$	$-\frac{V_{dc}}{2}$	$-\frac{V_{dc}}{2}$
V_{zo}	$\frac{V_{dc}}{2}$	$\frac{V_{dc}}{2}$	$\frac{V_{dc}}{2}$	$\frac{V_{dc}}{2}$	$\frac{V_{dc}}{2}$	$\frac{V_{dc}}{2}$	V_{zo}	$\frac{V_{dc}}{2}$	$\frac{V_{dc}}{2}$	$\frac{V_{dc}}{2}$	$-\frac{V_{dc}}{2}$	$-\frac{V_{dc}}{2}$	$-\frac{V_{dc}}{2}$
V_{no}	$\frac{V_{dc}}{2}$	$\frac{V_{dc}}{2}$	$-\frac{V_{dc}}{2}$	$-\frac{V_{dc}}{2}$	$-\frac{V_{dc}}{2}$	$\frac{V_{dc}}{2}$	V_{no}	$-\frac{V_{dc}}{2}$	$\frac{V_{dc}}{2}$	$-\frac{V_{dc}}{2}$	$-\frac{V_{dc}}{2}$	$\frac{V_{dc}}{2}$	$\frac{V_{dc}}{2}$
V_{mo}	$\frac{V_{dc}}{4}$	0	$-\frac{V_{dc}}{4}$	0	0	$\frac{V_{dc}}{4}$	V_{mo}	0	$\frac{V_{dc}}{4}$	0	$-\frac{V_{dc}}{4}$	$-\frac{V_{dc}}{4}$	0

3.7 Summary

The details description of mathematical modeling and working principle of three-phase four-leg inverter has been presented in this chapter. This chapter has also presented common mode voltage modeling of three-phase four-leg inverter. In order to apply Lyapunov function and near state vector selection-based model predictive control technique, voltage vectors structure and their switching state pattern of three-phase four-leg inverter has illustrated. The controller requires these mathematical models to control the power inverter and to increase the system performance, to mitigate the common mode voltage and to ensure the system stability. The finite control set model predictive control (FCS-MPC) technique has been extended based on Lyapunov function for three-phase

four-leg inverter topology and the FCS-MPC technique has also applied based on the near state vector selection for the same topology. The CMV weighting factor is introduced in the cost function and voltage vector pattern selection strategy is also introduced to mitigate common mode voltage of three-phase four-leg inverter. The proposed control techniques have verified theoretically in this chapter. The outcomes using these proposed control algorithms for the application in the three-phase four-leg inverter are discussed in the next chapter.

University of Malaya

CHAPTER 4: RESULT AND DISCUSSION

4.1 Introduction

The theoretical analysis of proposed control techniques described in chapter 3 are verified in this chapter. The verification has been accomplished with simulation as well as experimentally. The control techniques of three-phase four-leg inverter are simulated using MATLAB/Simulink software environment and the LabVIEW Field programmable gate array (FPGA) rapid prototyping controller is used to validate experimentally. LabVIEW FPGA Implementation procedure is briefly discussed in the next section and all simulation and experimental results are discussed in section 4.3.

4.2 LabVIEW FPGA Implementation Procedure

An FPGA project regarding the proposed control technique of three-phase four-leg inverter is created with graphical language for the RIO board in the LabVIEW environment. The displays in the LabVIEW are compatible for the design of control method such as different logic gates, signal generations, math functions, cluster manipulation, array, analog and digital I/O. The algorithm of the control method is designed using the combination of these functions and it is integrated with the FPGA device. The project code of LabVIEW virtual instrument (VI) must be required compilation for the FPGA. The required time for the compilation depends on the complexity of the control algorithm. The LabVIEW executes the project from the development computer as well as access the analog and digital I/O from the device when the target FPGA device is used. A LabVIEW Host VI is created after compilation of the LabVIEW FPGA project code and it is integrated with the hardware for the control system. The project creation and compilation in FPGA is illustrated in Figure 4.1.

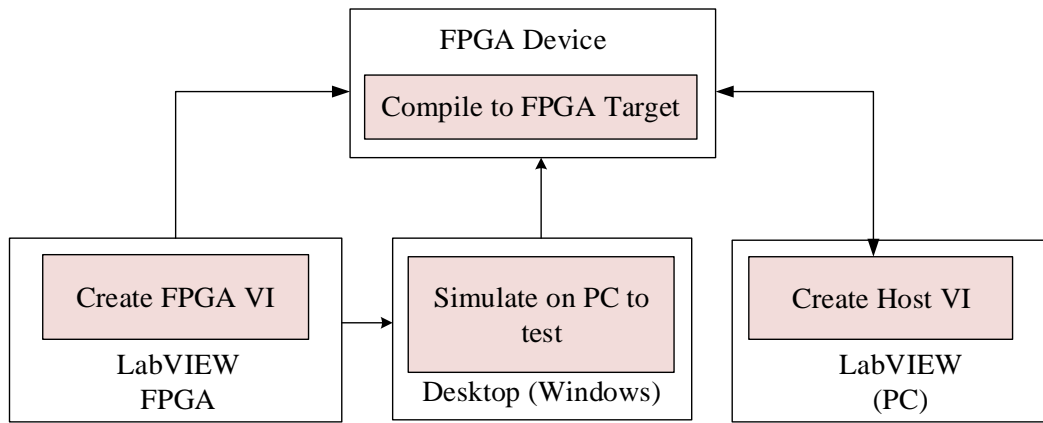


Figure 4.1: Applications development flow with FPGA compilation (Soghoyan, Suleiman, & Akopian, 2014)

The Host VI uses indicators and control and it transfer the data between the host processing unit and FPGA device from the front panel of FPGA VI. The model predictive model demands the feedback load variable to find out the error between the actual and the desired variable. The Figure 4.2 shows the feedback load currents acquiring system using analog input/output port of the FPGA module.

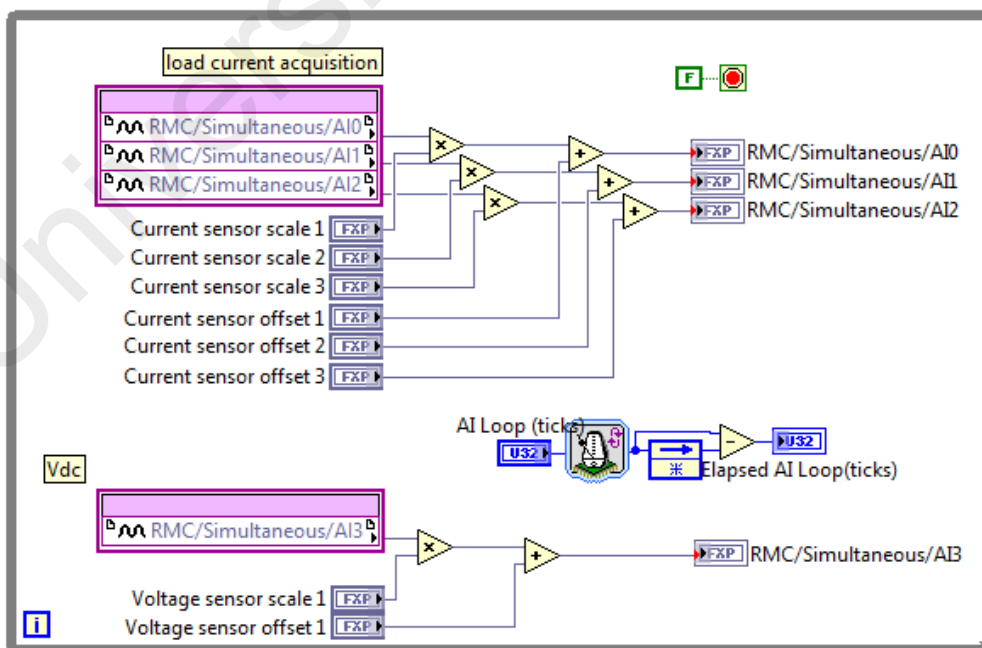


Figure 4.2: Inverter input DC voltage and output load current acquisition

The input DC voltage is also acquired for the predictive model. The current reference is required for the predictive model to compare with measured load current in the cost function. The generation of references are obtained using LabVIEW function blocks illustrated in Figure 4.3.

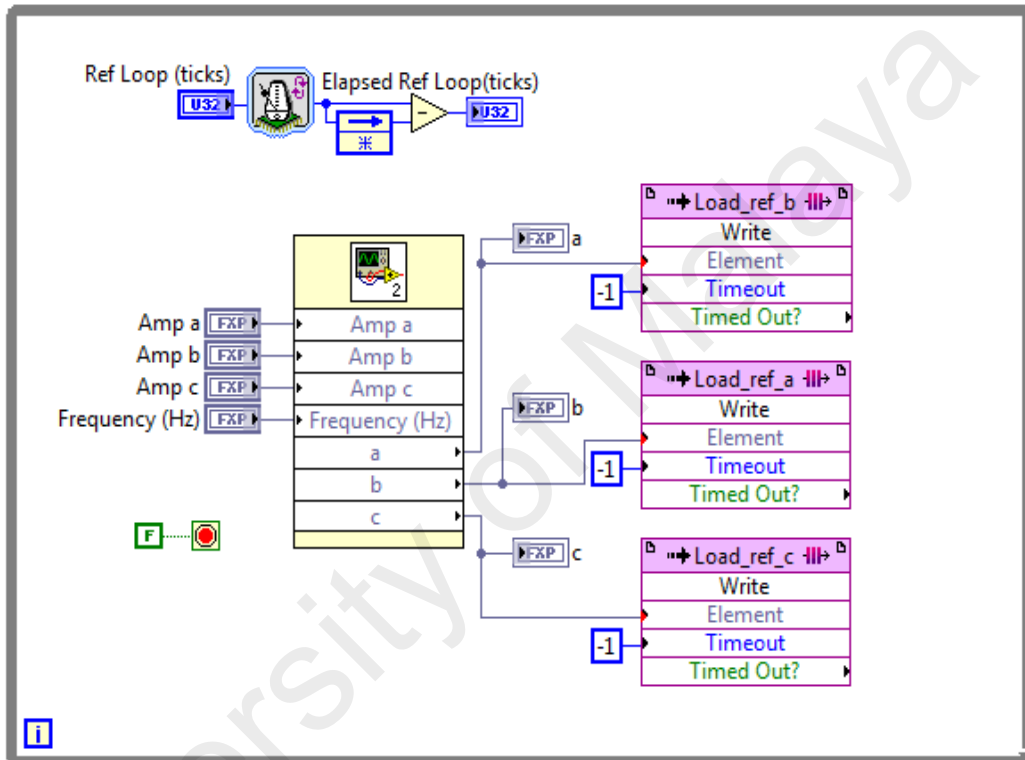


Figure 4.3 Reference current generation for the cost function

The acquisition algorithm has been implemented using graphical language based on LabVIEW functional blocks shown in Figure 4.4. The target LabVIEW FPGA acquisition unit is connected with FIFOs using IP node for communicating with the host VI. The target FPGA module can be connected to host computer through PCI.

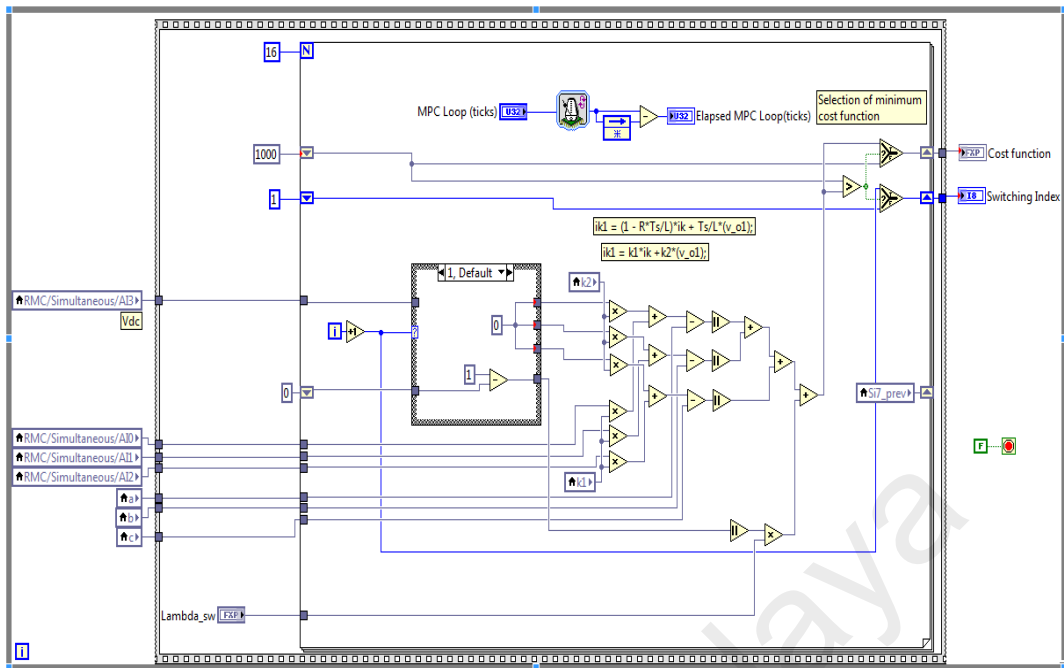


Figure 4.4: Algorithm acquisition using LabVIEW function blocks

4.3 Simulation and Experimental Results Analysis

Simulation results for the proposed controller was carried out in Matlab Simulink presented in this section. The current references are studied with NI LabVIEW FPGA 2015 module interfaced to a host computer. Figure 4.5 depicts the project set up in the laboratory. A National Instrument Single-Board RIO General Purpose Inverter Controller (GPIC) NI-sbRIO9606 with mezzanine card NI 9683 on-board is utilized to acquire analog input and generate the digital control signal output to the gate drive of the inverter. The pre-scaled current sensor LA25NP and voltage transducer LV25N are utilized to acquire appropriate analog signals before sending them to the simultaneous analog input from the GPIC board. The common mode voltage (CMV) is measured using Pintek DP-25 Differential Probe. The three-phase load currents and the CMV are obtained by LeCroy Wave Runner oscilloscope.

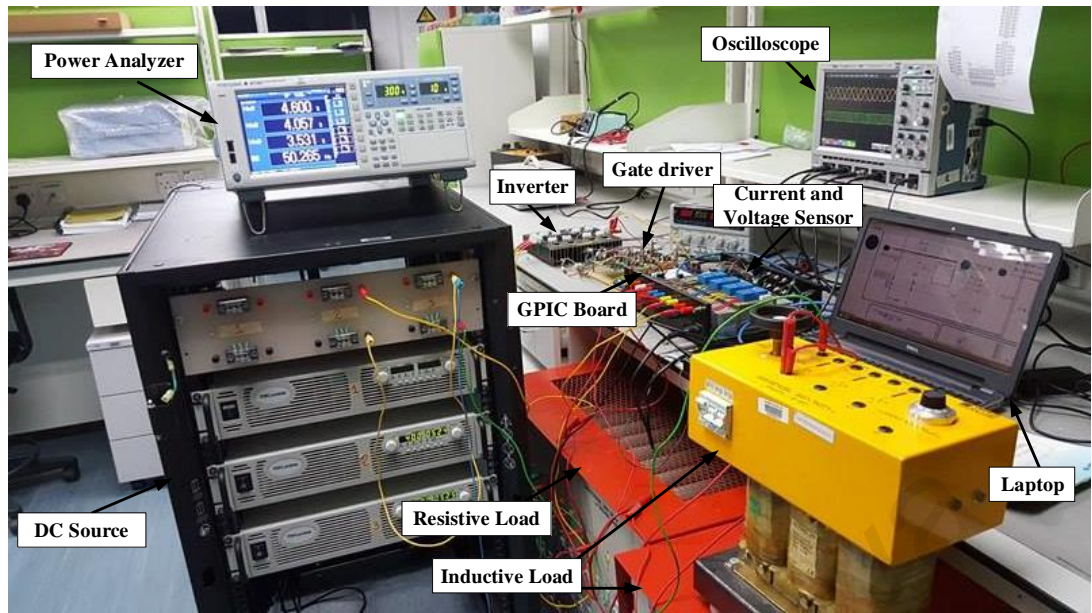


Figure 4.5: Experimental setup in the FPGA platform

4.3.1 MPC with CMV Mitigation of Three-Phase Four-Leg Inverter

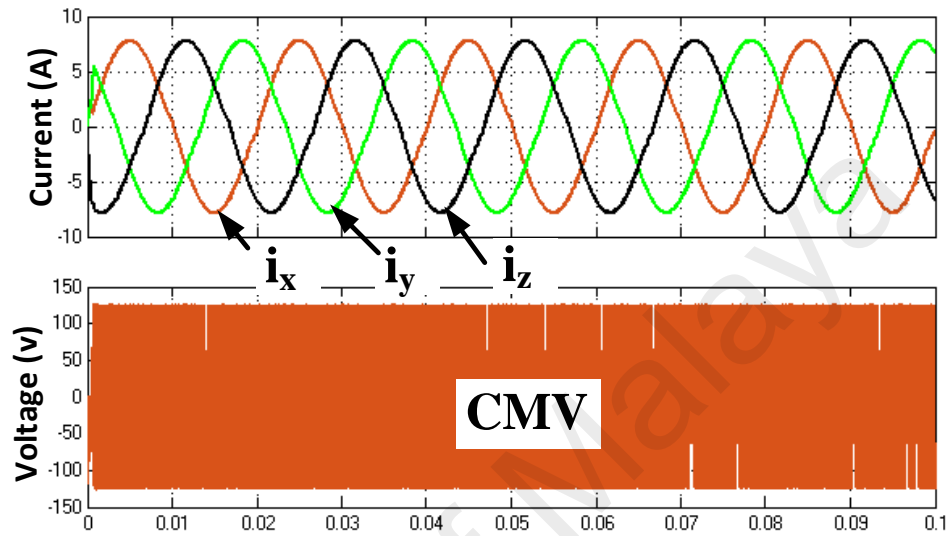
The different vector selection and CMV weighting factor based MPC has been validated with a simulation using Matlab/Simulink and experimentally implemented in a laboratory prototype of three-phase four-leg inverter with the parameters as specified in Table 4.1.

Table 4.1: Parameters of the simulation and experimental results

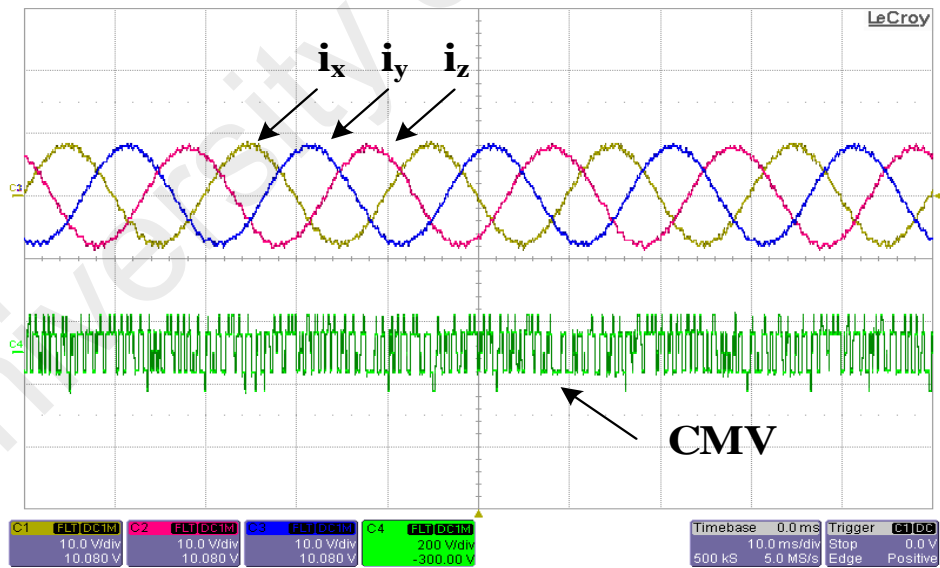
Variable	Parameter	Value
V_{dc}	dc-link voltage	250 V
C	dc-link capacitance	2.2 μ F
L_f	Filter inductance	12 mH
T_s	Sampling Time	50 μ s
R	Load resistance	10 Ω
R_f	Filter resistance	0.1 Ω
f^*	Reference nominal frequency	50 Hz
i^*	Reference nominal peak current	8 A
L_{fn}	Neutral leg inductance	8 mH

1st case: Model predictive control utilizes 16 switching vectors to predict the future reference vector in each control cycle. Hence the common mode voltage is high and

causes large computational burden owing to the high calculation time required to select the desired voltage vector. The peak value of CMV is oscillating between $-\frac{V_{dc}}{2}$ and $+\frac{V_{dc}}{2}$ owing to the use of two zero vectors alternatively in the control algorithm presented in Figure 4.6.



(a)

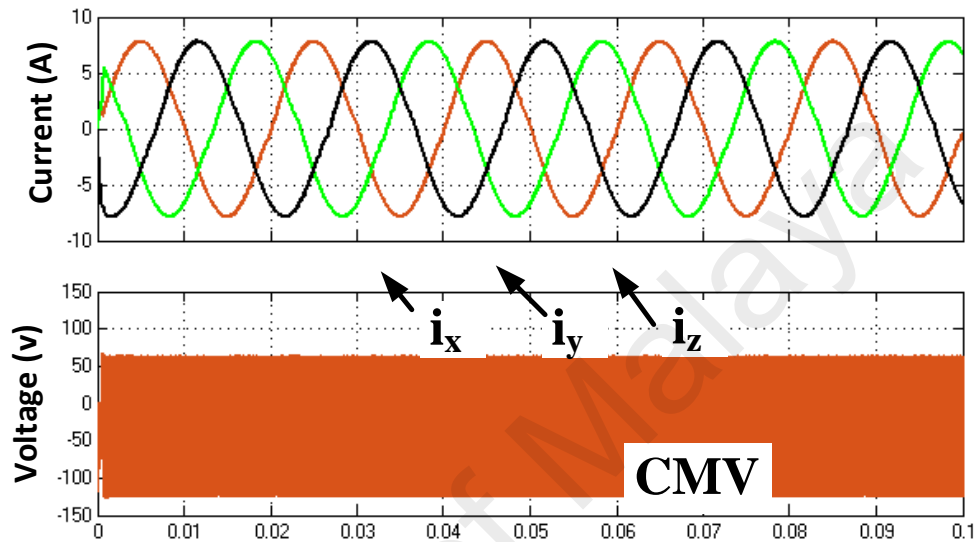


10A/div. 10ms/div.

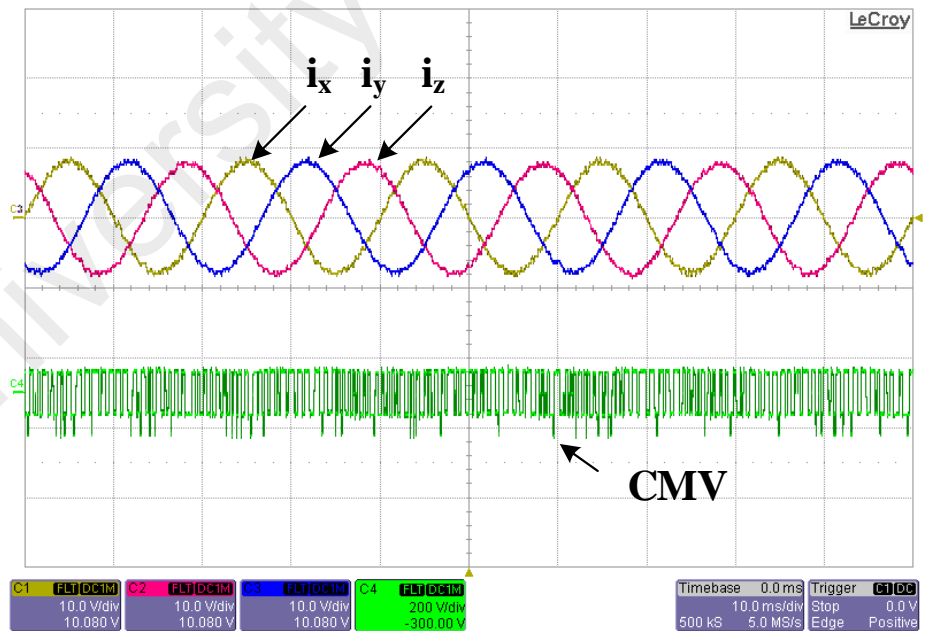
(b)

Figure 4.6: MPC based on all available voltage vector (a) Simulation result (b) Experimental result

2nd case: The MPC scheme can utilize only one zero vector either pppp or nnnn with 14 available active vectors at every sampling time. For this, the one-sided peak value of CMV is reduced and varied between $\frac{V_{dc}}{2}$ and $-\frac{V_{dc}}{6}$ or between $\frac{V_{dc}}{6}$ and $-\frac{V_{dc}}{2}$ respectively due to the use of only one zero vector shown in Figure 4.7 and Figure 4.8 respectively.



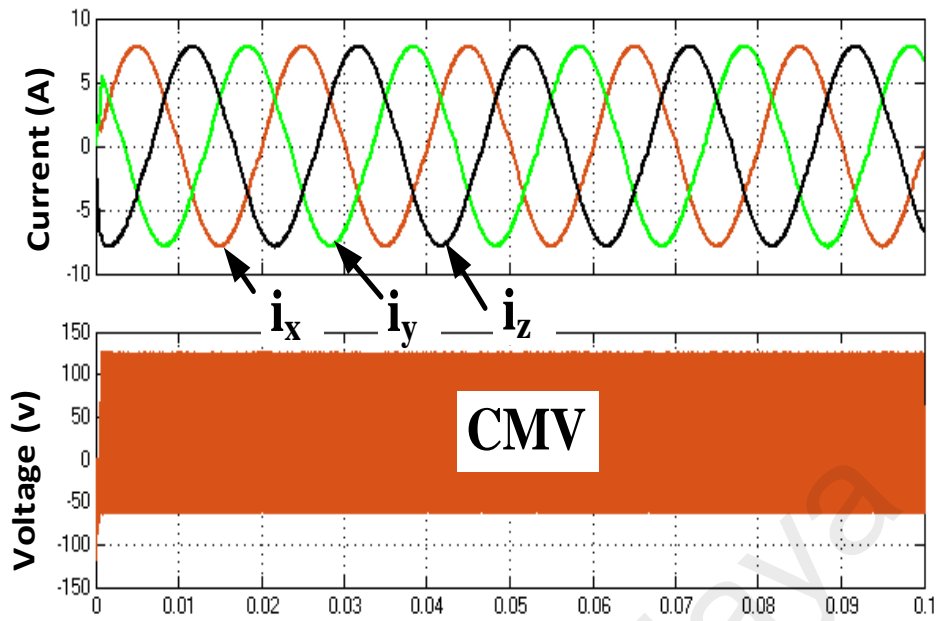
(a)



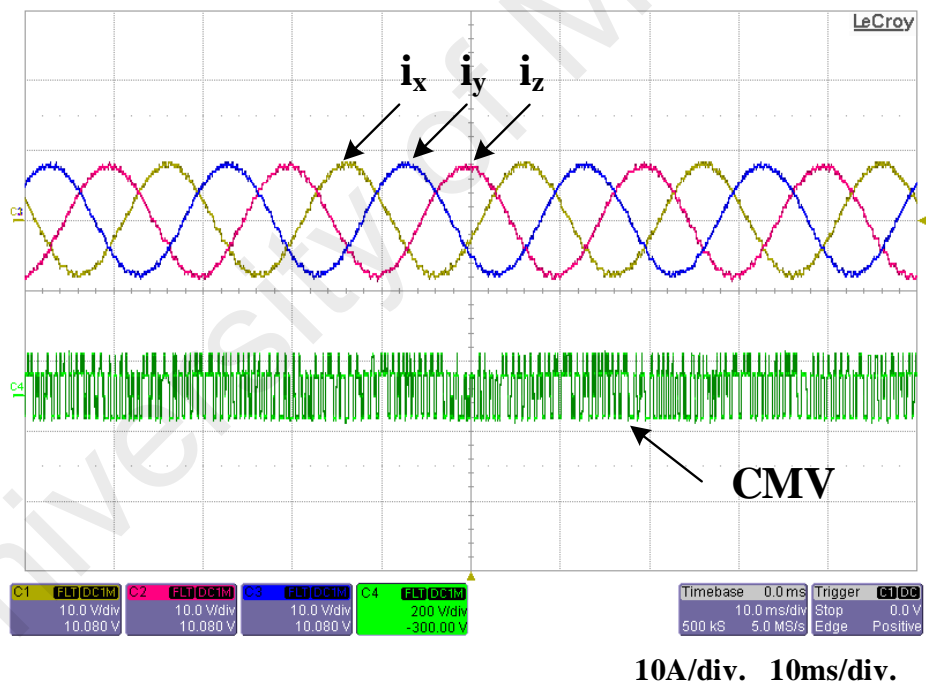
10A/div. 10ms/div.

(b)

Figure 4.7: MPC based on active vectors with one zero (pppp) vector (a) Simulation result (b) Experimental result



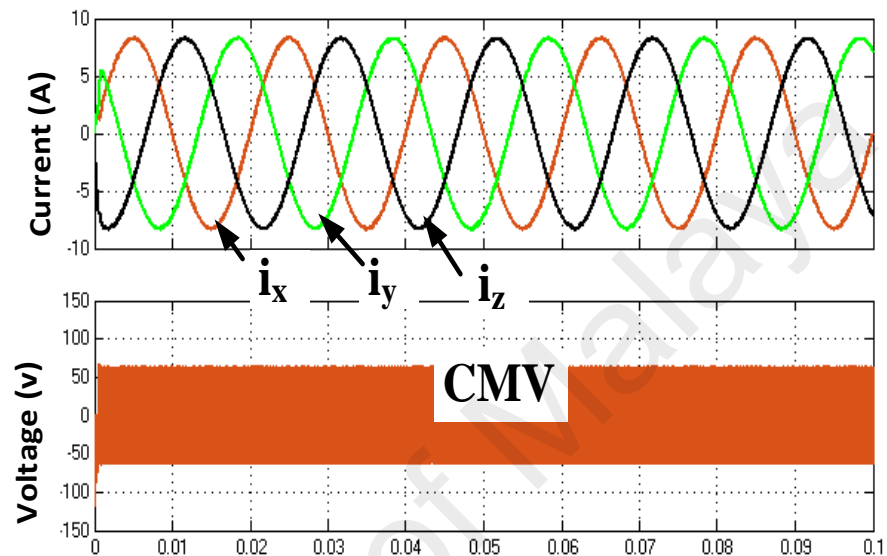
(a)



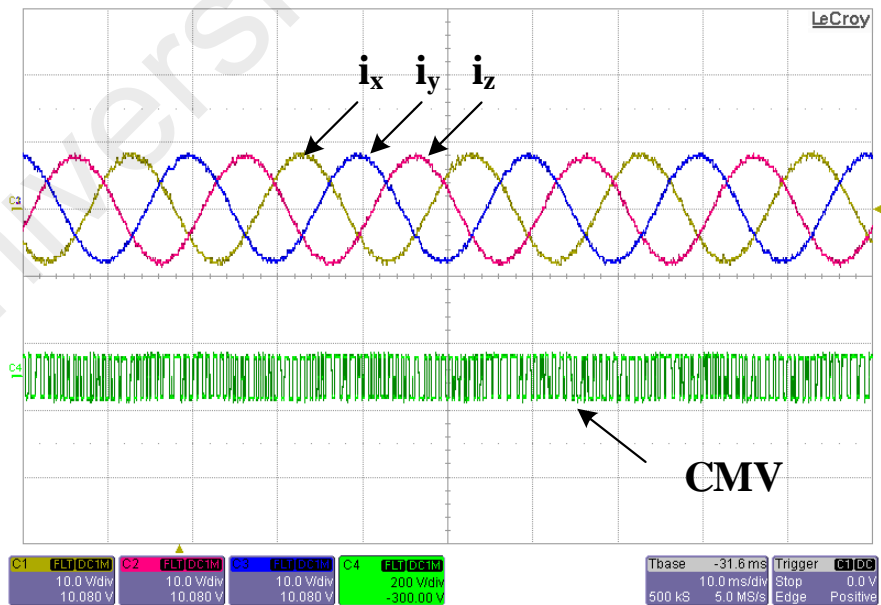
(b)

Figure 4.8: MPC based on active vectors with one zero (nnnn) vector (a) Simulation result (b) Experimental result

3rd case: When the CMV weighting factor is introduced in the cost, the waveform of CMV and load currents are shown in Figure 4.9. With addition of CMV factor, the CMV is mitigated significantly and also ripple content is reduced in the inverter output currents. An effective balance can be obtained between CMV and load currents using this CMV factor.



(a)



10A/div. 10ms/div.

(b)

Figure 4.9: The inverter output current and CMV using CMV weighting factor (a) Simulation result (b) Experimental result.

4.3.2 L-MPC for Three-Phase Four-Leg Inverter

The Lyapunov function based MPC algorithm has been validated with experimental implementation in a laboratory prototype of three-phase four-leg inverter with the parameters as specified in Table 4.2. All the results of this section are obtained without providing information of variation in the load and filter parameters into the controllers. The weighting factor $w_{swc} = 0.5$ is carried out in $(k + 1)$ th state because of not using delay compensation and sampling time $T_s = 50 \mu s$ is considered.

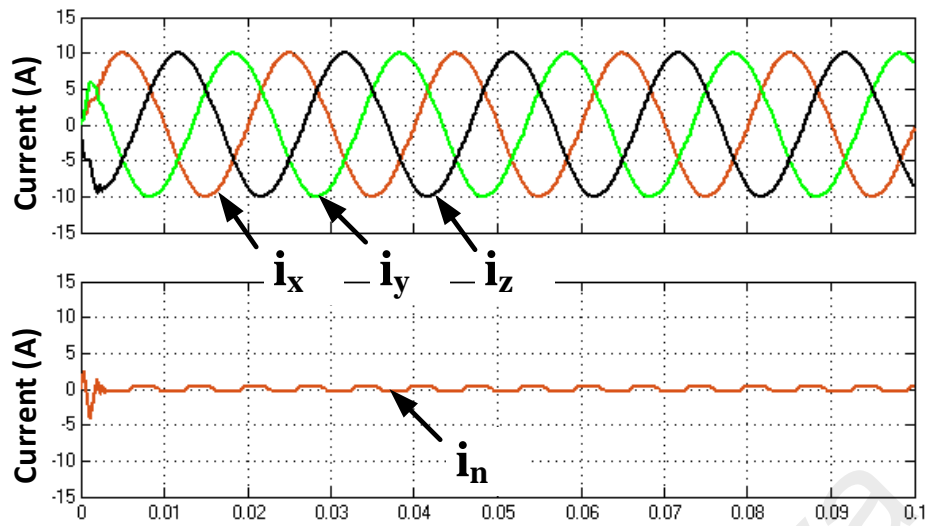
Table 4.2: Parameters of the simulation and experimental results

Variable	Parameter	Value
V_{dc}	dc-link voltage	220 V
L_f	Filter inductance	15 mH
T_s	Sampling Time	50 μs
R	Load resistance	12 Ω
R_f	Filter resistance	0.1 Ω
f*	Reference nominal frequency	50 Hz
i*	Reference nominal peak current	10 A
L_{fn}	Neutral leg inductance	7.5 mH

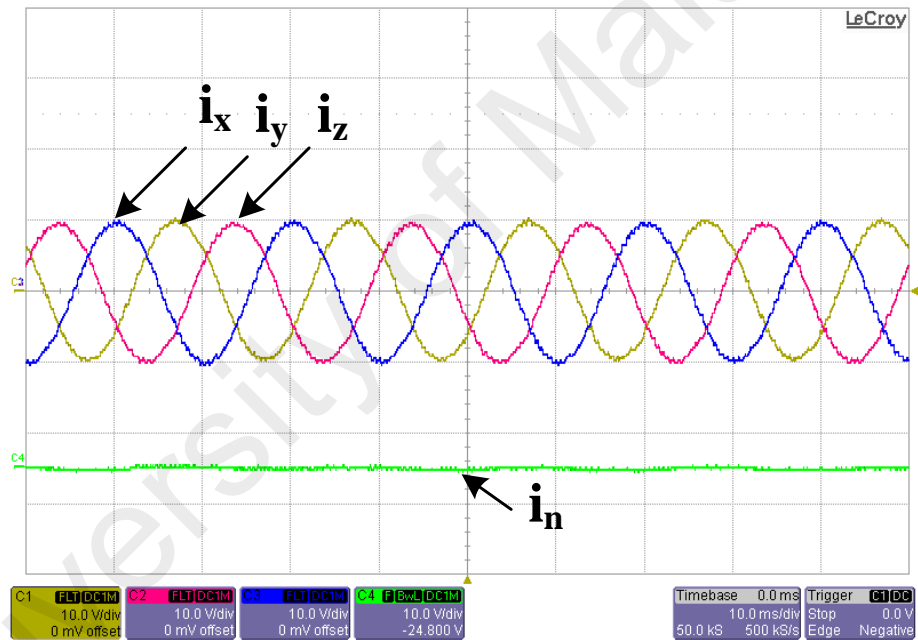
Case-1: Balanced references and balanced load;

$$i_x^* = i_y^* = i_z^* = 10A, R_{Tx} = R_{Ty} = R_{Tz} = 12 \Omega, L_{fx} = L_{fy} = L_{fz} = 15 \text{ mH} ;$$

The simulation and experimental results of balanced condition (ideal case) are shown in Figure 4.10, where the reference signals are balanced, and the loads are distributed equally in each phase. The results showed that no neutral current flows through the neutral leg and ripple content in the load currents with amplitude 10 A, which are same as the references.



(a)



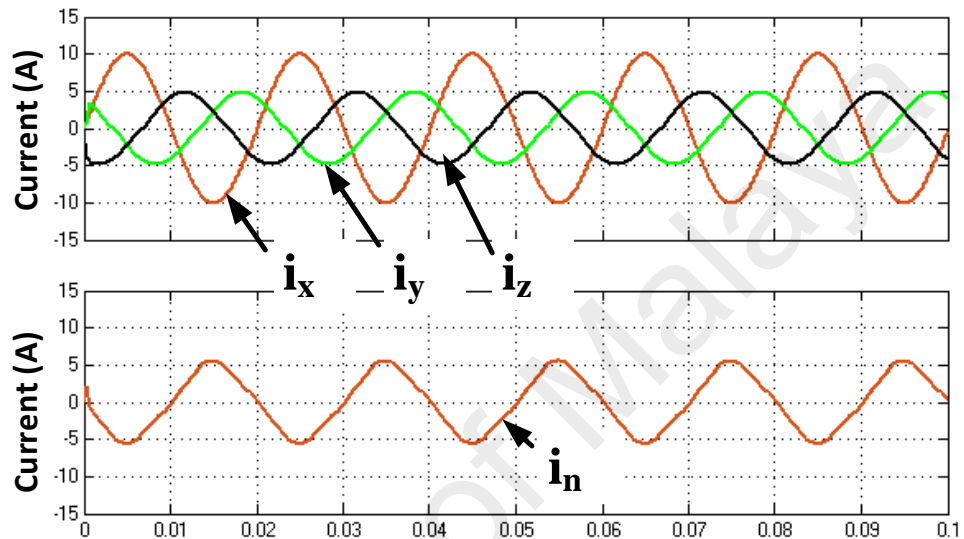
(b)

Figure 4.10: Case 1: Balanced references with balanced load and filter (a) Simulation result (b) Experimental Result

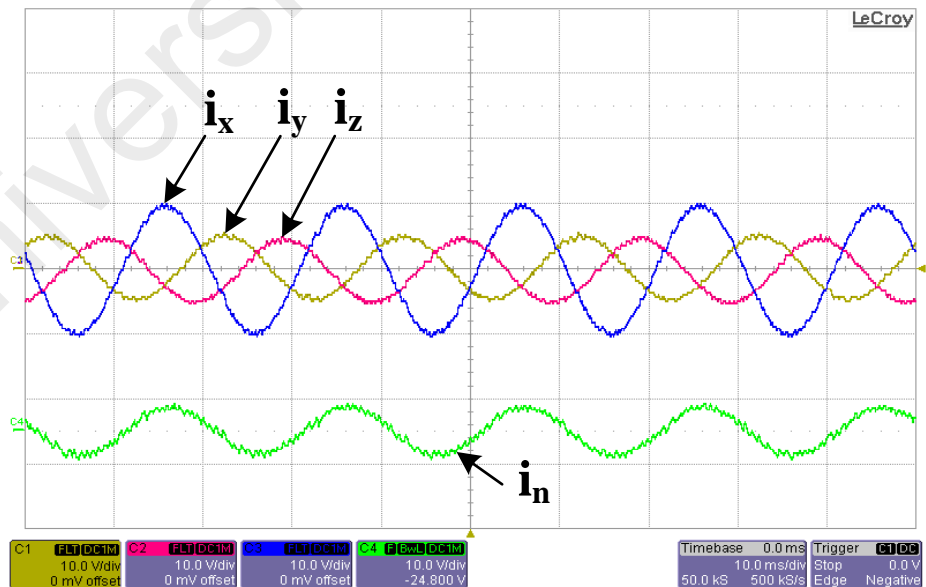
Case-2: Unbalanced references and balanced load;

$$i_x^* = 10A, i_y^* = i_z^* = 5A, R_{Tx} = R_{Ty} = R_{Tz} = 12 \Omega, L_{fx} = L_{fy} = L_{fz} = 15 \text{ mh} ;$$

This case represents the unbalanced reference connected to the balanced load. The results are shown in Figure 4.11. The neutral current circulates the unbalanced currents through the fourth leg. These references create an uneven harmonic distribution and produces the zero-sequence current. The load and neutral current are found with reduced total harmonic distortion.



(a)



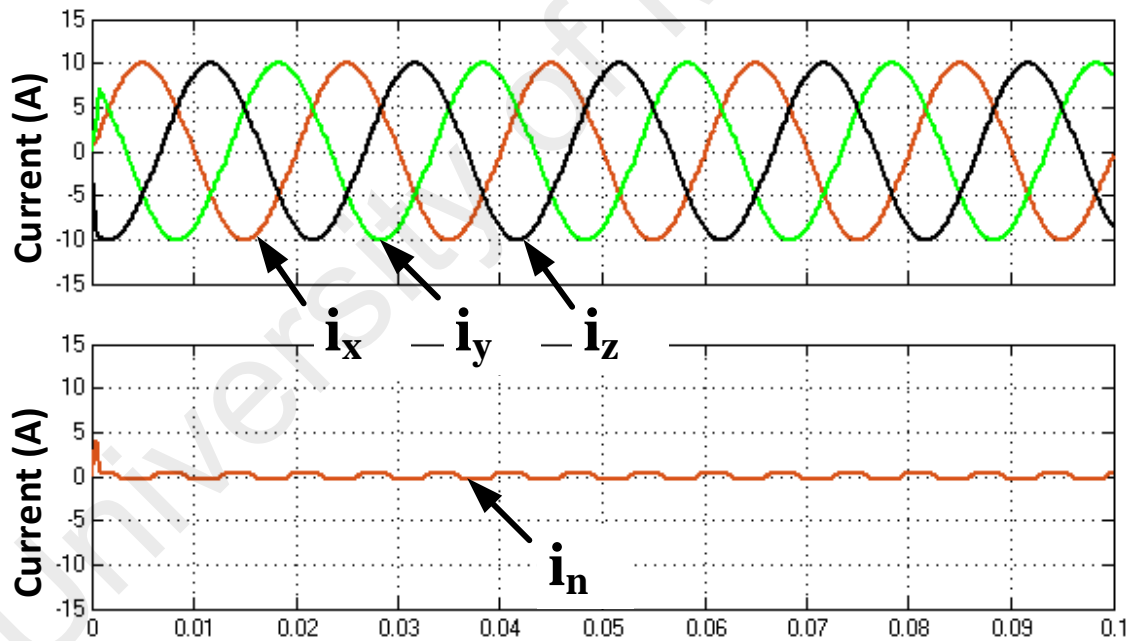
(b)

Figure 4.11: Case 2: Unbalanced references with balanced load and filter (a) Simulation result (b) Experimental Result.

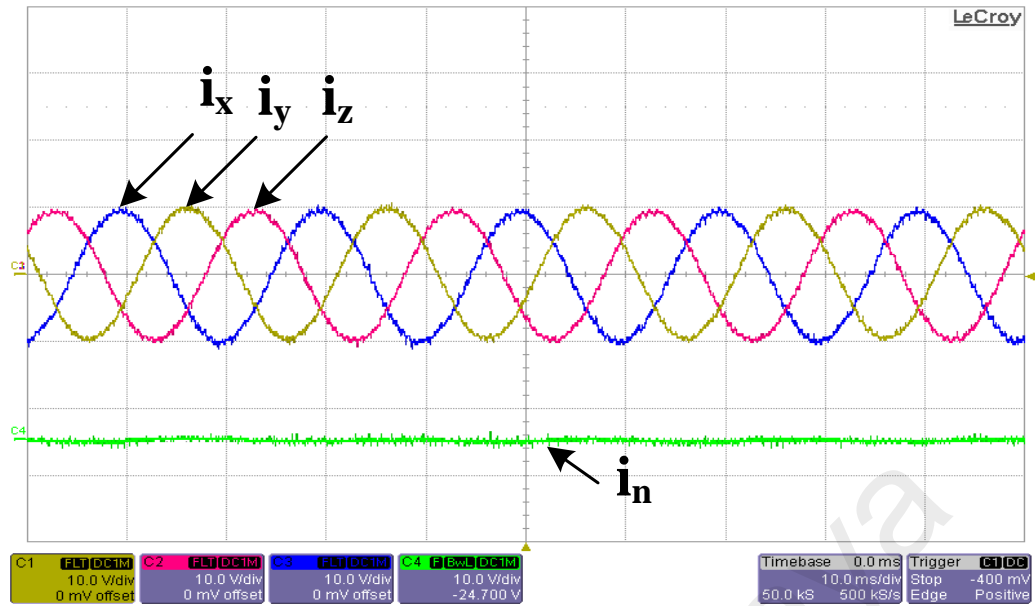
Case-3: Balanced references and unbalanced load;

$$i_x^* = i_y^* = i_z^* = 10A, R_{Tx} = 12 \Omega, R_{Ty} = R_{Tz} = 6 \Omega, L_{fx} = 15 \text{ mh}, L_{fy} = L_{fz} = 8 \text{ mh};$$

The same reference signals are applied to an unbalanced load distribution. This control strategy can generate very good load current with a sinusoidal waveform despite the unbalanced load distribution. The fast-dynamic response is obtained with practically no overshoot for all three output currents. The results are shown in Figure 4.12. Despite unbalanced load and filter parameters, the load currents generated exactly as their references with amplitude 10A.



(a)



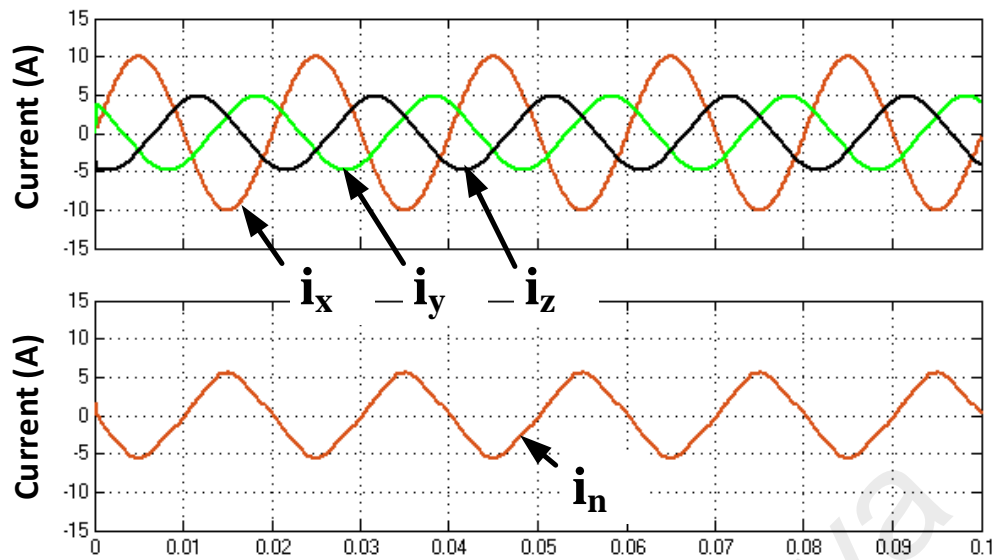
(b)

Figure 4.12: Case 3: Balanced references with unbalanced load and filter (a) Simulation result (b) Experimental Result

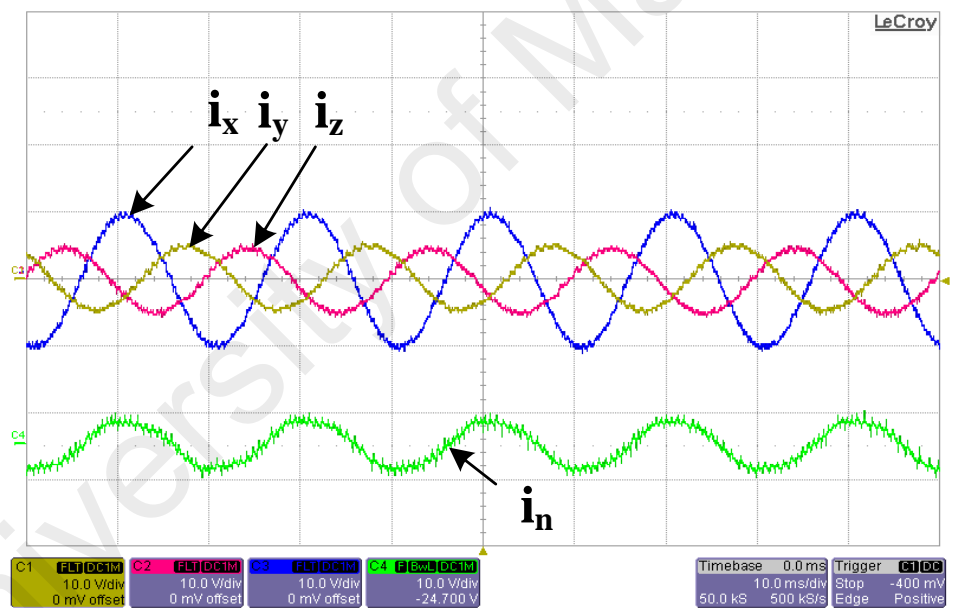
Case-4: Unbalanced references and unbalanced load;

$$i_x^* = 10A, i_y^* = i_z^* = 5A, R_{Tx} = 12 \Omega, R_{Ty} = R_{Tz} = 6 \Omega, L_{fx} = 15 \text{ mh}, L_{fy} = L_{fz} = 8 \text{ mh};$$

This case is to validate the effect of unbalanced references connected to the unbalanced three-phase RL loads. The control method is able to perform independent load current reference tracking. The generated load current follows the reference values, but with slightly higher distortion compared to that in case 3 because of the uneven load distribution. The load current and neutral current waveform imitates the one in case 3 because both cases are given the same reference load current. The simulation and experimental results for case 4 are presented in Figure 4.13. The load magnitude and neutral currents are found to be equal as case 2; thus, it is proven that the reference tracking does not depend upon the variation of load and filter parameters.



(a)



(b)

Figure 4.13: Case 4: Unbalanced references with unbalanced load and filter (a) Simulation result (b) Experimental Result

Figure 4.14 illustrates the transient result of the proposed L-MPC method in the load variation. A step change in the load from 10 A to 5 A is achieved. During transient

instant, the inverter load currents tracked their corresponding reference very well which shows the fast-dynamic response. Similarly, the fast-dynamic response is observed in step changing in the frequency with the variation from 50 Hz to 25Hz as shown in Figure 4.15.

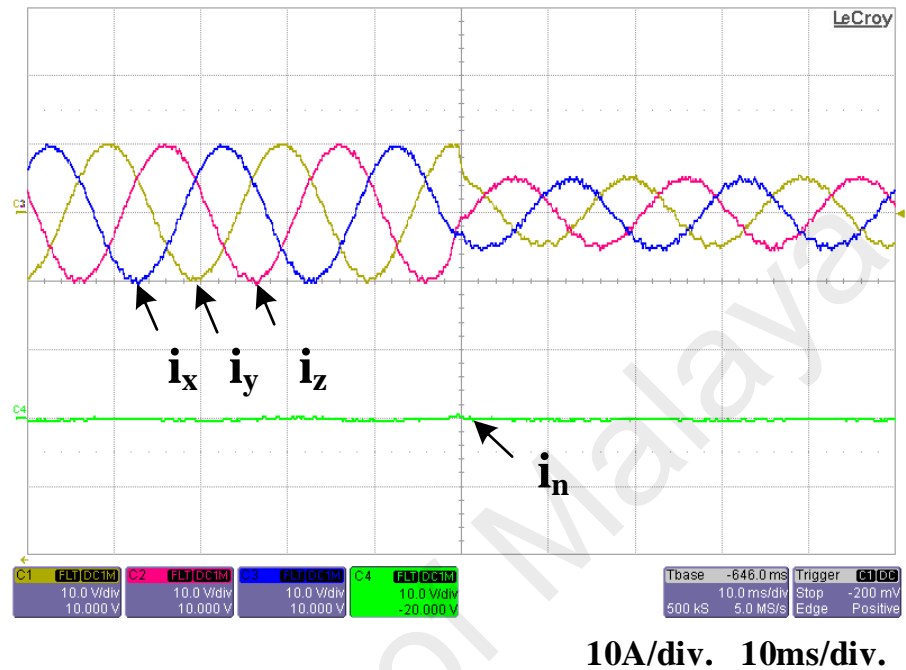


Figure 4.14: Experimental result with sudden variation in the load from 10 A to 5A of proposed L-MPC

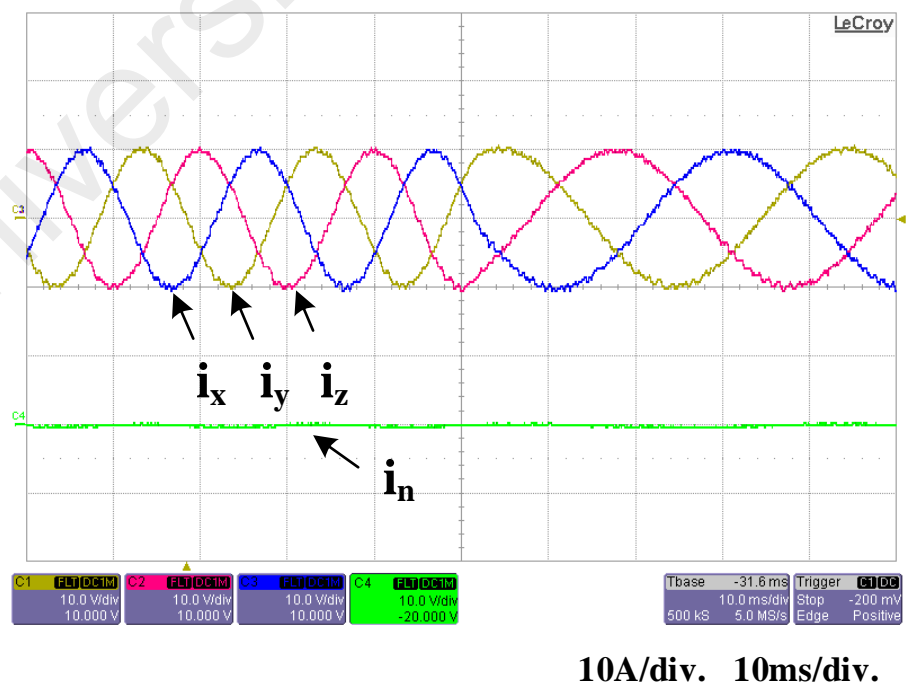


Figure 4.15: Experimental result with sudden variation in frequency from 50 Hz to 25Hz of L -MPC

4.3.3 Near State Vector Based Model Predictive Control for Three-Phase Four-Leg Inverter

The near state vector based MPC (NSV-MPC) has been validated with simulation and experimentally with the parameters as specified in Table 4.3. The experimental test is done using field programmable gate array (FPGA) based controller and it can be interfaced with parallel processing technique of model predictive controller for enhancing the system dynamic response.

Table 4.3: Parameters of the experimental results

Variable	Parameter	Value
V_{dc}	dc-link voltage	320 V
C	dc-link capacitance	2.2 μ F
L_f	Filter inductance	15 mH
T_s	Sampling Time	50 μ s
R	Load resistance	12 Ω
R_f	Filter resistance	0.1 Ω
f^*	Reference nominal frequency	50 Hz
i^*	Reference nominal peak current	10 A
L_{fn}	Neutral leg inductance	8 mH

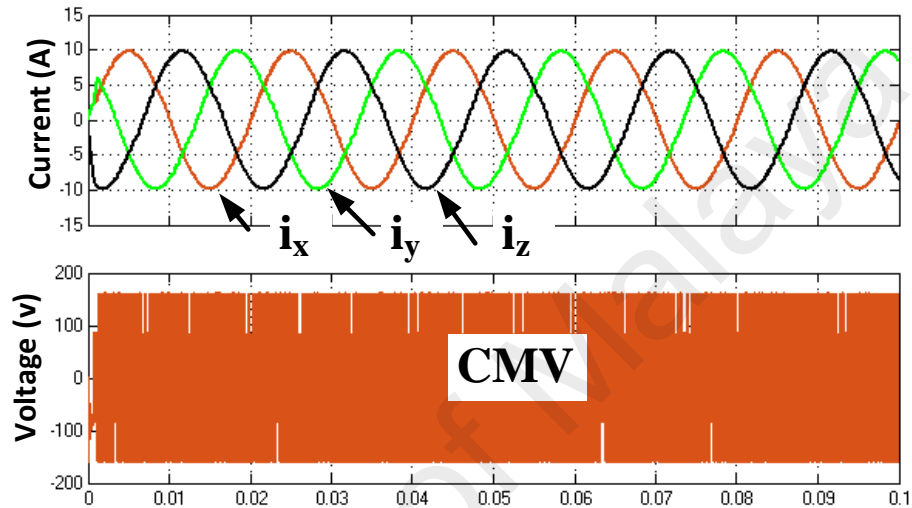
All the experimental results in this section are obtained using the weighting factor $w_{swc} = 0.5$ and sampling time $T_s = 50 \mu s$. All condition considered are same in both Conventional MPC and NSV-MPC. Four cases are considered:

Case 1: Two zero vectors with six active vectors in proposed NSV-MPC at every sampling time.

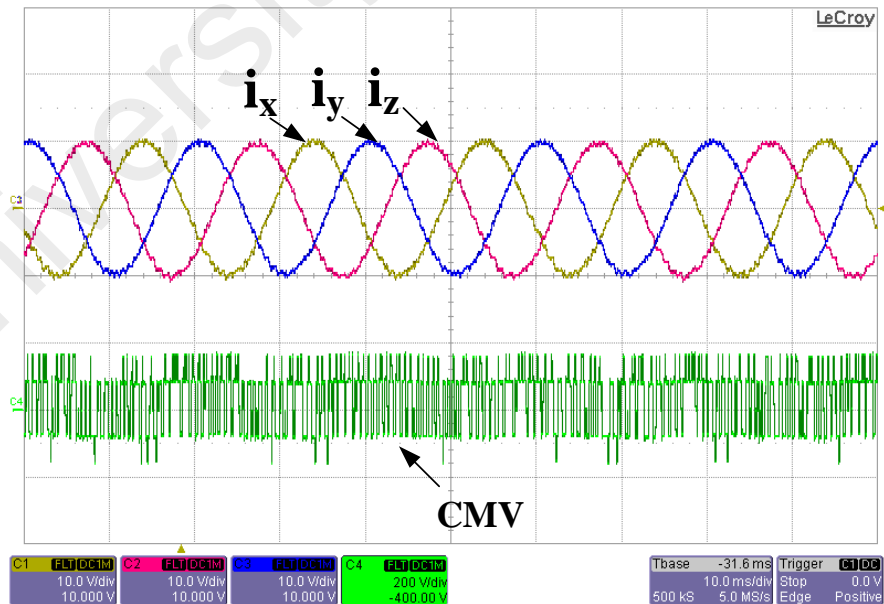
Case 2: One zero vector either pppp or nnnn with six active vectors in proposed NSV-MPC at every sampling time.

Case 3: Six active vectors in proposed NSV-MPC at every sampling time.

In the 1st case, The NSV-MPC utilize 8 switching vectors including both the zero vectors to predict the future reference vector in each control cycle, hence computational burden is reduced as reduced number of voltage vectors are used in the calculation. The magnitude of peak to peak value of CMV are same as conventional MPC varying between $-\frac{V_{dc}}{2}$ and $+\frac{V_{dc}}{2}$ presented in Figure 4.16.



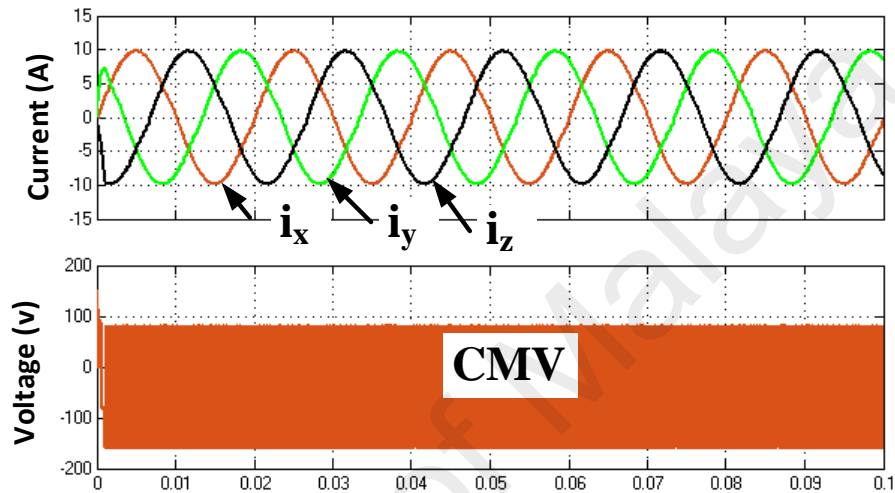
(a)



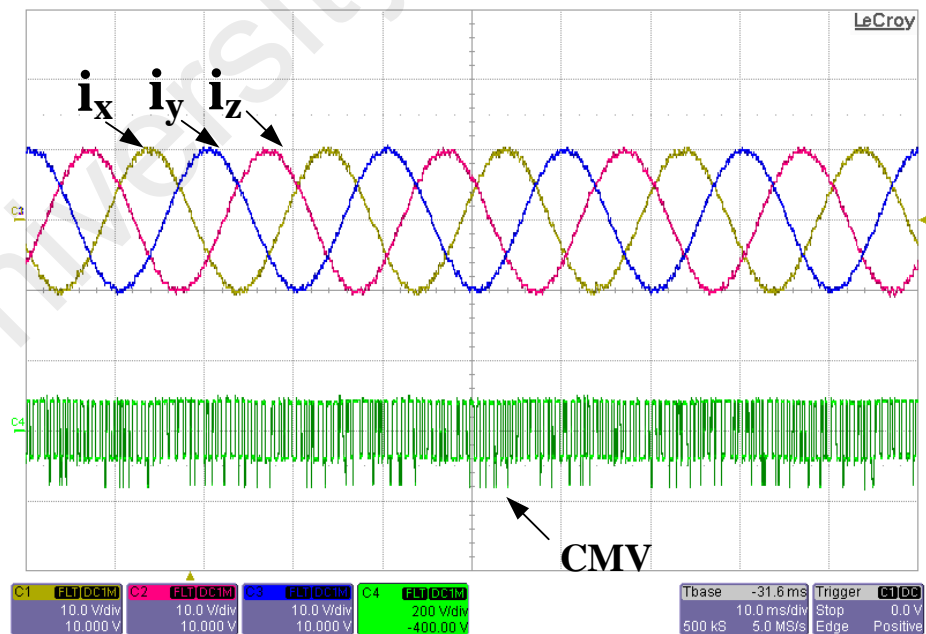
(b)

Figure 4.16: Each phase current and CMV for case 1 (a) Simulation result (b) Experimental result

In the 2nd case, the NSV- MPC scheme utilize only one zero vector either pppp or nnnn with 6 active vectors at every sampling time. The one-sided peak value of CMV is large and varies between $\frac{V_{dc}}{2}$ and $-\frac{V_{dc}}{4}$ or between $\frac{V_{dc}}{4}$ and $-\frac{V_{dc}}{2}$ respectively due to the use of only one zero vector shown in Figure 4.17 and Figure 4.18 respectively. This reduced the computational burden due to use of reduced number of switching state.

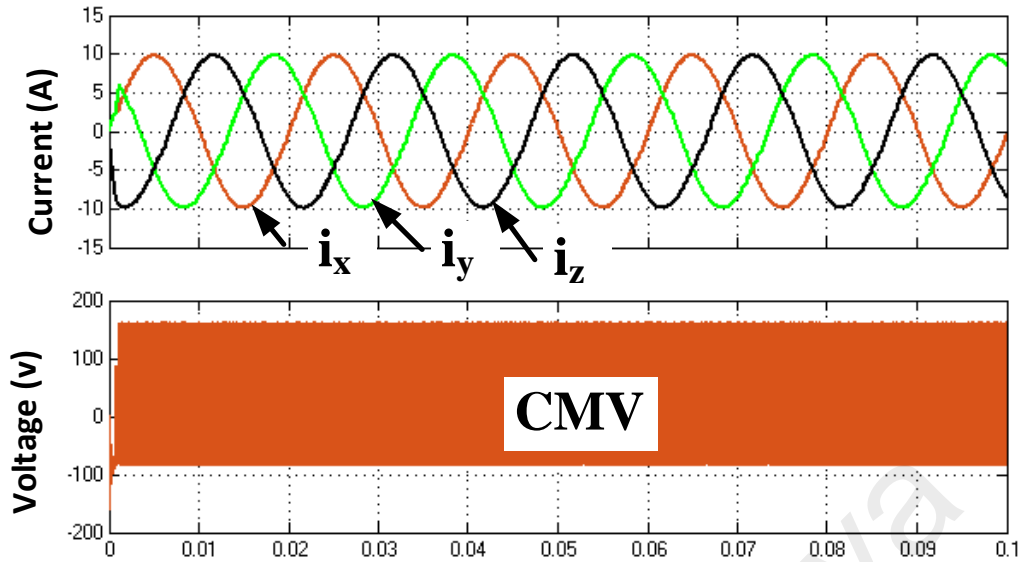


(a)

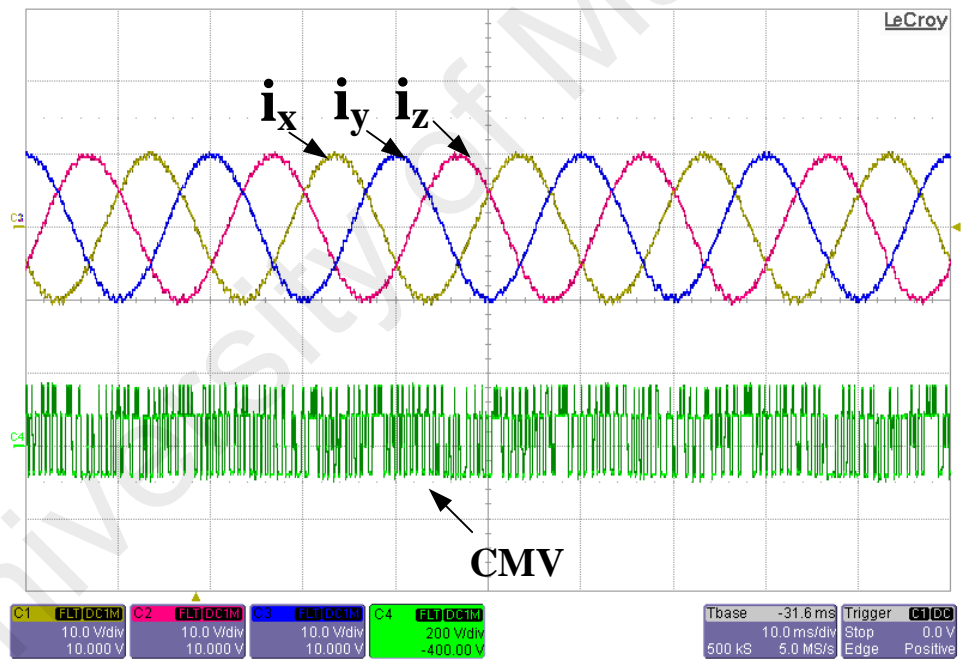


(b)

Figure 4.17: Each phase current and CMV for case 2 considering pppp switching state (a) Simulation result (b) Experimental result



(a)



(b)

Figure 4.18: Each phase current and CMV for case 2 considering nnnn switching state (a) Simulation result (b) Experimental result

For the 3rd case, the proposed NSV-MPC is applied using only six active vectors in each sampling instant to reduce the peak to peak value of CMV significantly. Consequently, the calculation time is also enhanced by using reduced switching vector.

Even though the ripple content in the load current comparatively higher which is still in allowable range, the CMV is confined within $\pm \frac{V_{dc}}{4}$ as shown in Figure 4.19.

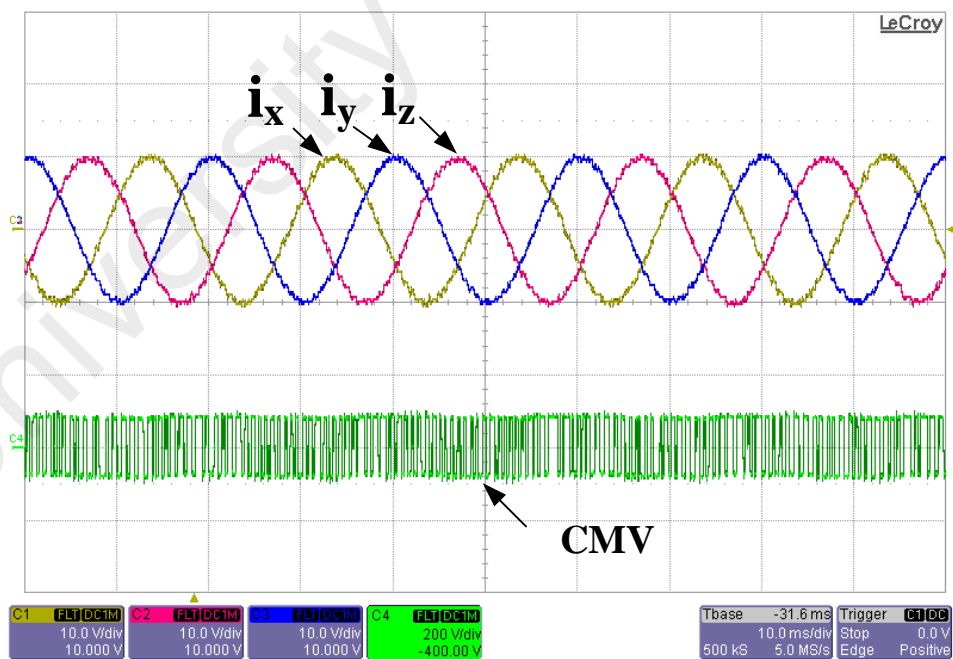
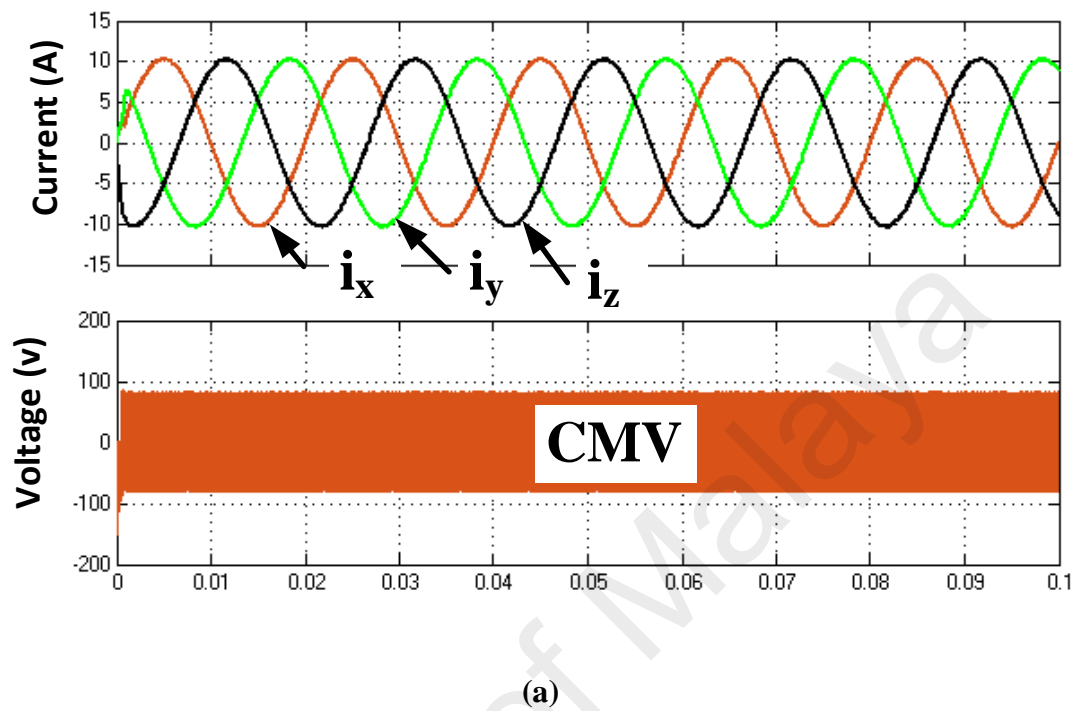


Figure 4.19: Each phase current and CMV for case 3 (a) Simulation result (b) Experimental result

The FFT analysis of CMV is done using powergui/FFT Analysis Toolbox of Matlab/Simulink software. The results of mentioned cases are illustrated in Figure 4.20 to Figure 4.23 based on this toolbox.

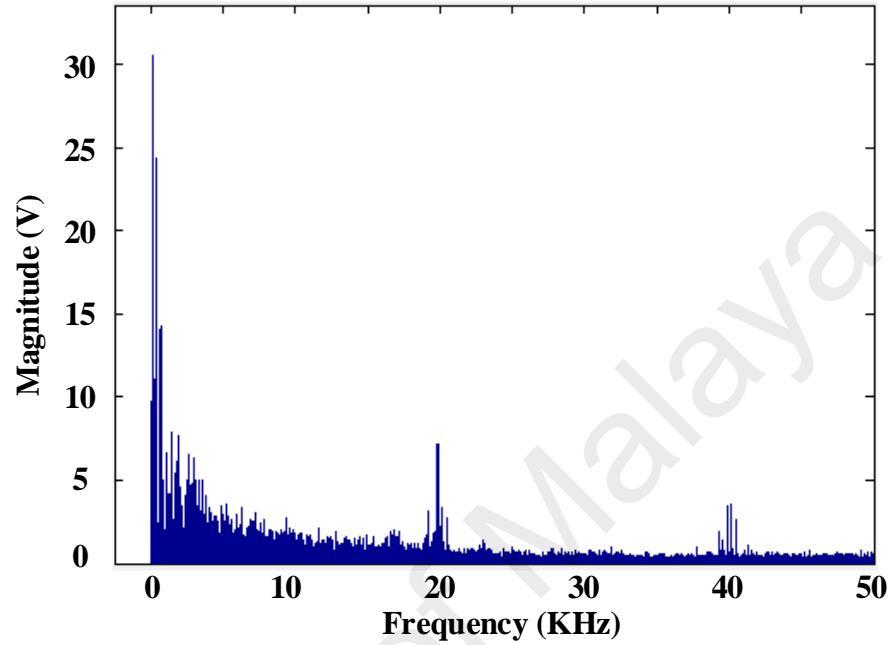


Figure 4.20: FFT analysis results of CMV for case 1- 8 vector based NSV-MPC

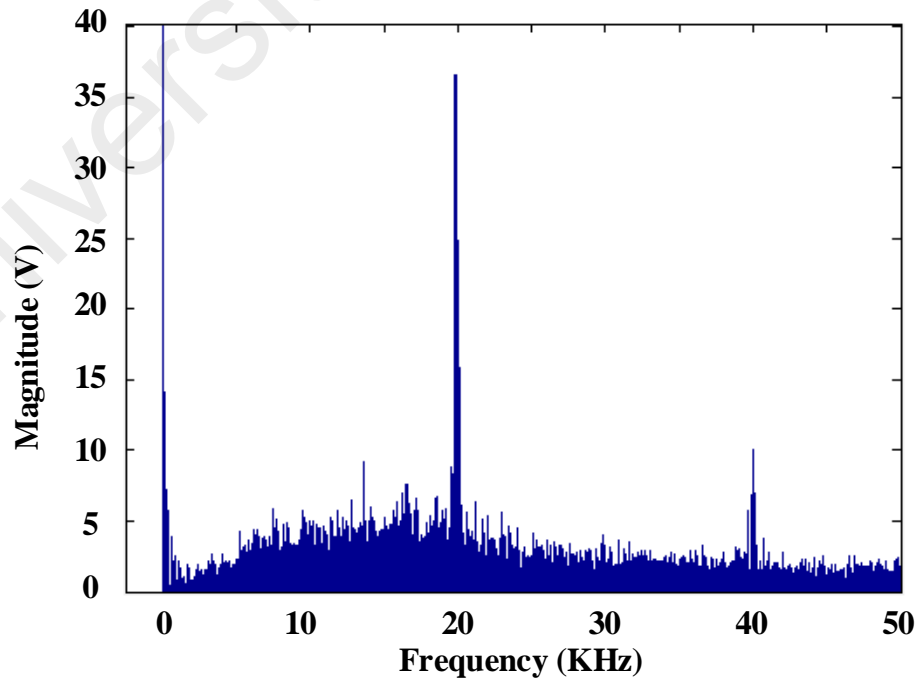


Figure 4.21: FFT analysis results of CMV for case 2 considering pppp switching state NSV-MPC

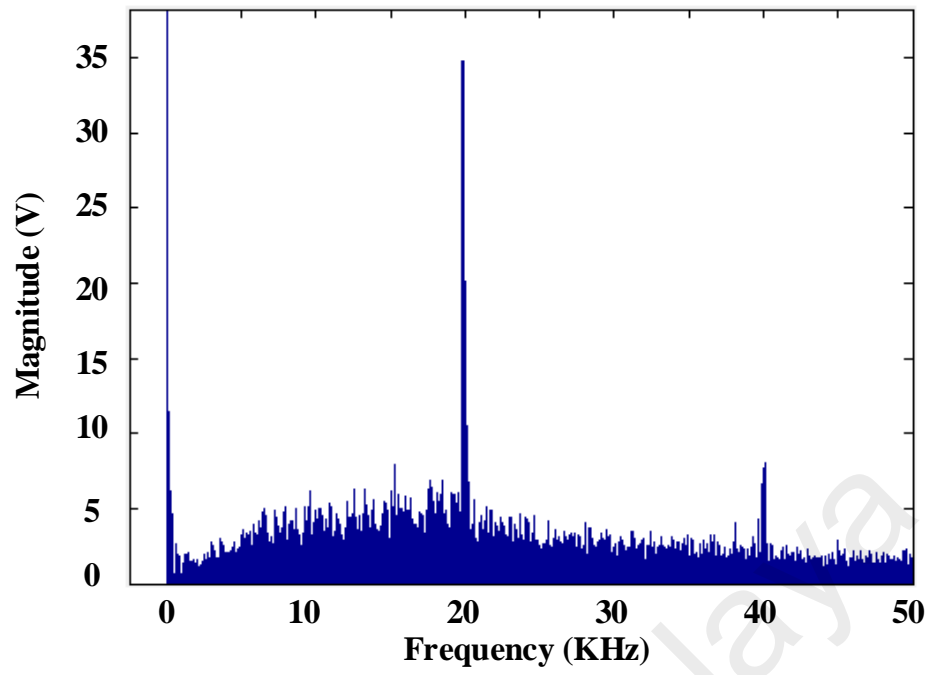


Figure 4.22: FFT analysis results of CMV for case 2 considering nnnn switching state NSV-MPC

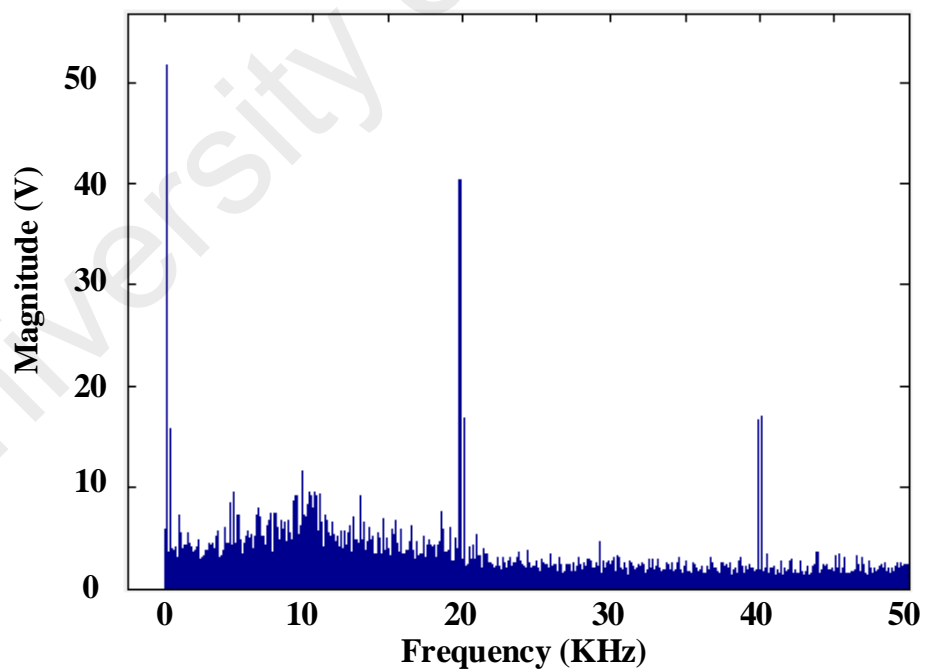


Figure 4.23: FFT analysis results of CMV for case 3 - NSV-MPC

4.4 Summary

All the control goals by the proposed control techniques are well achieved. The computational burden, ripple content in the current and the common mode voltage are mitigated of three-phase four-leg inverter. The outcomes of the results are summarized as follows:

4. Lyapunov function based MPC algorithm has reduced the computational burden by 23.8 % compared to the conventional MPC algorithm of three-phase four-leg inverter.
5. Near state voltage vector selection-based model predictive control (NSV-MPC) has mitigated the common mode voltage (CMV) with reduced computational burden of three-phase four-leg inverter.
6. The effectiveness of proposed control techniques has been validated in simulation and experimentally presented in this chapter.

CHAPTER 5: STABILITY ANALYSIS AND PERFORMANCE ASSESMENT

5.1 Introduction

Stability is an important requirement when Lyapunov function is introduced with model predictive control in the non-linear control engineering system. In order to analyze stability, a robustness test is also required to perform for ensuring the closed-loop behavior under model parameter uncertainties. At the end of this chapter, a comparative assessment of performance has been presented to show the effectiveness of the proposed control techniques of the three-phase four-leg inverter.

5.2 Stability Analysis of Three-phase Four-leg Inverter

In order to implement nonlinear control law-based L-MPC, closed-loop system is obtained globally stable based on the nonlinear model of the system and stability of the system is investigated with justification of Lyapunov control law and then proved the stability of the system with Lyapunov control law via backstepping control.

5.2.1 Lyapunov Law Justification

The Lyapunov control law can be written from chapter 4 as follows

$$\bar{\mathbf{v}}(k+1) = -\frac{\mathbf{P}}{\mathbf{Q}}\mathbf{i}(k) + \frac{1}{\mathbf{Q}}\mathbf{i}^*(k+1) \quad (5.1)$$

By applying Lyapunov control law $\bar{\mathbf{v}}(k+1)$ of equation (5.1), the rate of change of the Lyapunov function equation (3.34) can be written as follows.

$$\begin{aligned} \nabla \text{LFC} = & \frac{1}{2} \left[\left\{ \mathbf{P}\mathbf{i}(k) + \mathbf{Q} \left\{ -\frac{\mathbf{P}}{\mathbf{Q}}\mathbf{i}(k) + \frac{1}{\mathbf{Q}}\mathbf{i}^*(k+1) + \boldsymbol{\delta}(k+1) \right\} - \mathbf{i}^*(k+1) \right\}^T \left\{ \mathbf{P}\mathbf{i}(k) \right. \right. \\ & \left. \left. + \mathbf{Q} \left\{ -\frac{\mathbf{P}}{\mathbf{Q}}\mathbf{i}(k) + \frac{1}{\mathbf{Q}}\mathbf{i}^*(k+1) + \boldsymbol{\delta}(k+1) \right\} - \mathbf{i}^*(k+1) \right\} \right] \\ & - \frac{1}{2} \{ \mathbf{i}_{er}(k) \}^T \{ \mathbf{i}_{er}(k) \} \end{aligned}$$

$$= \frac{1}{2} [\{\mathbf{Q}\boldsymbol{\delta}(k+1)\}^T \{\mathbf{Q}\boldsymbol{\delta}(k+1)\}] - \frac{1}{2} \{\mathbf{i}_{er}(k)\}^T \{\mathbf{i}_{er}(k)\} \quad (5.2)$$

The voltage vector $\mathbf{v}(k+1)$ is bounded by a finite control set of voltage vector which is determined by the dc-link voltage according to switching action. As the inverter output current $\mathbf{i}(k)$ and the reference current $\mathbf{i}^*(k+1)$ are bounded by the control system, the error of load current is also bounded. A finite set of $\mathbf{i}^*(k+1)$ and $\bar{\mathbf{v}}(k+1)$ determines a compact set (Γ) for all $\mathbf{i}_{er}(k) \in \Gamma \subset \mathbb{R}^2$. There exists a constant $\sigma > 0$ satisfying $\|\boldsymbol{\delta}(k+1)\| \leq \sigma$ so, the rate of change of the Lyapunov function as follows.

$$\Delta LF(k) \leq -\frac{1}{2} \{\mathbf{i}_{er}(k)\}^T \{\mathbf{i}_{er}(k)\} + \frac{1}{2} \mathbf{Q}^2 \sigma \quad (5.3)$$

The Lyapunov control law is uniformly bounded (J.-J. E. Slotine, 1991) since $\mathbf{i}_{er}(k)$ and $\mathbf{i}_{er}(k+1)$ both are compact sets, there exists four positive constants c_1, c_2, c_3 and c_4 that make.

$$\left. \begin{aligned} LF(\mathbf{i}_{er}(k)) &\geq c_1 |\mathbf{i}_{er}(k)|^l, & \forall \mathbf{i}_{er}(k) \in G \\ LF(\mathbf{i}_{er}(k)) &\geq c_2 |\mathbf{i}_{er}(k)|^l, & \forall \mathbf{i}_{er}(k) \in \Gamma \\ LF(\mathbf{i}_{er}(k+1)) - LF(\mathbf{i}_{er}(k)) &< -c_3 |\mathbf{i}_{er}(k)|^l + c_4 \end{aligned} \right\} \quad (5.4)$$

Where, $l \geq 1, G \subseteq \mathbb{R}^n$ is a control positive invariant set and $\Gamma \subseteq G$ is a compact set.

The stability condition equation (5.4) is satisfied by defining.

$$c_1 = c_2 = 1; c_3 = \frac{1}{2}; c_4 = \frac{1}{2} \mathbf{Q}^2 \sigma^2 \quad (5.5)$$

This is found that all close loop signals in the L-MPC for four-leg inverter system is bounded uniformly. So, the rate of change of Lyapunov function in equation (5.3) is

$$\Delta LF(k) \leq -2c_3 LF(\mathbf{i}_{er}(k)) + c_4 \quad (5.6)$$

This variation denotes, the current control error vectors converged with time increasing in the compact set as

$$\Lambda = \mathbf{i}_{er} \|\mathbf{i}_{er}\| \leq \sqrt{\frac{c_4}{c_3}} \quad (5.7)$$

Thus, all signals are uniformly and ultimately bounded in the proposed L-MPC for three-phase four-leg inverter.

5.2.2 Lyapunov Stability Analysis with Backstepping Control

In order to show the proposed L-MPC is stable, the stability analysis is carried out through Lyapunov function with the help of backstepping control. Backstepping is a recursive technique for designing nonlinear controls and ensuring the stability of the whole system by generating negative derivatives of Lyapunov function. The stabilization technique via Backstepping control based on Lyapunov function must be reformed to conform the nonlinear system before applying it (Khalil & Grizzle, 1996). Consider nonlinear system of the form from equation (3.6):

$$\dot{\mathbf{x}} = \mathbf{Ax} + \mathbf{Bv} \quad (5.8)$$

$$\dot{\mathbf{v}} = \mathbf{u} \quad (5.9)$$

In equation (5.9), \mathbf{v} is used as a virtual control for the backstepping control. The first step of the backstepping procedure is to rearrange the system so that it contains an error variable which is the difference between the actual controller and the desired controller (Khalil & Grizzle, 1996) (Davila, 2013).

The inverter output current tracking error signal can be expressed as

$$\mathbf{i}_{er} = \mathbf{i} - \mathbf{i}_{ref} \quad (5.10)$$

The derivative of above equation and using equation (5.8), equation (5.11) can be written as follows

$$\begin{aligned}\dot{\mathbf{i}}_{er} &= \dot{\mathbf{i}} - \dot{\mathbf{i}}_{ref} \\ &= \mathbf{Ax} + \mathbf{Bv} - \dot{\mathbf{i}}_{ref}\end{aligned}\quad (5.11)$$

The error is to be minimized between the desired reference signal \mathbf{i}_{ref} and its actual value \mathbf{i} to make the system stable globally.

Considering the positive definite Lyapunov function to stabilize the system as

$$LF_1 = \frac{1}{2} \mathbf{i}_{er1}^2 \quad (5.12)$$

The derivative of equation (5.12) along its trajectory is

$$L\dot{F}_1 = \mathbf{i}_{er1} \dot{\mathbf{i}}_{er1} = \mathbf{i}_{er1} (\mathbf{Ax} + \mathbf{Bv} - \dot{\mathbf{i}}_{ref}) \quad (5.13)$$

From the Lyapunov function method, $L\dot{F}_1$ is needed to make negative definite to stabilize the system, the system equation (5.13) becomes asymptotically stable. $\boldsymbol{\varphi}_1$ is as the ideal value of \mathbf{v} that can control \mathbf{i} appropriately. Therefore,

$$\boldsymbol{\varphi}_1 = \frac{1}{\mathbf{B}} (-\mathbf{Ax} + \dot{\mathbf{i}}_{ref} + \mathbf{H}_1 \mathbf{i}_{er1}) \quad (5.14)$$

Consequently,

$$L\dot{F}_1 = \mathbf{H}_1 \mathbf{i}_{er1}^2 \leq 0 \quad (5.15)$$

Where, \mathbf{H}_1 is selected negative because of Hurwitz matrix \mathbf{H}_1 . From equation (5.15), the error \mathbf{i}_{er1} converges to zero exponentially due to $L\dot{F}_1$ negative definite. Hence, \mathbf{i} converges to \mathbf{i}_{ref} exponentially by virtue from Lyapunov control law of finding stability. In the next step, according to the backstepping method, consider the error between the desired ideal and its actual signal \mathbf{v} as

$$\mathbf{i}_{er2} = \mathbf{v} - \boldsymbol{\varphi}_1 \quad (5.16)$$

The next step is to write the total Lyapunov function as follows:

$$\mathbf{LF}_2 = \frac{1}{2} \mathbf{i}_{er1}^2 + \frac{1}{2} \mathbf{i}_{er2}^2 \quad (5.17)$$

Accordingly, $\dot{\mathbf{LF}}_2$ is

$$\begin{aligned} \dot{\mathbf{LF}}_2 &= \mathbf{i}_{er1} \dot{\mathbf{i}}_{er1} + \mathbf{i}_{er2} \dot{\mathbf{i}}_{er2} \\ &= \mathbf{i}_{er1} (\mathbf{Ax} + \mathbf{Bv} - \dot{\mathbf{i}}_{ref}) + \mathbf{i}_{er2} (\dot{\mathbf{v}} - \dot{\boldsymbol{\varphi}}_1) \\ &= \mathbf{i}_{er1} (\mathbf{Ax} + \mathbf{B}(\mathbf{i}_{er2} + \boldsymbol{\varphi}_1) - \dot{\mathbf{i}}_{ref}) + \mathbf{i}_{er2} (\mathbf{u} - \dot{\boldsymbol{\varphi}}_1) \end{aligned} \quad (5.18)$$

Replacing for $\boldsymbol{\varphi}_1$ from equation (5.14) Yields

$$\begin{aligned} \dot{\mathbf{LF}}_2 &= \mathbf{i}_{er1} \left(\mathbf{Ax} + \mathbf{B}(\mathbf{i}_{er2} + \frac{1}{\mathbf{B}}(-\mathbf{Ax} + \dot{\mathbf{i}}_{ref} + \mathbf{H}_1 \mathbf{i}_{er1})) - \dot{\mathbf{i}}_{ref} \right) + \mathbf{i}_{er2} (\mathbf{u} - \dot{\boldsymbol{\varphi}}_1) \\ &= \mathbf{H}_1 \mathbf{i}_{er1}^2 + \mathbf{i}_{er1} \mathbf{B} \mathbf{i}_{er2} + \mathbf{i}_{er2} (\mathbf{u} - \dot{\boldsymbol{\varphi}}_1) \end{aligned} \quad (5.19)$$

Finally, the control law via the Backstepping design method is

$$\mathbf{u} = (\dot{\boldsymbol{\varphi}}_1 + \mathbf{H}_2 \mathbf{i}_{er2} - \mathbf{B} \mathbf{i}_{er1}) \quad (5.20)$$

Replacing u from equation (5.20) into equation (5.19), the equation (5.21) can be written as

$$\mathbf{H}_1 \mathbf{i}_{er1}^2 + \mathbf{H}_2 \mathbf{i}_{er2}^2 \leq 0 \quad (5.21)$$

Where Hurwitz matrix, \mathbf{H}_2 is a negative value. Hurwitz matrix \mathbf{H}_1 and \mathbf{H}_2 provides the rate of convergence of \mathbf{i} and $\boldsymbol{\varphi}_1$ respectively (Davila, 2013). According to the Lyapunov stability criterion, \mathbf{i}_{er1} and \mathbf{i}_{er2} converge to zero exponentially where \mathbf{i} and $\boldsymbol{\varphi}_1$

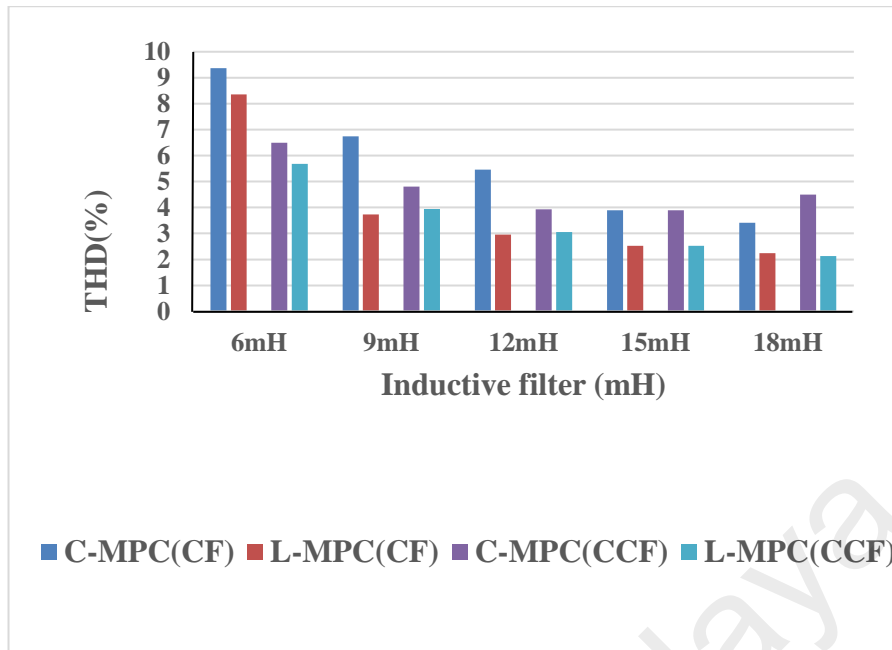
converge exponentially to \mathbf{i}_{ref} and \mathbf{v} respectively. These convergences imply that the control input equation (5.20) causes the output \mathbf{i} exponentially tracks the reference \mathbf{i}_{ref} .

5.3 Performance Assessment of L-MPC

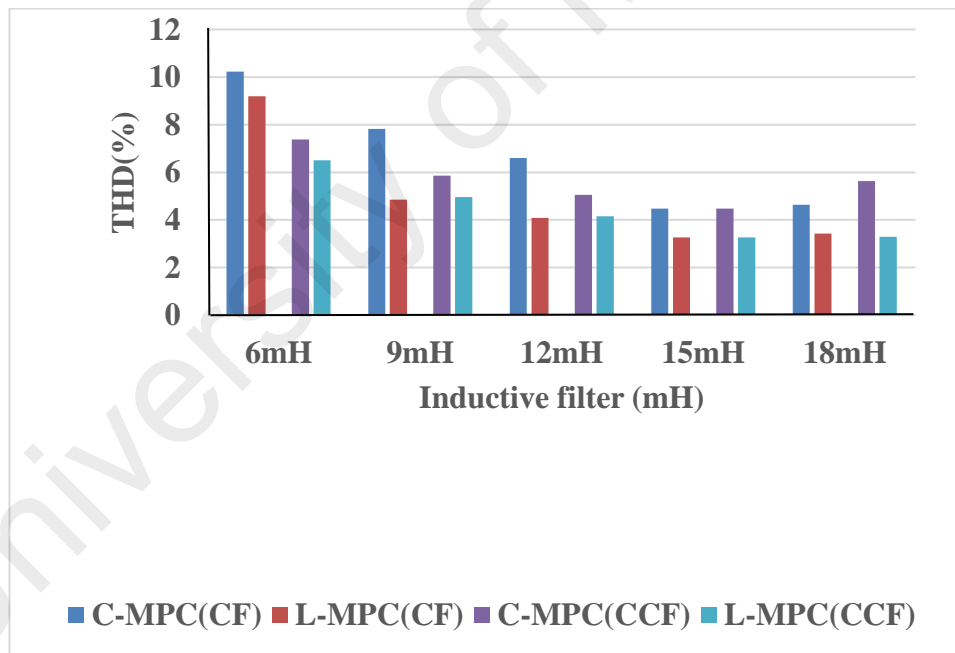
In this section, a comparison between the L-MPC and C-MPC is achieved for three-phase four-leg inverter. Robustness, control algorithm, reference tracking and THD are considered in this comparison.

5.3.1 Robustness Analysis of Model Parameter Variations

The modeling errors are used to compare the effectiveness for both C-MPC and L-MPC methods. The increase of ripple on the load current is due to the inductance variation (Jose & Patricio, 2012b). Thus, balanced references and the variation of filter's inductance are considered. Two cases are observed: a) CF: inductive filter changes and controller with no changes, where the filter's inductive changed from 6 mH to 18 mH without providing the information of filter changes to the controller. b) CCF: changes of filter as well as the controller, the changed filter values are given to the controller for evaluating the effectiveness comparison. In Figure 5.1, it is found that the THD (%) variation for both cases is very small but in each case, the proposed controller has better performance over the conventional controller. In both control method, THD is decreasing with the increase of inductive value and thus causes more power losses.



(a)



(b)

Figure 5.1: Comparison of THD between C-MPC and L-MPC with the filter changes (CF) and the controller and filter changes (CCF) at 50 μ s (a) Simulation result and (b) Experimental result

The percentage of reference tracking error with respect to load current is calculated from the reference and load current as follows.

$$\hat{i}_{error,m}(\%) = \frac{\frac{1}{a} \sum_k^a |i_m^*(k) - i_m(k)|}{i_m(k)_{rms}}, \quad (5.22)$$

Where $m = x, y, z$ and $a=2001$ is the number of samples used in simulation. For balanced, unbalanced references or loads cases, the current tracking error (%) is bounded and comparatively lower than C-MPC as shown in Figure 5.2.

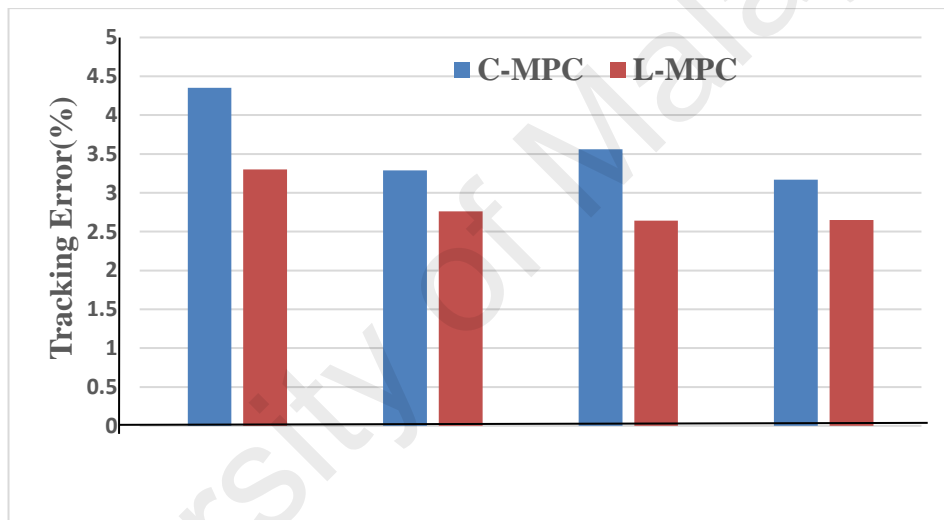


Figure 5.2: Reference tracking error (%) of L-MPC over C-MPC with model parameters variation

5.3.2 Control Algorithm and Implementation Procedure

The controller flowchart for both algorithms are presented in Figure 5.3. The L-MPC is based on voltage vector calculation, and the C-MPC is based on current vector calculation. The main difference is the reduction in the number of calculation inside the main loop without using the indicated portion (part A) in the proposed control algorithm. In the C-MPC system, the predictive voltage $\mathbf{v}(k + 1)$ is obtained based on switch control and then, phase currents $\mathbf{i}(k)$ are calculated in each iteration from the complex equation

with sampling time (T_s), predicted voltage $\mathbf{v}(k+1)$ and load-filter parameters Figure 5.3 (a), whereas in L-MPC system, only the predictive voltage $\mathbf{v}(k+1)$ is required to be obtained, and the reference voltage $\bar{\mathbf{v}}(k+1)$ vectors are calculated just once out of the main control loop Figure 5.3(b). Hence, the proposed L-MPC minimizes the number of operation in each iteration of the main loop. This is the remarkable improvement over the C-MPC in determining the predictive model in each control cycle.

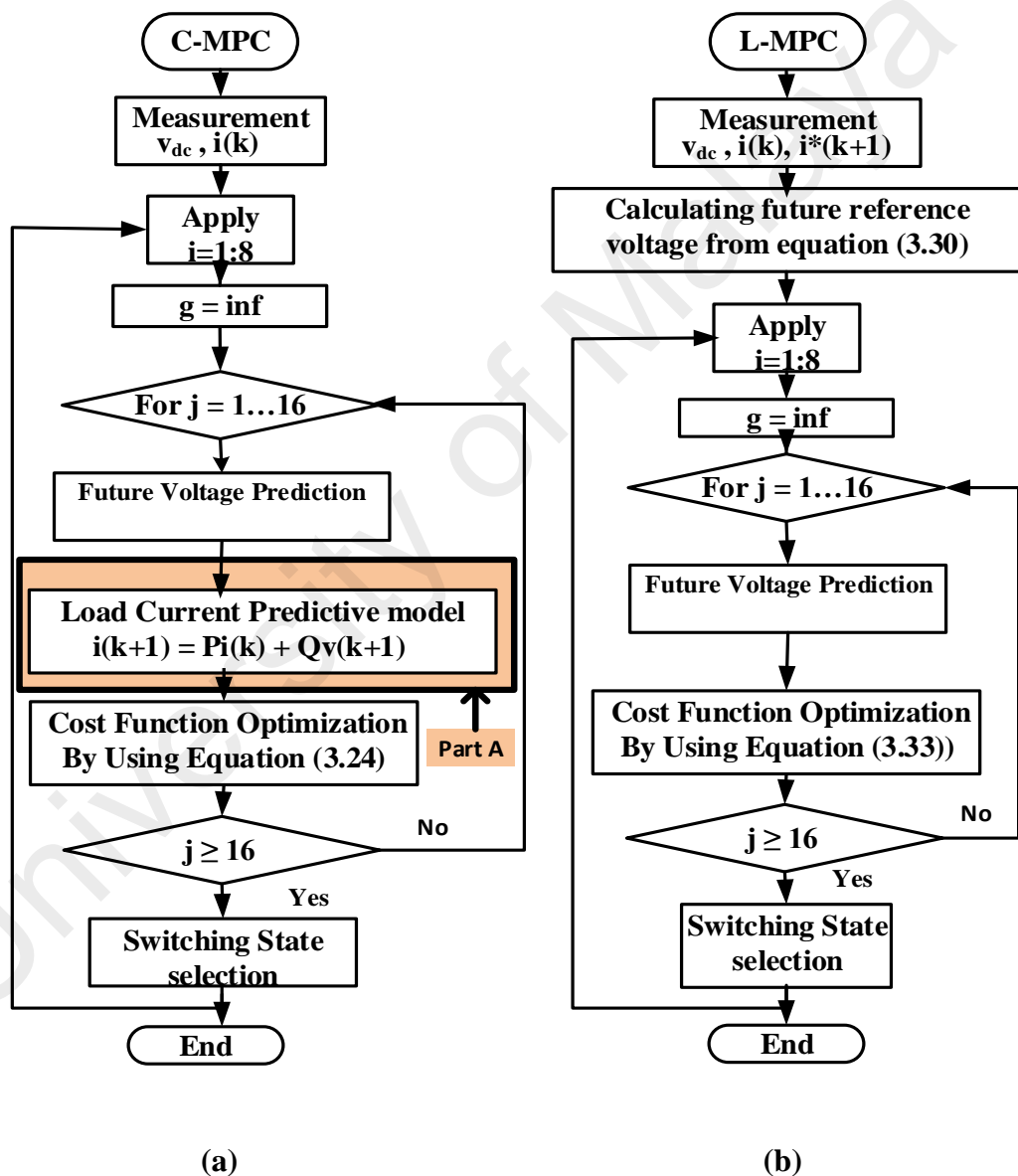


Figure 5.3: Flowcharts of the (a) C-MPC (Rivera, Yaramasu, Llor, et al., 2013) and (b) L-MPC

Table 5.1 shows the number of estimation operation in the four-leg inverter using both the conventional and Lyapunov controller respectively. The L-MPC has better performance as compared to the C-MPC. The algorithm of C-MPC needs 336 ticks per cycle whereas the L-MPC takes 256 ticks as shown in Table 5.2. Thus, the L-MPC improves the digital speed by reducing the processing time as compared to the C-MPC.

Table 5.1: The improvement of L-MPC over C-MPC per operation

Operations	C-MPC	L-MPC	Improvement (%)
Addition	96	52	46%
Absolute value	64	64	0
Subtraction	72	56	22%
Comparison	48	48	0
Division	48	2	96%
Multiplication	144	22	84%
Registers	1250	1206	3.52%
Xors	146	144	1.36%
Comparators	85	83	2.35%

Table 5.2: Execution time measurement

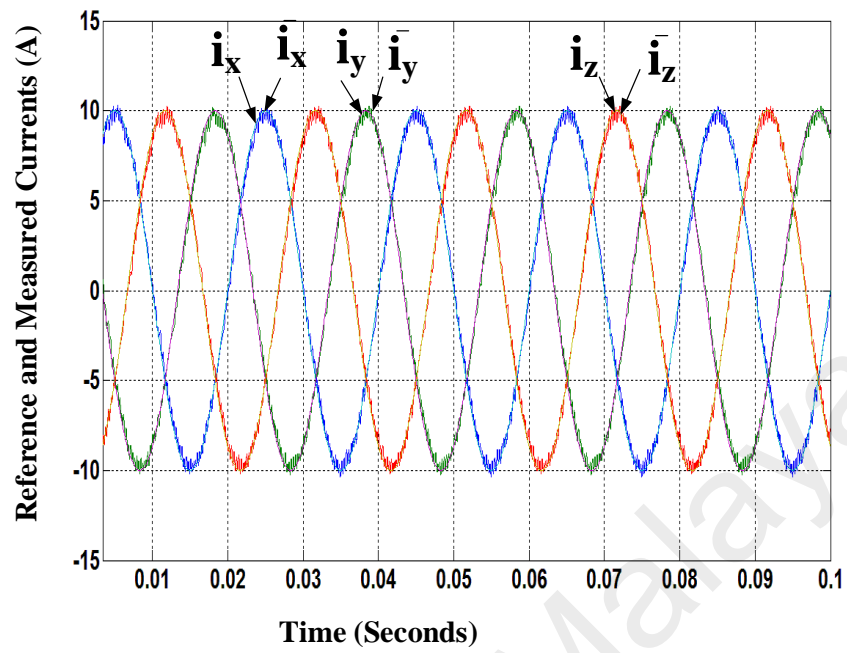
	C-MPC (1 tick=25 ns)	L-MPC (1 tick=25 ns)	Improvement (%)
Execution time (tick)	21*16 (8.4 μ s)	16*16(6.4 μ s)	23.8

The implementation procedure of C-MPC has already been described details in (Rivera, Yaramasu, Llor, et al., 2013) .

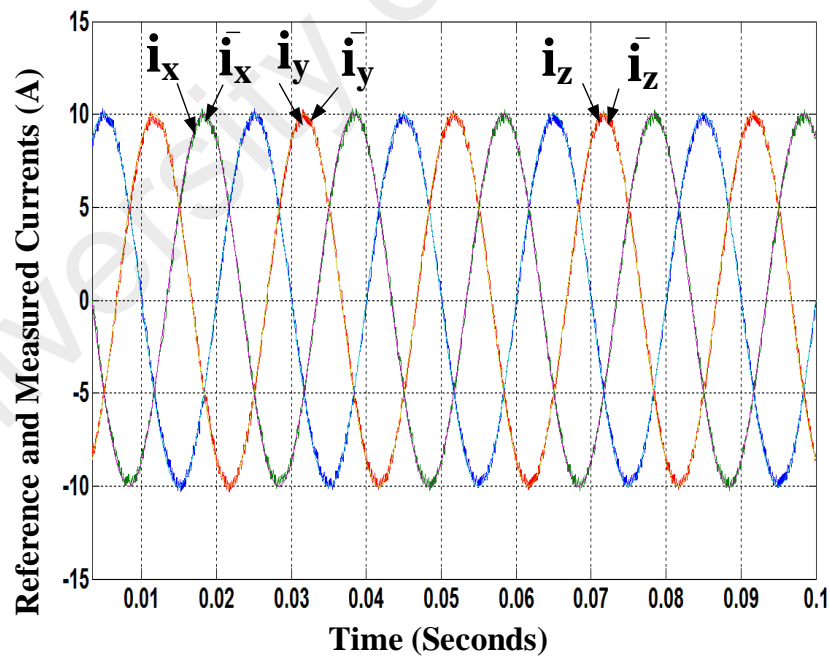
5.3.3 Current Reference Tracking and THD

In this section, Performance assessments are conducted to evaluate tracking error and THD assessment. The three-phase four-leg inverter controls the zero-sequence voltage or current by generating independent voltage on each leg. The references track the inverter load currents very well. In Figure 5.4 and Figure 5.5, the result shows that the proposed controller is more accurate in load current tracking, though the variations of current error of L-MPC and C-MPC are confined within (0.65A and 0.83A respectively)

acceptable limit. In figures, i indicates load currents and i^* indicates reference currents.

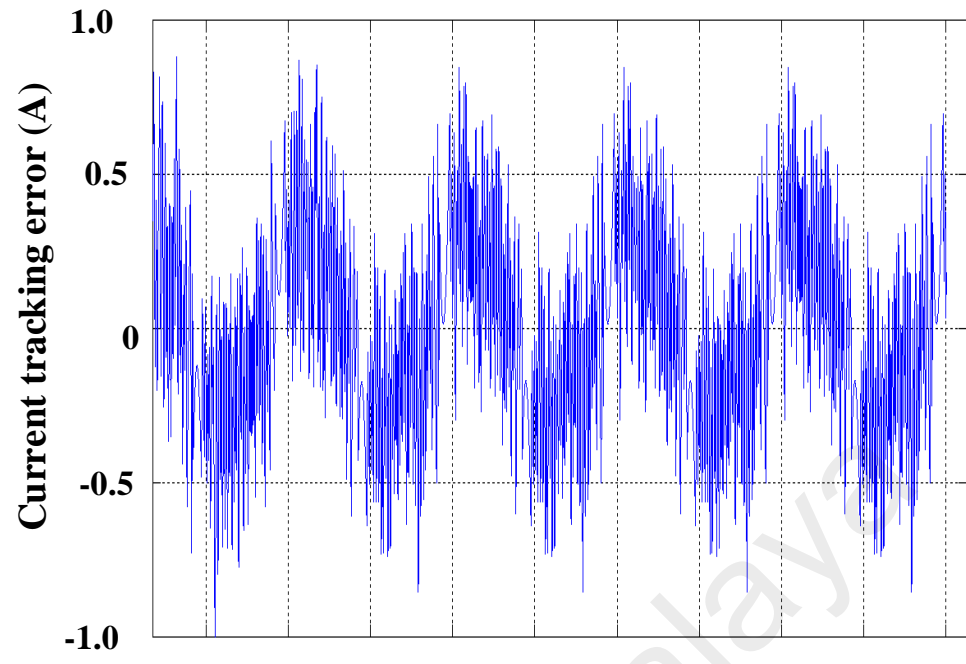


(a)



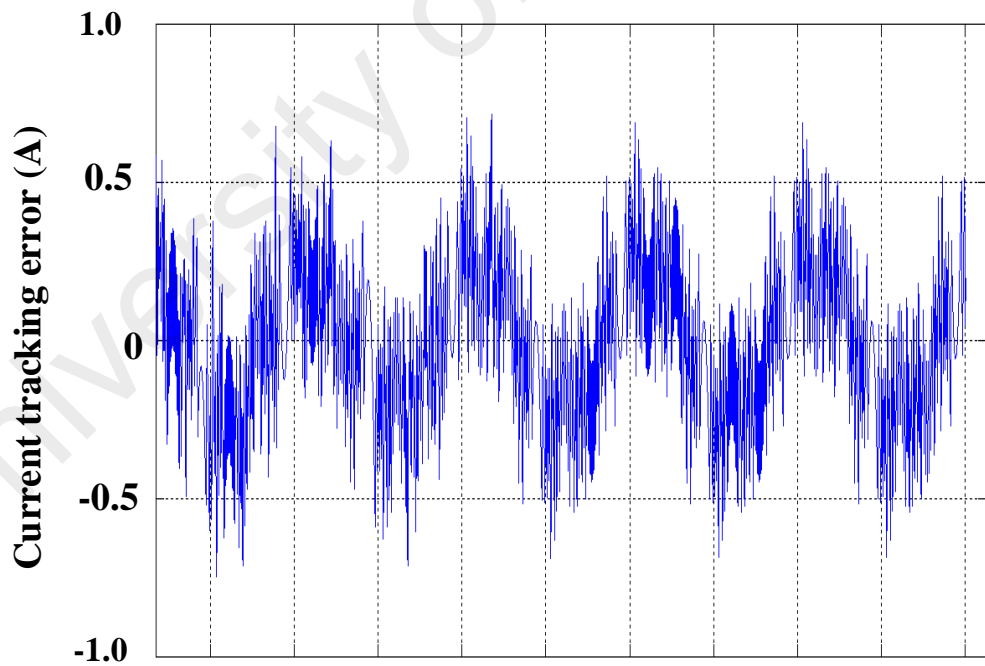
(b)

Figure 5.4: Three-phase references and measured load currents (a) C-MPC and (b) L-MPC.



Sample = 2001

(a)

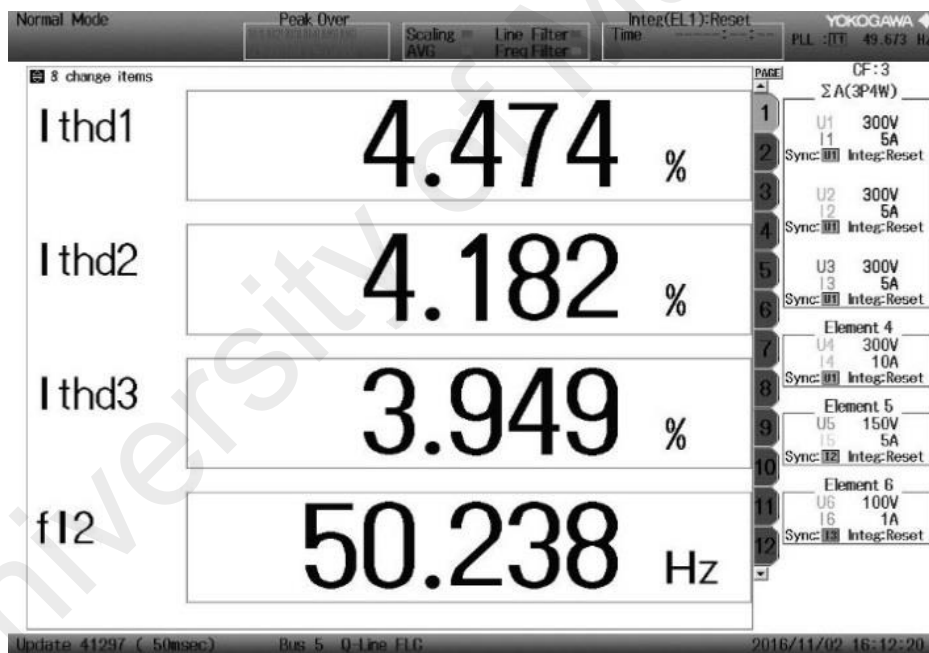


Sample = 2001

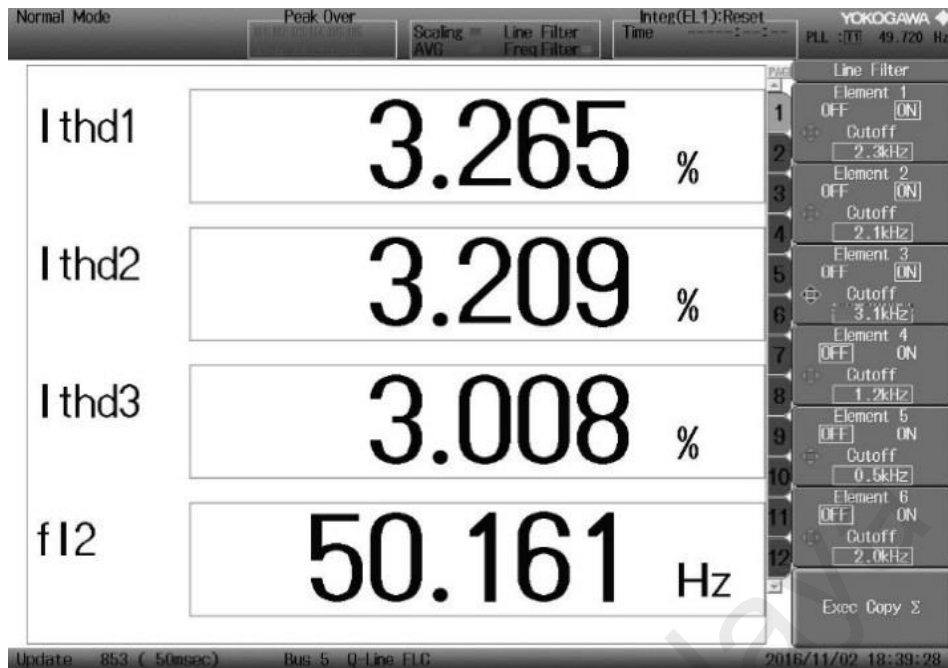
(b)

Figure 5.5: Current tracking error of Phase X (a) C-MPC and (b) L-MPC

Due to fast controlling and accurate reference tracking, the percentages of total harmonic distortion (THD) of proposed control method for every case are less as compared to C-MPC method at the same sampling time 20 μ s, 50 μ s and 100 μ s. The result (THD Comparison between C-MPC and L-MPC) of case 1 has been shown in Figure 5.6, and detail simulation and experimental results in Table 5.3. Since the proposed L-MPC is the modified MPC, the proposed Lyapunov MPC is only compared to the conventional MPC method to show the effectiveness of the proposed method. Other than that, the performance of the proposed method is compared to previous works in Table 5.4. In every case, THD (%) is obtained in experiment marginally higher than the simulation result due to add gate drive circuit, switching loss, etc.



(a)



(b)

Figure 5.6: Experimental result for balanced references with balanced loads (a) C-MPC and (b) L-MPC.

Table 5.3 : THD comparison between C-MPC and L-MPC

Case	Phase	C-MPC (Simulation /Experimental results)			L-MPC (Simulation/Experimental results)		
		20 μ s	50 μ s	100 μ s	20 μ s	50 μ s	100 μ s
Sampling time							
Balanced references with balanced load	X	1.69/3.17	3.89/4.47	5.72/6.93	1.01/2.52	2.53/3.26	4.87/6.01
	Y	1.76/2.96	3.90/4.18	5.33/6.16	1.02/2.47	2.41/3.21	4.59/5.64
	Z	1.73/2.58	3.75/3.94	5.41/5.75	1.02/2.29	2.59/3.00	4.98/5.09
Unbalanced references with balanced load	X	1.23/2.94	3.06/4.38	5.20/6.24	0.99/2.37	2.46/3.27	4.62/5.39
	Y	2.56/4.14	6.52/8.23	12.45/14.01	2.00/3.68	4.70/5.82	9.19/11.41
	Z	2.43/4.18	6.38/7.73	11.85/12.65	1.96/3.78	4.21/5.17	8.69/10.07
Balanced references	X	1.44/2.51	3.48/3.96	6.07/7.32	1.11/2.33	2.62/3.08	4.77/6.05

with unbalanced load	Y	1.87/3.29	4.61/5.58	7.73/8.29	1.60/2.92	3.50/4.97	6.72/7.31
	Z	1.90/3.21	4.52/5.61	8.62/8.98	1.62/3.12	3.59/4.12	6.45/8.01
Unbalanced references with unbalanced load	X	1.24/2.89	3.15/4.02	4.91/5.74	1.10/2.28	2.58/3.24	4.93/5.62
	Y	3.57/5.71	8.45/9.84	14.90/15.71	2.83/4.22	6.26/7.82	12.73/15.13
	Z	3.58/5.04	8.57/9.92	13.90/15.11	2.78/4.34	6.22/9.01	12.52/14.46

Table 5.4 : THD Comparison of Proposed Control Method with Previous Works of Four-leg Inverter

Previous Works	Phase	Balanced references with balanced load	Unbalanced references with balanced load	Balanced references with unbalanced load	Unbalanced references with unbalanced load
Digital Predictive Current Control with 150 V dc-link, 12mH/6 mH, 66 us sampling time (Rivera, Yaramasu, Llor, et al., 2013)	X	4.61%	6.03%	5.17%	6.89%
	Y	5.72%	11.5%	6.38%	12.66%
	Z	5.81%	13.05%	9.39%	21.38%
Model Predictive Current Control with 300V dc-link, 15mH, 50 us (Rivera, Yaramasu, Rodriguez, et al., 2013)	X	5.71%	4.68%	5.47%	5.42%
	Y	5.66%	5.78%	6.93%	6.87%
	Z	5.81%	7.44%	0 (I =0 A)	0 (I=0A)
Proposed Control Method At 50 μs	X	3.47%	3.77%	4.31%	4.52%
	Y	3.49%	7.21%	7.63%	15.92%
	Z	3.29%	7.77%	7.91%	16.05%

5.4 Performance Assessment of NSV-MPC

The performance and robustness analysis of proposed control scheme are performed in the following assessments.

5.4.1 Robustness Analysis of Model Parameter Variations

The controller accuracy depends upon the system parameters and discrete predictive model. The effectiveness of the near state vector based MPC is tested by robustness analysis in the parameter variations. The inductive filter variation is analysed through simulations and experiments. Two cases are observed: a) CF: inductive filter changes and controller with no changes, where the filter's inductive changed from 6 mH to 18 mH without providing the information of filter changes to the controller. b) CCF: changes of filter as well as the controller, the changed filter values are given to the controller for evaluating the effectiveness. In Figure 5.7, the percentages of THD with respect to variation of inductive value have been shown. In Figure, 6v, 7v and 8v represents the number of voltage vectors.

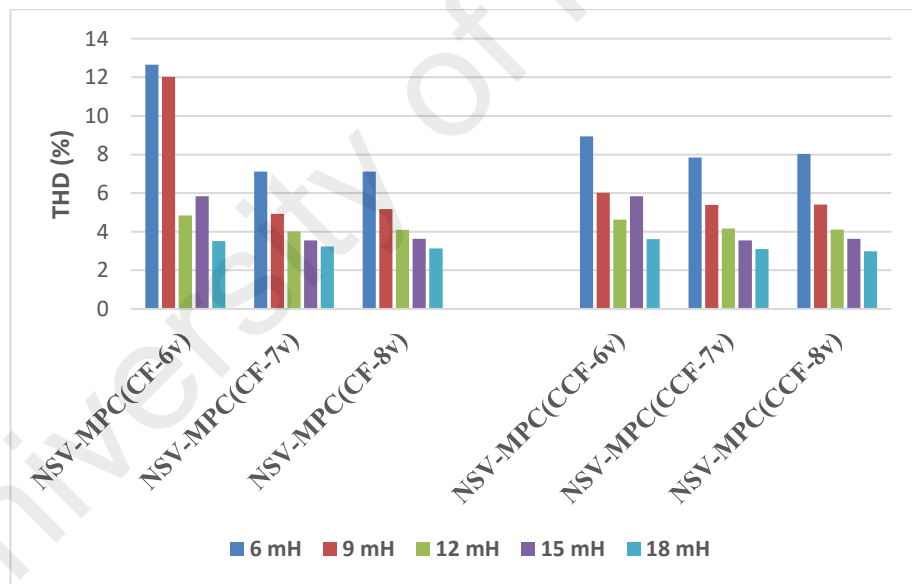


Figure 5.7: The percentages of THD with respect to variation of inductive value

5.4.2 Performance Assessment

The performance assessment is achieved considering the parameters of peak to peak value of CMV, THD (%) of load current and execution time. The proposed NSV-MPC technique improved the processing time by reducing the computational burden due to

utilize a reduced number of voltage vector at every control cycle. The number of tick (1 tick=25 ns) required in proposed controller is less than conventional controller for completing each iteration in the control loop with LabVIEW FPGA based control platform. The improvement of NSV-MPC compared to C-MPC are illustrated in Table 5.5 and Table 5.6. The proposed NSV-MPC is compared to the C-MPC method to show the effectiveness of the proposed control method. The performance of the proposed NSV-MPC are also analyzed under different weighting factor shown in Table 5.7. Other than that, the proposed method is compared to the previous works in Table 5.8.

Table 5.5: Execution time measurement

Strategy	Conventional MPC (1tick=25 ns)	Execution time (tick)	Proposed NSV-MPC (1 tick=25 ns)	Execution time (tick)	Improve ment (%)
No. of Switching Vectors	14	294	6	187	36.40
	15	317	7	201	36.59
	16	336	8	213	32.36

Table 5.6: CMV and percentage of THD and Current tracking error variation at different sampling time

Strategy	CMV Variat ion	THD (%)	Current Tracking Error (%)	THD (%)	Current Trackin g Error (%)	THD (%)	Current Tracking Error (%)
		Sampling frequency 50 KHz		Sampling frequency 20 KHz		Sampling frequency 10 KHz	
C-MPC	-160 to 160	3.47 %	3.58 %	3.90 %	4.68 %	6.65%	6.59 %
NSV-MPC with PPPP vector	-160 to 80	3.24 %	3.36 %	3.83 %	4.26 %	6.34 %	6.11 %
NSV-MPC with NNNN vector	-80 to 160	3.24 %	3.36 %	3.83 %	4.26 %	6.33 %	6.13 %
NSV-MPC with active vectors	-80 to 80	3.62 %	3.22 %	4.37 %	4.05 %	6.58 %	5.87 %

Table 5.7: THD (%), Current tracking error variation and average switching frequency at different weighting factor

Weighting Factor	Current THD (%)	Current Tracking Error (%)	Average switching frequency
0	3.71	3.29	13000
0.1	3.82	3.52	11500
0.3	4.08	3.82	10250
0.5	4.37	4.05	8500
0.7	4.51	4.18	8000
0.9	4.64	4.37	7500
1	4.79	4.5	7000

Table 5.8: Comparison between proposed control technique and previous works

Strategy	No. of Voltage vector used per sampling period	CMV Variation	Load current THD (%)
PWM based control technique for four-leg inverter (X. Guo et al., 2016)	16	$\pm \frac{V_{dc}}{2}$	-
Digital predictive current control for four-leg inverter (Rivera, Yaramasu, Llor, et al., 2013)	16	-	5.72 %
RCMV-MPC for three-leg inverter (Kwak & Mun, 2015)	6 among available 8	$\pm \frac{V_{dc}}{6}$	5.53 %
Proposed NSV-MPC technique for four-leg inverter	6 among available 16	$\pm \frac{V_{dc}}{4}$	4.37 %

5.5 Summary

This chapter has presented the stability analysis and comparative performance assessment of Lyapunov function and near state vector selection-based model predictive control with conventional model predictive control for the three-phase four-leg inverter. The robustness has been tested with the model parameter variations. The direct Lyapunov control law with the help of backstepping control has been used for the stability analysis of the three-phase four-leg inverter. The analysis of stability confirmed that the proposed

model predictive control based on Lyapunov function is stable for the operation of three-phase four-leg inverter. The performance of proposed Lyapunov function based MPC has compared to the previous work in terms of THD (%). The reference tracking error and execution time for the algorithm operation are also compared to show the fast controlling of the proposed control technique.

University of Malaya

CHAPTER 6: CONCLUSION AND FUTURE WORK

6.1 Conclusion

The outcome of the research work presented in this progress report has achieved the major contribution in the improvement of the control scheme. The proposed control techniques are very promising innovations in the development of existing control techniques. This dissertation focuses the model predictive control based on Lyapunov function and near state vector based for the three-phase four-leg inverter with resistive-inductive load. The MPC technique utilizes the discrete nature of the system to predict the future behavior of that system. The dissertation has reviewed different types of control technique and the model predictive control is an interesting control technique due to inclusion of constraints and non-linearity applied to the three-phase four-leg inverter. The MPC technique has been extended with Lyapunov function and near state vector selection has introduced in the MPC technique. The stability issue has been established owing to introduce Lyapunov control law in the cost function of MPC technique.

6.1.1 Summary of Major Contributions

The conclusions with major contributions of this dissertation work are summarized as follows.

- 1) Lyapunov function based model predictive control has applied to the three-phase four-leg inverter. This control technique improves the digital speed by 23.8 % over conventional MPC technique. The total harmonic distortion and current reference tracking are obtained 3.97 and ± 0.65 respectively in the balanced condition. The stability analysis has been performed to show the effectiveness of the proposed control technique for the three-phase four-leg inverter.
- 2) Near state vector selection-based model predictive control technique is also applied successfully to the three-phase four-leg inverter. This control technique mitigates

the common mode voltage with reduced computational burden. The CMV is bounded within $\pm \frac{V_{dc}}{4}$.

- 3) The CMV weighting factor in the cost function and voltage vector strategy are introduced to mitigate the common mode voltage of the three-phase four-leg inverter.
- 4) The performances of proposed control techniques are evaluated with respect to conventional model predictive control.
- 5) Simulation and experimental verification are conducted using Matlab/Simulink and LabVIEW FPGA respectively for the system operation.

It can be concluded that the validities of the dissertation results are justified with fast response, accurate reference tracking, no overshoots, low ripple content, low execution time as well as obtained the reduced computational burden of the operation of power inverter.

6.2 Future Work

The future research works are suggested as an extensive improvement to knowledge presented in this dissertation as following.

- 1) The model predictive control can be applied based upon the combination of Lyapunov function and near state vector selection strategy.
- 2) The proposed controller can also be applied to dynamic load especially in industrial application with electrical machine drive.
- 3) The comparison of proposed controller performance can be carried out with classical controller such as PI based, SVM/PWM based controller.

REFERENCES

- Alexandrou, A. D., Adamopoulos, N. K., & Kladas, A. G. (2016). Development of a Constant Switching Frequency Deadbeat Predictive Control Technique for Field-Oriented Synchronous Permanent-Magnet Motor Drive. *IEEE Transactions on Industrial Electronics*, 63(8), 5167-5175.
- Barros, J. D., & Silva, J. F. (2008). Optimal Predictive Control of Three-Phase NPC Multilevel Converter for Power Quality Applications. *IEEE Transactions on Industrial Electronics*, 55(10), 3670-3681.
- Barros, J. D., Silva, J. F. A., & Jesus, E. G. A. (2013). Fast-Predictive Optimal Control of NPC Multilevel Converters. *IEEE Transactions on Industrial Electronics*, 60(2), 619-627.
- Basri, H. M., & Mekhilef, S. (2016, 22-26 May 2016). Model predictive torque and flux control of induction motor fed by Three Level Indirect Matrix Converter with unity power factor strategy. Paper presented at the 2016 IEEE 8th International Power Electronics and Motion Control Conference (IPEMC-ECCE Asia).
- Bayhan, S., Abu-Rub, H., & Balog, R. (2016). Model Predictive Control of Quasi-Z Source Four-Leg Inverter. *IEEE Transactions on Industrial Electronics*, PP(99), 1-1.
- Bibian, S., & Jin, H. (2002). High performance predictive dead-beat digital controller for DC power supplies. *Ieee Transactions on Power Electronics*, 17(3), 420-427
- Bordons, C., & Montero, C. (2015). Basic Principles of MPC for Power Converters: Bridging the Gap Between Theory and Practice. *IEEE Industrial Electronics Magazine*, 9(3), 31-43.
- Bose, B. K. (2000). Energy, environment, and advances in power electronics. *IEEE Transactions on Power Electronics*, 15(4), 688-701.
- Calle-Prado, A., Alepuz, S., Bordonau, J., Nicolas-Apruzzese, J., Cortes, P., & Rodriguez, J. (2015). Model Predictive Current Control of Grid-Connected Neutral-Point-Clamped Converters to Meet Low-Voltage Ride-Through Requirements. *IEEE Transactions on Industrial Electronics*, 62(3), 1503-1514.
- Chee-Shen, L., Levi, E., Jones, M., Rahim, N. A., & Wooi-Ping, H. (2014). A Comparative Study of Synchronous Current Control Schemes Based on FCS-

MPC and PI-PWM for a Two-Motor Three-Phase Drive. *IEEE Transactions on Industrial Electronics*, 61(8), 3867-3878.

Chen, Q., Luo, X., Zhang, L., & Quan, S. (2017). Model Predictive Control for Three-Phase Four-Leg Grid-Tied Inverters. *IEEE Access*, 5, 2834-2841.

Choi, D. K., & Lee, K. B. (2015). Dynamic Performance Improvement of AC/DC Converter Using Model Predictive Direct Power Control With Finite Control Set. *IEEE Transactions on Industrial Electronics*, 62(2), 757-767.

Cortes, P., Kazmierkowski, M. P., Kennel, R. M., Quevedo, D. E., & Rodriguez, J. (2008). Predictive Control in Power Electronics and Drives. *IEEE Transactions on Industrial Electronics*, 55(12), 4312-4324.

Cortes, P., Kouro, S., La Rocca, B., Vargas, R., Rodriguez, J., Leon, J. I., Franquelo, L. G. (2009, 10-13 Feb. 2009). Guidelines for weighting factors design in Model Predictive Control of power converters and drives. Paper presented at the. *IEEE International Conference on Industrial Technology*, 2009

Cortes, P., Wilson, A., Kouro, S., Rodriguez, J., & Abu-Rub, H. (2010). Model Predictive Control of Multilevel Cascaded H-Bridge Inverters. *IEEE Transactions on Industrial Electronics*, 57(8), 2691-2699.

Davila, J. (2013). Exact Tracking Using Backstepping Control Design and High-Order Sliding Modes. *IEEE Transactions on Automatic Control*, 58(8), 2077-2081.

Dora, G. S., & Madhulita, M. (2013). Control techniques for power system stabilisation.

Druant, J., Belie, F. D., Sergeant, P., & Melkebeek, J. (2016). Field-Oriented Control for an Induction-Machine-Based Electrical Variable Transmission. *IEEE Transactions on Vehicular Technology*, 65(6), 4230-4240.

Duran, M. J., Riveros, J. A., Barrero, F., Guzman, H., & Prieto, J. (2012). Reduction of Common-Mode Voltage in Five-Phase Induction Motor Drives Using Predictive Control Techniques. *IEEE Transactions on Industry Applications*, 48(6), 2059-2067.

Fengjiang, W., Xiaoguang, L., Fan, F., & Hoay Beng, G. (2015). Modified Cascaded Multilevel Grid-Connected Inverter to Enhance European Efficiency and Several Extended Topologies. *IEEE Transactions on Industrial Informatics*, 11(6), 1358-1365.

- Fernandes, D. A., Costa, F. F., & Santos, E. C. d. (2013). Digital-Scalar PWM Approaches Applied to Four-Leg Voltage-Source Inverters. *IEEE Transactions on Industrial Electronics*, 60(5), 2022-2030.
- Gao, J., & Hu, Y. (2010). Direct Self-Control for BLDC Motor Drives Based on Three-Dimensional Coordinate System. *IEEE Transactions on Industrial Electronics*, 57(8), 2836-2844.
- Garcia, C. E., Prett, D. M., & Morari, M. (1989). Model predictive control: theory and practice—a survey. *Automatica*, 25(3), 335-348.
- George, V., & Mishra, M. K. (2009). User-defined constant switching frequency current control strategy for a four-leg inverter. *IET Power Electronics*, 2(4), 335-345.
- Geyer, T., & Quevedo, D. E. (2014). Multistep Finite Control Set Model Predictive Control for Power Electronics. *Ieee Transactions on Power Electronics*, 29(12), 6836-6846.
- Geyer, T., & Quevedo, D. E. (2015). Performance of Multistep Finite Control Set Model Predictive Control for Power Electronics. *IEEE Transactions on Power Electronics*, 30(3), 1633-1644.
- Ghate, V. N., & Dudul, S. V. (2011). Cascade Neural-Network-Based Fault Classifier for Three-Phase Induction Motor. *IEEE Transactions on Industrial Electronics*, 58(5), 1555-1563.
- Guo, L., Zhang, X., Yang, S., Xie, Z., & Cao, R. (2016). A Model Predictive Control Based Common-Mode Voltage Suppression Strategy for Voltage Source Inverter. *IEEE Transactions on Industrial Electronics*, PP(99), 1-1.
- Guo, X., He, R., Jian, J., Lu, Z., Sun, X., & Guerrero, J. M. (2016). Leakage Current Elimination of Four-Leg Inverter for Transformerless Three-Phase PV Systems. *Ieee Transactions on Power Electronics*, 31(3), 1841-1846.
- Hava, A. M., & Ün, E. (2011). A High-Performance PWM Algorithm for Common-Mode Voltage Reduction in Three-Phase Voltage Source Inverters. *IEEE Transactions on Power Electronics*, 26(7), 1998-2008.
- Hedayati, M. H., Acharya, A. B., & John, V. (2013). Common-Mode Filter Design for PWM Rectifier-Based Motor Drives. *IEEE Transactions on Power Electronics*, 28(11), 5364-5371.

- Hoseini, S. K., Adabi, J., & Sheikholeslami, A. (2014). Predictive modulation schemes to reduce common-mode voltage in three-phase inverters-fed AC drive systems. *IET Power Electronics*, 7(4), 840-849.
- Huang, J., & Shi, H. (2014). Reducing the Common-Mode Voltage through Carrier Peak Position Modulation in an SPWM Three-Phase Inverter. *IEEE Transactions on Power Electronics*, 29(9), 4490-4495.
- Hurng-Liahng, J., Jinn-Chang, W., Kuen-Der, W., Wen-Jung, C., & Yi-Hsun, C. (2005). Analysis of zig-zag transformer applying in the three-phase four-wire distribution power system. *IEEE Transactions on Power Delivery*, 20(2), 1168-1173.
- J, B., Freudenberg, B., The, A., & Dieckerhoff, S. (2015). Experimental Comparison of Model Predictive Control and Cascaded Control of the Modular Multilevel Converter. *Ieee Transactions on Power Electronics*, 30(1), 422-430.
- J.-J. E. Slotine, W. L. (1991). *Applied Nonlinear Control* Applied Nonlinear Control (Vol. 199). Prentice-Hall: Englewood Cliffs, NJ ,USA.
- Jose, R., & Patricio, C. (2012a). Cost Function Selection Predictive Control of Power Converters and Electrical Drives (pp. 145-161): Wiley-IEEE Press.
- Jose, R., & Patricio, C. (2012b). Effect of Model Parameter Errors Predictive Control of Power Converters and Electrical Drives (pp. 191-202): Wiley-IEEE Press.
- Jou, H. L., Wu, K. D., Wu, J. C., & Chiang, W. J. (2008). A Three-Phase Four-Wire Power Filter Comprising a Three-Phase Three-Wire Active Power Filter and a ZigZag Transformer. *IEEE Transactions on Power Electronics*, 23(1), 252-259.
- Jung, J. W., Vu, N. T. T., Dang, D. Q., Do, T. D., Choi, Y. S., & Choi, H. H. (2014). A Three-Phase Inverter for a Standalone Distributed Generation System: Adaptive Voltage Control Design and Stability Analysis. *IEEE Transactions on Energy Conversion*, 29(1), 46-56.
- Kadri, R., Gaubert, J. P., & Champenois, G. (2011). An Improved Maximum Power Point Tracking for Photovoltaic Grid-Connected Inverter Based on Voltage-Oriented Control. *IEEE Transactions on Industrial Electronics*, 58(1), 66-75.

- Kerekes, T., Teodorescu, R., Liserre, M., Klumpner, C., & Sumner, M. (2009). Evaluation of Three-Phase Transformerless Photovoltaic Inverter Topologies. *IEEE Transactions on Power Electronics*, 24(9), 2202-2211.
- Khalil, H. K., & Grizzle, J. (1996). *Nonlinear systems (Vol. 3)*: Prentice hall New Jersey.
- Kouro, S., Cortés, P., Vargas, R., Ammann, U., & Rodríguez, J. (2009). Model predictive control—A simple and powerful method to control power converters. *IEEE Transactions on Industrial Electronics*, 56(6), 1826-1838.
- Kwak, S., & Mun, S. k. (2015). Model Predictive Control Methods to Reduce Common-Mode Voltage for Three-Phase Voltage Source Inverters. *IEEE Transactions on Power Electronics*, 30(9), 5019-5035.
- Liu, Z., Liu, J., & Li, J. (2013). Modeling, Analysis, and Mitigation of Load Neutral Point Voltage for Three-Phase Four-Leg Inverter. *IEEE Transactions on Industrial Electronics*, 60(5), 2010-2021.
- Maheshwari, R., Munk-Nielsen, S., & Busquets-Monge, S. (2013). Design of Neutral-Point Voltage Controller of a Three-Level NPC Inverter With Small DC-Link Capacitors. *Industrial Electronics, IEEE Transactions on*, 60(5), 1861-1871.
- Mohd, A., Ortjohann, E., Hamsic, N., Sinsukthavorn, W., Lingemann, M., Schmelter, A., & Morton, D. (2010). Control strategy and space vector modulation for three-leg four-wire voltage source inverters under unbalanced load conditions. *IET Power Electronics*, 3(3), 323-333.
- Morales-Caporal, R., & Pacas, M. (2008, 24-27 Aug. 2008). Digital implementation of a direct mean torque control for AC servo drives based on a hybrid DSP/FPGA controller system. Paper presented at the 11th IEEE International Power Electronics Congress.
- Morari, M., & Lee, J. H. (1999). Model predictive control: past, present and future. *Computers & Chemical Engineering*, 23(4), 667-682.
- Nauman, M., & Hasan, A. (2016). Efficient Implicit Model-Predictive Control of a Three-Phase Inverter With an Output Filter. *IEEE Transactions on Power Electronics*, 31(9), 6075-6078.
- Nguyen, T., Nguyen, N., & Prasad, N. (2016). Novel Eliminated Common-Mode Voltage PWM Sequences and an Online Algorithm to Reduce Current Ripple for a Three-Level Inverter. *Ieee Transactions on Power Electronics*, PP(99), 1-1.

- Ortjohann, E., Mohd, A., Hamsic, N., & Lingemann, M. (2009, 8-10 Sept. 2009). Design and experimental investigation of space vector modulation for three-leg four-wire voltage source inverters. Paper presented at the 13th European Conference on Power Electronics and Applications.
- Panwar, N. L., Kaushik, S. C., & Kothari, S. (2011). Role of renewable energy sources in environmental protection: A review. *Renewable and Sustainable Energy Reviews*, 15(3), 1513-1524.
- Pettersson, S., Salo, M., & Tuusa, H. (2005). Improving the performance of a three-leg four-wire active power filter with a neutral wire filter inductor. Paper presented at the IEEE Compatibility in Power Electronics, 2005.
- Philip, J., Jain, C., Kant, K., Singh, B., Mishra, S., Chandra, A., & Al-Haddad, K. (2016). Control and Implementation of a Standalone Solar Photovoltaic Hybrid System. *IEEE Transactions on Industry Applications*, 52(4), 3472-3479.
- Pichan, M., & Rastegar, H. (2017). Sliding Mode Control of Four-Leg Inverter with Fixed Switching Frequency for Uninterruptible Power Supply Applications. *IEEE Transactions on Industrial Electronics*, PP(99), 1-1.
- Pozo-Palma, M., & Pacas, M. (2013, 10-13 Nov. 2013). Predictive torque control for an induction machine with a virtual multilevel inverter. Paper presented at the Industrial Electronics Society, IECON 2013 - 39th Annual Conference of the IEEE.
- Pozo-Palma, M., & Pacas, M. (2014, 2-5 Sept. 2014). Predictive control for a PMSM with LC-filter and a virtual multilevel inverter. Paper presented at the International Conference on Electrical Machines (ICEM), 2014.
- Prabhakar, N., & Mishra, M. K. (2010). Dynamic Hysteresis Current Control to Minimize Switching for Three-Phase Four-Leg VSI Topology to Compensate Nonlinear Load. *Ieee Transactions on Power Electronics*, 25(8), 1935-1942.
- Priya, N. A., & Mabel, M. C. (2012, 15-16 March 2012). Control methods for four-leg voltage source inverter. Paper presented at the International Conference on Devices, Circuits and Systems (ICDCS), 2012.
- PVPS, I. (2014). Trends in photovoltaic applications. Survey report of selected IEA countries between 1992 and 2013: Report IEA-PVPS T1–25.

- Rivera, M., Rodriguez, J., Yaramasu, V., & Wu, B. (2012, 4-6 Sept. 2012). Predictive load voltage and capacitor balancing control for a four-leg NPC inverter. Paper presented at the Power Electronics and Motion Control Conference (EPE/PEMC), 2012 15th International.
- Rivera, M., Yaramasu, V., Llor, A., Rodriguez, J., Wu, B., & Fadel, M. (2013). Digital Predictive Current Control of a Three-Phase Four-Leg Inverter. *Industrial Electronics, IEEE Transactions on*, 60(11), 4903-4912.
- Rivera, M., Yaramasu, V., Rodriguez, J., & Bin, W. (2013). Model Predictive Current Control of Two-Level Four-Leg Inverters Part II: Experimental Implementation and Validation. *Power Electronics, IEEE Transactions on*, 28(7), 3469-3478.
- Rodriguez, C. T., Fuente, D. V. d. l., Garcera, G., Figueres, E., & Moreno, J. A. G. (2013). Reconfigurable Control Scheme for a PV Microinverter Working in Both Grid-Connected and Island Modes. *IEEE Transactions on Industrial Electronics*, 60(4), 1582-1595.
- Rodriguez, J., & Cortes, P. (2012). *Model Predictive Control Predictive Control of Power Converters and Electrical Drives* (pp. 31-39): Wiley-IEEE Press.
- Rodriguez, J., & Cortes, P. (2012). *Predictive control of power converters and electrical drives* (Vol. 40): John Wiley & Sons.
- Rodriguez, J., Kazmierkowski, M. P., Espinoza, J. R., Zanchetta, P., Abu-Rub, H., Young, H. A., & Rojas, C. A. (2013). State of the Art of Finite Control Set Model Predictive Control in Power Electronics. *Industrial Informatics, IEEE Transactions on*, 9(2), 1003-1016.
- Rojas, F., Kennel, R., Cardenas, R., Repenning, R., Clare, J. C., & Diaz, M. (2017). A New Space-Vector-Modulation Algorithm for a Three-Level Four-Leg NPC Inverter. *IEEE Transactions on Energy Conversion*, 32(1), 23-35.
- Rossiter, J. A. (2003). *Model-based predictive control: a practical approach*: CRC press.
- Scoltock, J., Geyer, T., & Madawala, U. K. (2015). Model Predictive Direct Power Control for Grid-Connected NPC Converters. *IEEE Transactions on Industrial Electronics*, 62(9), 5319-5328.

- Seung-Hee, R., Dong-Gyun, W., Min-Kook, K., & Byoung-Kuk, L. (2016). Analysis and Design of Modified Half-Bridge Series-Resonant Inverter With DC-Link Neutral-Point-Clamped Cell. *IEEE Transactions on Power Electronics*, 31(3), 2282-2295.
- Singh, B., & Sharma, S. (2012). Design and Implementation of Four-Leg Voltage-Source-Converter-Based VFC for Autonomous Wind Energy Conversion System. *IEEE Transactions on Industrial Electronics*, 59(12), 4694-4703.
- Soghoyan, A., Suleiman, A., & Akopian, D. (2014). A Development and Testing Instrumentation for GPS Software Defined Radio With Fast FPGA Prototyping Support. *IEEE Transactions on Instrumentation and Measurement*, 63(8), 2001-2012.
- Sonawane, A. J., Gawande, S. P., Kadwane, S. G., & Ramteke, M. R. (2016). Nearly constant switching frequency hysteresis-based predictive control for distributed static compensator applications. *IET Power Electronics*, 9(11), 2174-2185.
- Song, W., Ma, J., Zhou, L., & Feng, X. (2016). Deadbeat Predictive Power Control of Single-Phase Three-Level Neutral-Point-Clamped Converters Using Space-Vector Modulation for Electric Railway Traction. *IEEE Transactions on Power Electronics*, 31(1), 721-732.
- Song, Z., Tian, Y., Yan, Z., & Chen, Z. (2016). Direct Power Control for Three-Phase Two-Level Voltage-Source Rectifiers Based on Extended-State Observation. *IEEE Transactions on Industrial Electronics*, 63(7), 4593-4603.
- Tallam, R. M., Skibinski, G. L., Shudarek, T. A., & Lukaszewski, R. A. (2011). Integrated Differential-Mode and Common-Mode Filter to Mitigate the Effects of Long Motor Leads on AC Drives. *IEEE Transactions on Industry Applications*, 47(5), 2075-2083.
- Teodorescu, R., Liserre, M., & Rodríguez, P. (2011). *Grid Converters for Photovoltaic and Wind Power Systems* (pp. 237-287): Wiley-IEEE Press.
- Tomlinson, M., Mouton, H. d. T., Kennel, R., & Stolze, P. (2016). A Fixed Switching Frequency Scheme for Finite-Control-Set Model Predictive Control, Concept and Algorithm. *IEEE Transactions on Industrial Electronics*, 63(12), 7662-7670.
- Trabelsi, M., Bayhan, S., Ghazi, K. A., Abu-Rub, H., & Ben-Brahim, L. (2016). Finite-Control-Set Model Predictive Control for Grid-Connected Packed-U-Cells Multilevel Inverter. *IEEE Transactions on Industrial Electronics*, 63(11), 7286-7295.

- Trinh, Q. N., F. H. C., & Wang, P. (2017). A Control Strategy to Eliminate Impact of Voltage Measurement Errors on Grid Current Performance of Three-Phase Grid-Connected Inverters. *IEEE Transactions on Industrial Electronics*, PP(99), 1-1.
- Uddin, M., Mekhilef, S., & Rivera, M. (2015). Experimental validation of minimum cost function-based model predictive converter control with efficient reference tracking. *IET Power Electronics*, 8(2), 278-287.
- Un, E., & Hava, A. M. (2009). A Near-State PWM Method With Reduced Switching Losses and Reduced Common-Mode Voltage for Three-Phase Voltage Source Inverters. *IEEE Transactions on Industry Applications*, 45(2), 782-793.
- Vazquez, S., Leon, J. I., Franquelo, L. G., Rodriguez, J., Young, H. A., Marquez, A., & Zanchetta, P. (2014). Model Predictive Control: A Review of Its Applications in Power Electronics. *Industrial Electronics Magazine, IEEE*, 8(1), 16-31.
- Vazquez, S., Montero, C., Bordons, C., & Franquelo, L. G. (2013, 10-13 Nov. 2013). Design and experimental validation of a Model Predictive Control strategy for a VSI with long prediction horizon. Paper presented at the Industrial Electronics Society, IECON 2013 - 39th Annual Conference of the IEEE.
- Wang, Z., Xiong, R., Huang, J., Yao, C., & Hu, X. (2008, 3-5 June 2008). Study on common mode voltage suppression based on three-phase four-leg inverter. Paper presented at the 2008 3rd IEEE Conference on Industrial Electronics and Applications.
- Xia, C., Wang, S., Wang, Z., & Shi, T. (2016). Direct Torque Control for VSI& PMSMs Using Four-Dimensional Switching-Table. *Ieee Transactions on Power Electronics*, 31(8), 5774-5785.
- Xiliang, C., Wenjie, C., Yaqiang, H., Yilin, S., Heyuan, Q., & Xu, Y. (2016, 22-26 May 2016). Predictive current control method to reduce common-mode interference for three-phase induction motor. Paper presented at the 2016 IEEE 8th International Power Electronics and Motion Control Conference (IPEMC-ECCE Asia).
- Yaramasu, V., Bin, W., Rivera, M., Narimani, M., Kouro, S., & Rodriguez, J. (2015). Generalised approach for predictive control with common-mode voltage mitigation in multilevel diode-clamped converters. *IET Power Electronics*, 8(8), 1440-1450.

- Yaramasu, V., Rivera, M., Bin, W., & Rodriguez, J. (2013). Model Predictive Current Control of Two-Level Four-Leg Inverters Part I: Concept, Algorithm, and Simulation Analysis. *IEEE Transactions on Power Electronics*, 28(7), 3459-3468.
- Akter, M. P., Mekhilef, S., Tan, N. M. L., & Akagi, H. (2016). Modified Model Predictive Control of a Bidirectional AC- DC Converter Based on Lyapunov Function for Energy Storage Systems. *IEEE Transactions on Industrial Electronics*, 63(2), 704-715.
- Yaramasu, V., Rivera, M., Narimani, M., Bin, W., & Rodriguez, J. (2014). Model Predictive Approach for a Simple and Effective Load Voltage Control of Four-Leg Inverter With an Output Filter. *IEEE Transactions on Industrial Electronics*, 61(10), 5259-5270.
- Yaramasu, V., Wu, B., Rivera, M., & Rodriguez, J. (2012, 4-6 Sept. 2012). Enhanced model predictive voltage control of four-leg inverters with switching frequency reduction for standalone power systems. Paper presented at the Power Electronics and Motion Control Conference (EPE/PEMC), 2012 15th International.
- Yaramasu, V., Wu, B., Rivera, M., Rodriguez, J., & Wilson, A. (2012, 5-9 Feb. 2012). Cost-function based predictive voltage control of two-level four-leg inverters using two step prediction horizon for standalone power systems. Paper presented at the Applied Power Electronics Conference and Exposition (APEC), 2012 Twenty-Seventh Annual IEEE.
- Zhang, F., & Yan, Y. (2009). Selective Harmonic Elimination PWM Control Scheme on a Three-Phase Four-Leg Voltage Source Inverter. *IEEE Transactions on Power Electronics*, 24(7), 1682-1689.
- Zhang, M., Atkinson, D. J., Ji, B., Armstrong, M., & Ma, M. (2014). A Near-State Three-Dimensional Space Vector Modulation for a Three-Phase Four-Leg Voltage Source Inverter. *IEEE Transactions on Power Electronics*, 29(11), 5715-5726.
- Zhang, R., Prasad, V. H., Boroyevich, D., & Lee, F. C. (2002). Three-dimensional space vector modulation for four-leg voltage-source converters. *Ieee Transactions on Power Electronics*, 17(3), 314-326.
- Uddin, M., Mekhilef, S., & Rivera, M. (2015). Experimental validation of minimum cost function-based model predictive converter control with efficient reference tracking. *IET Power Electronics*, 8(2), 278-287.

Zhang, X., Wang, Y., Yu, C., Guo, L., & Cao, R. (2016). Hysteresis Model Predictive Control for High-Power Grid-Connected Inverters With Output LCL Filter. *IEEE Transactions on Industrial Electronics*, 63(1), 246-256.

University of Malaya

LIST OF PUBLICATIONS AND PAPERS PRESENTED

List of Journal Paper

1. Abdul Mannan Dadu, Saad Mekhilef, Tey Kok Soon, Mehdi Seyedmahmoudian and Ben Horan “Near State Vector Selection-Based Model Predictive Control with Common Mode Voltage Mitigation for a Three-Phase Four-Leg Inverter” in *Energies* (Accepted)
2. Abdul Mannan Dadu, Saad Mekhilef and Tey Kok Soon “Lyapunov Model Predictive Control to Optimize Computational Burden, Reference Tracking and THD of Three-Phase Four-leg Inverter” in *IEEE Journal of Emerging and Selected Topics in Power Electronics* (Under review)

List of Conference Paper

1. Abdul Mannan Dadu, Saad Mekhilef, Tey Kok Soon and Mutsuo Nakaoka “Lyapunov Law Based Model Predictive Control Scheme for Grid Connected Three-phase Three Level Neutral Point Clamped Inverter” *Proceedings on ECCE-Asia 2017* (Accepted).